FRUSTRATED MAGNETIC LADDERS: A DMRG STUDY

A THESIS SUBMITTED FOR THE DEGREE OF

DOCTOR OF PHILOSOPHY (SCIENCE)

IN PHYSICS (THEORETICAL)

by

DEBASMITA MAITI

Department of Physics

University of Calcutta

2019

Dedicated to

My Parents

ACKNOWLEDGEMENTS

PUBLICATIONS

PAPERS TO BE INCLUDED IN THE PH.D. THESIS

- **An efficient density matrix renormalization group algorithm for chains with periodic boundary condition**, Dayasindhu Dey, Debasmita Maiti, and Manoranjan Kumar, Papers in Physics **8**, 080006 (2016).

- **Frustrated spin-1/2 ladder with ferro- and antiferromagnetic legs**, Debasmita Maiti, Dayasindhu Dey and Manoranjan Kumar, Journal of Magnetism and Magnetic Materials **446**, 170 (2018).

- **Melting of ferromagnetic order on a trellis ladder**, Debasmita Maiti and Manoranjan Kumar, Journal of Magnetism and Magnetic Materials **486**, 165266 (2019).

- **Quantum phase diagram of a frustrated spin-1/2 system on a trellis ladder**, Debasmita Maiti and Manoranjan Kumar, arXiv:1907.04709 [cond-mat.str-el].

- **Ground state properties of mixed-spin(1,1/2) ladder**, Dayasindhu Dey, Debasmita Maiti and Manoranjan Kumar (in preparation).

CONTENTS

LIST OF FIGURES

INTRODUCTION

Our daily life can not be imagined without the applications of various electronic devices. We exploit transport, optical or magnetic properties of materials in these devices. The magnetic properties play important roles in designing a wide range of devices like MRI machines, refrigerators, magnetic sensors, data storage devices used in electronic devices like computers, mobiles etc. To understand different magnetic phenomena, theoretical modeling of magnetic materials is crucial; therefore, study of magnetism is one of the frontier areas of the modern research. The itinerant or localized magnetic moment which consists of both angular and spin magnetic moments of electrons is responsible for magnetism in the material [1]. The concept of diamagnetism and paramagnetism can be understood without considering any explicit interaction between electrons exhibiting magnetic moments [2]. However, the interactions between electrons may lead to many interesting properties e.g., spontaneous magnetic order in ferromagnetic (FM) and antiferromagnetic (AFM) phases [3]. In these phases electronic charge degrees of freedom are localized; however, spins sitting at neighboring sites can exchange their orientations. The arrangement of spins depends on the nature of spin exchange interactions in the system [4]. The spin arrangements can be FM where all spins are aligned in one direction, AFM where nearest neighbor spins are aligned in opposite direction, or canted ferromagnet where the neighboring spins have a relative pitch angle θ ($0 < \theta < \pi$).

Ferromagnetic materials like K_2CuF_4 [5], $CdCr_2Se_4$ [6], EuO [7], EuS [8], Rb_2CrCl_4 [9], $CrBr_3$ [10] and antiferromagnetic materials like MnO [11], $EuTe$ [12], $RbMnF_3$ [13], Rb_2MnCl_4 [14] are experimentally synthesized. There are ferrimagnetic materials e.g., $EuSe$ [15], where

spins are partially polarized. Majority of the materials are insulators and magnetic contribution comes from localized magnetic moments of their partially filled d or f electronic shells. There are also some materials like Fe, Ni, Co and their alloys, in which valance electrons are involved in both electrical conductivity and magnetism. The itinerant electrons of these materials are highly interacting. However, in non-interacting limit tight binding theory gives the band structure of electrons moving in an effective periodic potential created by the nuclei. On the other hand, the Hartree-Fock calculation deals with interacting electrons which are under the influence of both the effective field produced by the nuclei and the effective field created by surrounding electrons [16]. However, in both of these models electrons are dealt considering single particle basis. The electronic band theory successfully classifies a large number of materials as metals or insulators, but the single particle theory is unable to identify Mott insulators where electron-electron interaction induces gap in the energy levels [17]. The band theory is also unable to explain the ferromagnetic behavior in certain metals like Fe, Co, Ni etc. The strong electron-electron interaction is responsible for spontaneous magnetic order in these materials [18]. However, inclusion of electron-electron correlation explicitly in a model Hamiltonian makes it many body in nature. In this context, we need a many body basis to deal with this Hamiltonian. In many body basis the degrees of freedom increase as m^N, where m is the local degrees of freedom and N is the size of the system. In the next two sections we will give a brief description about some of these model Hamiltonians, in particular the Hubbard model and the Heisenberg model. We will also discuss a few numerical techniques to solve these many body Hamiltonians in the next chapter.

1.1 BEYOND THE BAND THEORY: HUBBARD MODEL

Due to the failure of the band structure theory in describing some of the magnetic phenomena, some toy models like Hubbard model, Anderson model, Heisenberg model etc. are proposed to explain magnetism in strongly correlated materials. In 1963, the Hubbard model was introduced simultaneously by Gutzwiller [19], Hubbard [20], and Kanamori [21]. This model includes kinetic energy term or hopping of electrons to neighboring sites and the

electron-electron repulsion term restricted to the same site i.e., electrons repel each other if they are at the same site. This model can be written in the second quantization form as

$$H = t \sum_{i,\sigma}(c_{i,\sigma}^\dagger c_{i+1,\sigma} + h.c.) + U \sum_i n_{i,\sigma} n_{i,\sigma'}, \qquad (1.1)$$

where $c_{i,\sigma}^\dagger$ is creation operator at site i and $c_{i+1,\sigma}$ is annihilation operator at site $i+1$ with spin σ. $n_{i,\sigma}$ is number operators with spin σ. t is the hopping amplitude and U is the on-site Coulomb repulsion. The Hamiltonian is not analytically solvable, except in one dimension [22], due to the presence of electron-electron interaction term. This is the simplest many body Hamiltonian, where two competing terms can explain interesting phenomenon like metal-insulator transition [23]. The kinetic energy or electron hopping term tries to delocalize the electrons and leads the system to behave like metal, whereas the second term i.e. electron-electron interaction attempts to localize the electron onto a site and drives the system to an insulating state, which is generally magnetic. The large $t >> U$ limit corresponds to the band picture of non-interacting particles, while in the limit of $U >> t$ electrons are completely localized. Depending on the nature of U i.e., attractive ($U < 0$) or repulsive ($U > 0$) the Hubbard Hamiltonian describes various phases. Phases like paramagnetic metallic [24], ferromagnetic metallic [25], antiferromagnetic insulating [26] phases arise in the limit of $U > 0$ i.e, repulsive U. On the other hand, attractive U explains normal Fermi-liquid [27], superconductivity [28] etc. The Hubbard model offers complex phase diagrams in the parameter space of t, U, temperature T and chemical potential μ for various lattice structures and dimensions [24, 29–33].

1.2 LARGE U/t LIMIT: HEISENBERG MODEL

The magnetic properties of many insulating materials can be well described by the Heisenberg model. In the large U limit i.e., for $U >> t$, we can consider the coulomb term as the unperturbed part of the Hubbard Hamiltonian in Eq. 1.1. The ground state (gs) of the unperturbed Hamiltonian has one electron occupying each lattice site. Now we can treat

the kinetic energy term as a perturbation. The second order degenerate perturbation theory produces the effective Hamiltonian given by

$$H = \sum_{<ij>} J_{ij} \mathbf{S}_i \cdot \mathbf{S}_j, \tag{1.2}$$

where $\mathbf{S}_i$ and $\mathbf{S}_j$ are the spin operators localized at sites i and j. The single bracket holds for only the nearest neighbors, and J_{ij} represents spin exchange interaction strength between sites i and j. The second order perturbation theory gives the value $J = 4t^2/U$. The positive J value gives rise to the AFM alignment of spins in the gs, whereas negative J favors parallel alignment of spins. In this limit the charge degrees of freedom are frozen, and each lattice site is occupied by a single unpaired electron. Therefore, at every site there are two possible spin configurations; either spin up or spin down. In this case, electrons can exchange their spins but they can not move.

The isotropic or anisotropic Heisenberg model with various kinds of spins and exchange interactions play important roles in understanding the phase transitions driven by quantum fluctuations at temperature $T = 0$ [34]. This simple model can also explain various complex physical phenomena in real materials with localized electronic spins. The details of exotic quantum phases for various spin models and their realizations in several materials are discussed in the following sections.

1.3 MAPPING OF MAGNETIC MATERIALS TO LOW-DIMENSIONAL SPIN MODELS

There are plenty of magnetic materials where the dominant exchange interactions are confined in certain directions only. Therefore, these materials effectively behave like low dimensional magnetic systems. To be more specific dominant exchange interactions acting along a particular direction drive the system into behaving similar to one-dimensional (1D) spin chain, while dominant exchange interactions confined in a two-dimensional (2D) plane turn the system into an effectively 2D spin system. In low-dimensional spin systems the intra-chain or intra-layer exchange coupling is about $10^2 - 10^5$ times the inter-chain or inter-layer exchange coupling. Hence, the magnetic properties of these systems can be explained

by simple low-dimensional spin models. The low-dimensional materials have advantage over bulk materials in modeling and interpreting the experimental properties like susceptibility, specific heat, magnetization etc. Most of the investigated spin-1/2 materials consist of Cu^{2+} ions and Ni^{2+} ions for spin-1 materials. Some of the examples of spin-1/2 AFM chains are $CuCl_2.2N(C_5D_5)$ [35], $KCuF_3$ [36], $KCuGaF_6$ [37] etc. The 1D materials like $LiCuVO_4$ [38], $LiCuSbO_4$ [39], $LiCu_2O_2$ [40], Li_2ZrCuO_4 [41] have FM nearest neighbor (NN) and AFM next nearest neighbor (NNN) interactions. The frustration due to competing exchange interactions induces an incommensurate magnetic order in most of these materials. The research on coupled-chains has been stimulated by the synthesis of 2-leg ladder materials e.g., $SrCu_2O_3$ [42], $(VO)_2P_2O_7$ [43, 44] etc. and $Sr_2Cu_3O_5$ [45] with 3-legs. $Ba_3Cu_3Sc_4O_{12}$, $Ba_3Cu_3Sc_4O_{12}$ [46, 47] are the realizations of spin-1/2 half-twist ladder. The experimental manifestations of interacting chains with NN and NNN exchange couplings are Cu_2GeO_4 [48], $BiCu_2PO_6$ [49] etc.

The discovery of high temperature superconductor with the parent compound composed of copper oxide layers evokes much interest in low-dimensional physics. La_2CuO_4 is the first discovered high temperature superconductor where the dominant AFM interactions between Cu^{2+} ions lies on CuO_2 plane [50], whereas K_2CuF_4 is one of the materials which shows 2D FM order [51]. The field of 2D quantum magnetism is quite broad due to the presence of various possible 2D lattice structures with different coordination numbers. The most common 2D lattice structures are square lattice, triangular lattice, kagome lattice, honeycomb lattice etc. In some undoped copper oxide insulators like La_2CuO_4 and YBa_2CuO_6 [50], the AFM exchange interactions among spin-1/2 of Cu^{2+} ions form square lattice like structure. The study of spin-1/2 AFM triangular Heisenberg model is relevant to certain inorganic salts like $LiNiO_2$ [52], Cs_2CuCl_4 [53], organic compounds like $\kappa-(BEDT-TTF)_2Cu_2(CN)_3$ [54], $\kappa-(ET)_2Cu_2(CN)_3$ [55] etc. Iridates like Na_2IrO_3 and Li_2IrO_3 [56, 57] have attracted special attention as the Ir^{+4} ions of these materials are arranged in a layered honeycomb lattice structure. There are many vanadates like CaV_2O_5, MgV_2O_5 [58, 59] which are predicted to be consisted of interacting ladders through zigzag bonds. The lattice structure that is exhibited by the interaction between spin-1/2 V^{4+} ions in these materials is shown to be trellis

lattice. The magnetic properties of $SrCu_2(BO_3)_2$ can be understood by the celebrated Shastry-Sutherland model [60].

The spin-1 magnetic systems where each effective spin is composed of two spin-1/2 show Haldane phase in 1D [61]. Some of the examples of the 1D spin-1 systems are $CsNiCl_3$ [62], $CsNiF_3$ [63], $Ni(C_2H_8N_2)_2NO_2(ClO_4)$ [64], $Ni(C_5H_{14}N_2)_2N_3(PF_6)$ [65] etc. In the bipartite substance $[NiCu(pba)(D_2O)_3].2D_2O$, Cu^{2+} and Ni^{2+} sit at alternative positions along one axis and give rise to spin-1/2 and 1 mixed-spin chain which can have ferrimagnetic gs [66].

The low-dimensional spin model systems provide an opportunity to study the interesting quantum phenomena in the field of exotic quantum phases and quantum phase transitions driven by quantum fluctuations. However, it is known that there is no long-range order (LRO) in the 1D and 2D Heisenberg spin systems at a finite temperature as stated in the Mermin-Wagner theorem [67], but LRO may exist in these systems at $T = 0$. The LRO in a frustrated system can be destroyed due to the presence of disorder and frustration. The chain and ladder compounds may exhibit either quasi-long-range order (QLRO) or short-range order (SRO) [68]. The roles of quantum fluctuations and geometrical frustrations in the gs are still under extensive investigation, and it is one of the most active areas of research. A large variety of theoretical approaches like perturbation theory with higher order series expansions [69], spin wave theory [70], Schwinger boson mean field theory [71], renormalization group (RG) method [72, 73], field theoretical approaches like bosonization [74], semi-classical non linear σ-model [61] etc. are proposed to deal with these many body systems. Though some of the 1D quantum spin models can have exact analytical solutions, but analytical solutions of most of these model systems are either inaccurate or can not be solved. Therefore, the of computational studies become important in these cases.

The exact numerical calculations of the many body Hamiltonian are computationally expensive. Therefore, for large system size these calculations are impossible. To deal with large system sizes a series of approximate methods are developed viz., numerical renormalization group method [75], density matrix renormalization group (DMRG) method [76, 77] to tackle frustrations in large 1D or quasi 1D systems, quantum Monte Carlo (QMC) method [78] to solve higher dimensional unfrustrated spin models etc. In recent years, the tensor network is another promising tool for the investigation of the many body systems [79].

Before going to discuss about my thesis problem, let us make a brief review of the exotic phases in 1D and quasi-1D magnetic systems. We shall provide a short discussion on 2D magnetic systems, thereafter.

1.4 ONE DIMENSIONAL SPIN SYSTEMS: SPIN CHAINS

The study of low-dimensional magnetism started with the investigation of 1D Ising model by Ernst Ising in 1925. In this model spin interactions are confined only along the easy-axis, say z-axis. But spins can have interaction along all three direction with various amplitudes, and the model Hamiltonian can be written as

$$H = \sum_{<ij>} J_x S_i^x S_j^x + J_y S_i^y S_j^y + J_z S_i^z S_j^z. \tag{1.3}$$

J_x, J_y and J_z are the anisotropic exchange interactions; whereas S^x, S^y and S^z are components of the spins along x, y, and z directions, respectively. When $J_x = J_y = 0$, Eq. 1.3 turns into Ising model. For $J^z < 0$, the gs configuration of the Ising model has either all spins up or all spins down at $T = 0$. On the other hand, no LRO appears in the gs for $T \neq 0$. The conditions J_x, $J_y \neq 0$ and $J_z = 0$ correspond to the XY model. In 1D, the XY model for S=1/2 is exactly solvable where spin operators are transformed to spin-less fermions through the Jordan-Wigner transformation [80, 81]. The spin correlation is one of the essential quantities to characterize gs. For a spin chain the spin correlation between i^{th} and $(i + r)^{th}$ spins is written as

$$C(r) = < \mathbf{S}_i \cdot \mathbf{S}_{i+r} > \tag{1.4}$$

where $\mathbf{S}_i$ and $\mathbf{S}_{i+r}$ are the spins of ith site and $(i + r)^{th}$ site, respectively. At $T = 0$, both the transverse correlations i.e., $< S_i^x S_{i+r}^x >$ and $< S_i^y S_{i+r}^y >$ show power law variation w.r.t. r for the isotropic 1D XY model with $J_x = J_y < 0$ [82]. In the anisotropic XY model, the gs develops LRO in $< S_i^x S_{i+r}^x >$ or $< S_i^y S_{i+r}^y >$ for stronger J_x or J_y interaction, respectively, at $T = 0$ [82]. The correlation decays exponentially for nonzero temperature as predicted by the Mermin-Wagner theorem [67].
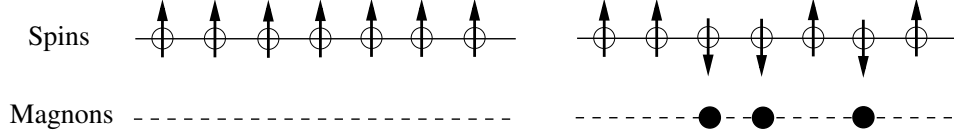
Figure 1.1: Flipping of spin-1/2 spins create magnons; here three spins are flipped which create three magnons represented by black solid circles.

For 1D isotropic Heisenberg model i.e, when $J_x = J_y = J_z = J$, the gs shows FM order for $J < 0$ and AFM order for $J > 0$. The gs energy in FM state is $\epsilon_0 = NJS^2$ for a 1D spin-S chain with N number of lattice sites. The FM gs is a maximally polarized state i.e, $S_{tot}^z = NS$, and this gs is $(2NS + 1)$ fold degenerate. The low-lying excitations can be created flipping the spins one by one and the dispersion relation can be described by means of the linearized spin wave theory. Originally the spin wave theory for the FM state was proposed by Bloch [83, 84], and Holstein and Primakoff [85], whereas it was later extended by Anderson [86], Kubo [87], and Oguchi [88] for the AFM Néel state. Flipping one spin in the FM state changes the value of S_{tot}^z from NS to $(NS - 1)$. Instead of flipping one spin, if all the spins are tilted by a certain angle with respect to their neighboring spins so that S_{tot}^z becomes $(NS - 1)$ then the arising excitation is called spin wave. The quasi-particles associated with the spin wave excitations are called magnons. These are the magnetic analog of phonons associated with lattice vibration. If S_{tot}^z of the system goes from NS to $(NS - n)$, then the number of magnons created in the excited state in n as shown in Fig. 1.1. In the case of the 1D FM chain the dispersion relation obtained from the spin wave theory is $\omega_k = 2|J|S(1 - \cos k)$. The spectrum is gapless in the isotropic FM Heisenberg limit. Two-magnon bound state can be found with two spin deviations on neighboring sites which creates two domain walls, and the lowest excitation energy remains unaffected in the presence of domain wall [89, 90]. The FM long range order in 1D vanishes at any finite temperature.

In the AFM gs of $S = 1/2$ 1D isotropic AFM Heisenberg model, quantum fluctuations destroy long-range Néel order and show power law decay in spin-spin correlation. This model can be exactly solved using 'Bethe ansatz', where gs energy is given by $\epsilon_0 = \frac{NJ}{4} - JNln2$ [91]. Using the Bethe ansatz, des-Cloizeaux and Pearson obtained a dispersion relation $\omega_k = \frac{\pi}{2}J|\sin k|$ [92]. The excitations associated with this dispersion are usually called spinons. Spinons are spin-1/2 objects and combination of two spinons gives low-lying excitations [93].
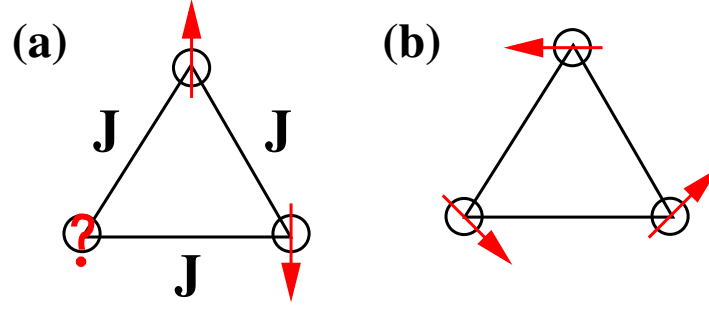
Figure 1.2: (a) Frustration on a triangle with AFM nearest neighbor interactions (b) classical ground state: the angle between two nearest neighbor spins is 120°

The gs is in singlet state ($S_{tot}^z = 0$) and the lowest excited state is the triplet state ($S_{tot}^z = 1$) for 1D $S = 1/2$ AFM chain. The singlet-triplet gap, alternatively called spin gap, vanishes in the thermodynamic limit [94]. The gs spin correlation function decays as $(-1)^r/r$ for the isotropic 1D AFM Heisenberg chain [95].

In the anisotropic limit i.e, $J_x = J_y \neq J_z$, the Heisenberg model is called XXZ model. For $J_x = J_y = 1$ and $J_z < -1$, the XXZ chain shows FM gs, whereas for $J_z > 1$ this model shows AFM ordered gs. In the limit, $-1 < J_z < 1$, XXZ chain behaves like 1D XY model [96].

The frustration in the low-dimensional spin models makes the physics more interesting. The concept of frustration arises in the system where no spin configurations can satisfy all the interactions between every pair of spins simultaneously. There are two types of frustration; one is induced due to the geometry of the system and the other one appears due to the presence of competing exchange interactions in the system. An example of geometrical frustration is a triangular lattice with nearest neighbor AFM interaction J, as shown in Fig. 1.2(a). All the spins on a triangle can not be antiparallel with both their neighbors simultaneously. If we treat these spins classically, then the minimum energy can be achieved with the spin configuration where each spin is at 120° angle with respect to its nearest neighbors, as shown in Fig. 1.2(b). The quantum phases proposed to arise in this system are discussed in the Sec. 1.6. On the other hand, the interaction induced frustration can be investigated in a linear spin-1/2 chain with nearest neighbor (nn) J_1 and next nearest neighbor (nnn) J_2 interactions. The system is frustrated for AFM J_2 interaction irrespective of the nature of J_1.

The $J_1 - J_2$ model has been studied extensively in the last couple of decades. The Heisenberg Hamiltonian of this model can be written as

$$H = J_1 \sum_i \mathbf{S}_i \cdot \mathbf{S}_{i+1} + J_2 \sum_i \mathbf{S}_i \cdot \mathbf{S}_{i+2}. \tag{1.5}$$

This model shows the existence of various exotic phases in different $\alpha = J_2/J_1$ limits. For AFM J_1 and J_2, the system shows a quantum phase transition from a gapless AFM phase to a gapped dimer phase at the critical point $\alpha_c = 0.2411$. This transition point has been shown by Okamoto and Nomura considering the crossover between energy gaps where the first excited state goes from triplet to singlet state [97]. On the other hand, Bosonization approach gives this quantum phase transition point at $\alpha_c = 1/6$ [98]. The exact dimer state is found at the Majumder-Ghosh point i.e., $\alpha = 1/2$ [99, 100]. The Majumder-Ghosh model (i.e., $J_1 - J_2$ model at $\alpha = 1/2$) shows the gs is doubly degenerate with the singlet gs energy $\epsilon_0 = -\frac{3}{8}J_1N$. The wave function of an exact dimer phase can be represented as a product of singlet pairs and this phase has an excitation gap to the first excited state which is the triplet state. The presence of dimerization is found in a broad region i.e., $\alpha_c < \alpha < 2.5$ [101]. The largest dimerization occurs approximately at $\alpha = 0.5781$. The incommensurate gapped spiral phase appears for approximately $0.5 < \alpha < 2.5$. The spin correlation in the incommensurate phase decays following $e^{-r/\xi}r^{-\frac{1}{2}}$, where ξ is correlation length. The exact upper limit of α for incommensurate phase is found at $1/\alpha = 0.44$ by exact diagonalization (ED) and DMRG calculations, and for $1/\alpha < 0.44$ the system behaves like two independent (decoupled) Heisenberg AFM chains with the structure factor $S(q)$ diverging at wave vector $q = \pi/2$, whereas below the critical point α_c, $S(q)$ diverges at $q = \pi$ [102, 103].

The $J_1 - J_2$ model with FM J_1 and AFM J_2 shows the presence of gapless FM phase at low $\alpha = J_2/|J_1|$. The level crossing between fully polarized FM state and singlet state occurs at $\alpha = 0.25$ and in this point gs is doubly degenerate with the energy $\epsilon_0 = -\frac{3}{16}N|J_1|$ [104, 105]. For $0.25 < \alpha < 0.67$, incommensurate spiral spin order appears with periodicity $2\pi/q$. The pitch angle lies between $0 < q < \pi/2$ in this phase [102, 103]. In incommensurate phase, spin gap for FM J_1 - AFM J_2 chain is finite but very small compared to that in AFM J_1 - AFM J_2. Hence, dimerization and incommensurate spiral order coexist for this model also [106]. The highest spin gap appears at $\alpha \approx 0.6$. For $\alpha > 0.67$, the system behaves like

spin−1/2   spin−1/2
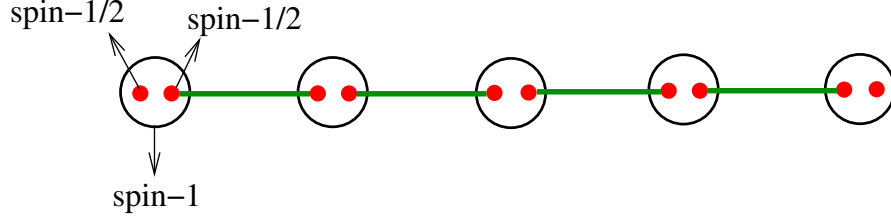
spin−1

Figure 1.3: Valance bond solid state in spin-1: Every $S = 1$ spin consists of two $S = 1/2$ spins and each spin-1/2 forms singlet bond with another spin-1/2 on neighboring $S = 1$ site

two decoupled gapless AFM chain with $q = \frac{\pi}{2}$. This model has attracted much attention also for manifesting different exotic phases like vector chiral, multipolar phases in the presence of magnetic field [107–111] or anisotropic exchange [112, 113].

The AFM Heisenberg integer and half integer spin chains behave very differently, as first discovered by Haldane [61, 114]. The gs of AFM Heisenberg integer-S chain shows a finite spin gap, whereas it is gapless for AFM Heisenberg half-integer-S chain. This finite gap for integer-S spin chain is given by $\Delta_{Haldane} = JSe^{-\pi S}$, which is known as Haldane gap [115]. Generally, the existence of a gap in a spin system is accompanied by a disordered gs. The short range correlation in the disordered gs follows $C(r) \propto e^{-r/\xi}$. The numerical renormalization group study finds the $\xi \approx 6.03$ for AFM Heisenberg $S = 1$ chain [75]. The same study shows the gs energy per site is $\epsilon_0 \approx -1.40$ and the Haldane gap is $\Delta \approx 0.41$. The Haldane chain shows an important property called string order. This can be measured from the relation

$$O^\alpha(i, i+r) = < S_i^\alpha e^{i\pi \sum_{j=i+1}^{i+r-1} S_j^\alpha} S_{i+r}^\alpha >, \qquad \alpha = x, y, z \tag{1.6}$$

as $r \to \infty$. The finite value of this order parameter indicates that after removing all the sites with $S^z = 0$, spin-1 sites with $S^z = +1$ and $S^z = -1$ locate at alternate positions along the chain between ith and $i + r$th spins. This hidden order creates Néel order in spin-1 chain. The value of string order in spin-1 chain is approximately 0.37 [75]. Moreover, open ended spin-1 chain addresses the presence of effective $S = 1/2$ spins at each end of the chain. This property can be explained easily using valance bond state (VBS) picture, as shown in Fig. 1.3. A VBS can be written as the product of the singlet states produced by two $S = 1/2$ spins [116]. The notion of valance bonds can also be extended to higher spins. The gs of

spin-1 Heisenberg chain is constructed using valance bonds by Affleck, Kennedy, Lied and Tasaki (AKLT) [117]. Each $S = 1$ spin can be considered as a combination of two $S = 1/2$ spins. In the VBS state one spin-1/2 of the pair on a site is linked to one of the spin-1/2 pair on the nearest neighbor site with a singlet bond, as shown in Fig. 1.3. If all the spins are connected to its nearest neighbors in this manner, then there will always be unpaired spin-1/2 left at the each end of a spin-1 chain with open boundary condition. These extra $S = 1/2$ spins form the edge modes in the gs which is four-fold degenerate. AKLT model captures all the properties of the Haldane phase. The behavior of higher S has been also explained implementing the VBS concept [118].

The studies on mixed spin chains containing two kinds of spins (S_1, S_2) situated at alternative positions have been done extensively. According to Lieb-Mattis theorem [119], the alternating or mixed spin chains exhibit the ferrimagnetic ground state with total spin $S_{tot} = N(S_1 - S_2)$, where N is the number of unit cells. The linearized spin wave theory (LWST) and DMRG calculations show that the correlation length in spin correlation reduces to 1.44 for a mixed spin chain with $S_1 = 1$ and $S_2 = 1/2$ [120]. The frustration arisen due to the inclusion of NNN interaction in a mixed spin chain provides quantum phase transition from ferromagnetic state to singlet state as predicted by Ivanov et al. using LSWT and DMRG calculations [121].

1.5 QUASI-ONE DIMENSIONAL SPIN SYSTEMS: SPIN LADDERS

Now let us make a brief review on quasi-1D spin systems. The frustrated spin chains with anisotropy and alternating exchange interactions, spin ladders with even or odd numbers of legs are generally considered in this class of spin systems. Spin ladders having two or more spin chains form a bridge between one- and two-dimensional systems and thus play an important role to understand many interesting phenomena in the crossover between 1D and 2D systems. The Heisenberg Hamiltonian of a 2-leg ladder is written as

$$H = \sum_i \sum_{l=1,2} J_L \mathbf{S}_{i,l} \cdot \mathbf{S}_{i+1,l} + \sum_i J_R \mathbf{S}_{i,1} \cdot \mathbf{S}_{i,2}, \tag{1.7}$$

with exchange couplings J_L along the legs and J_R on rungs. i and l represent spin and leg indices, respectively. The gs of spin-1/2 ladder with AFM J_L and J_R is a singlet gs with short range spin correlation and have finite singlet-triplet gap. The gs is a spin liquid state. In $J_R/J_L = 0$ limit, a 2-leg AFM ladder behaves like two decoupled AFM Heisenberg chains which follow power law decaying spin correlation on each leg and zero spin gap. For $J_L = J_R = J > 0$, correlation length in the gs is $\xi \approx 3.19$, and singlet-triplet energy gap $\Delta \approx 0.504J$ obtained from the DMRG study [122]. It is predicted that Δ vanishes only for $J_R/J_L = 0$ [44]. $\Delta > 0$ for any finite value of J_R. At strong $J_R/J_L >> 1$ limit, the ladder acts like a system of decoupled rung singlet dimers with excitation gap $\Delta_{dimer} = J_R$. On increasing the number of legs, a dramatic difference is found between the gs properties of an even and an odd-leg ladder. While ladders with even number of legs possess spin gap and exponential decay of spin correlation, the ladders with odd number of legs show gapless behavior with spin correlation following a power law [44]. The properties of a $S = 1/2$ odd-leg ladder is similar to a $S = 1/2$ AFM Heisenberg chain, whereas the properties exhibited by a $S = 1/2$ even-leg ladder is like that in $S = 1$ AFM Heisenberg chain. Using the resonating valence bond state formalism, the presence of spin-1/2 defects can be shown at the end of an even-leg ladder and this is very similar to the effective spin-1/2 edge modes at the ends of an open $S = 1$ chain [123]. The spin gap reduces on increasing the number of legs in even-leg ladder system and vanishes as the system approaches 2-dimension. Furthermore, the anisotropic AFM XXZ ladder has been studied extensively and phase diagrams are constructed in different anisotropy limits [124–126].

Ladders with AFM J_L and FM J_R undergo a transition between decoupled phase in which the system behaves like two decoupled AFM $S = 1/2$ chains, and the Haldane phase where the system behaves effectively as a $S = 1$ AFM Heisenberg chain. At large $|J_R|/J_L$ two spins along a rung form triplet and thus this spin pair acts effectively as a spin-1. Numerical diagonalization and projector Monte Carlo study by Hida shows that the gap for $|J_R|/J_L < 0.6$ is small, and the critical transition point is proposed to be around $|J_R|/J_L \approx 0.6$ above which Haldane gap appears [127]. Moreover, the phase between the decoupled (gapless) and the Haldane (gapped) phases in the same system with anisotropy along the legs is studied using non-linear σ model [128]. It is shown that the decoupled phase exists only
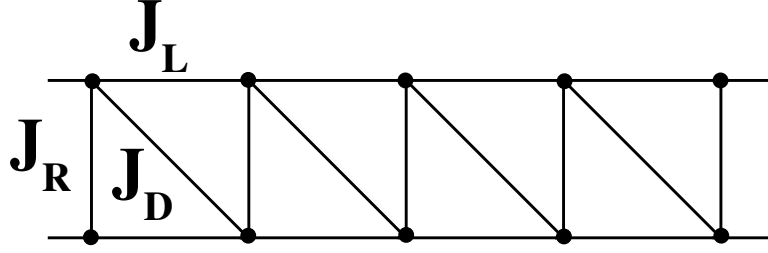
Figure 1.4: Ladder structure with single plaquette diagonal: this reduces to normal ladder when $J_D = 0$ and zigzag ladder when $J_R = J_D$.

for $|J_R|/J_L = 0$ in the isotropic case. The gs phase diagram for XXZ ladder model has been constructed in the intra-chain anisotropy and FM rung coupling plane using DMRG study by Narishima et al. [129].

The $S = 1/2$ FM J_L and AFM J_R ladder model has been studied numerically by Roji and Miyashita [130]. When $J_R = 0$, FM LRO is developed along each chain and rung dimers are formed for large J_R. Any finite J_R opens a gap which is shown both analytically [126, 131] and numerically [130]. This ladder model in the isotropic limit does not show any transition, but in the presence of a finite easy-axis anisotropy along legs, transition between FM and dimer phases can be observed. A rich phase diagram for this ladder has been constructed by different groups in various anisotropy limits [131, 132].

In the above mentioned ladder models, a gap is always generated due to the presence of any arbitrarily small AFM or FM rung coupling. The relation between the ladder gap and the Haldane gap can be understood by string order parameter. The concept of string order given in Eq. 1.6 can be extended to $S = 1/2$ ladders by considering composite spin-1 units where each unit is made up of two $S = 1/2$ spins, both located along a rung or a diagonal plaquette. It is found that gapped ladders possess finite values of string order [133]. The gs phases of ladders with single diagonal as shown in Fig. 1.4 or both diagonal interactions have been also explained using the idea of string order parameter. When rung coupling is large, singlet or triplet dimers are formed along rungs of the ladder for AFM or FM rung coupling, respectively. Interacting triplet rung dimers show Haldane gap like $S = 1$ Heisenberg chain. On the other hand, dimer gap for interacting rung singlets evolves to the Haldane gap when two neighboring dimers interact with each other through a plaquette diagonal FM coupling and form a composite spin $S = 1$ unit along the diagonal. Recent DMRG study of FM J_1 -
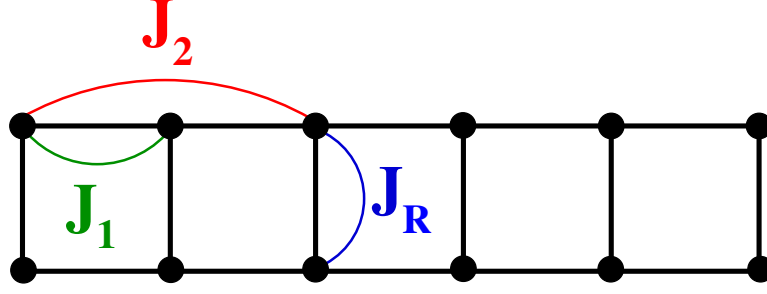
Figure 1.5: Two interacting $J_1 - J_2$ chains through rung coupling J_R.

AFM J_2 zigzag ladder ($J_R = J_D = J_1$ and $J_L = J_2$ in Fig. 1.4), alternatively called $J_1 - J_2$ chain, reveals the coexistence of spin-singlet dimer order between third neighbor sites and string order which is maximum at around $J_2/|J_1| \approx 0.55$ [106].

Several works on the spin-1/2 ladder model with two frustrated $J_1 - J_2$ legs, as shown in Fig. 1.5, display various kinds of dimer or gapped phases in different interaction limits [134–136]. For AFM J_1, J_2 and J_R, the phase diagram presents two kind of phases; one is called rung singlet (RS) and another one is columnar dimer (CD) [134, 135]. In the RS phase, singlets are formed along the rungs due to strong antiferromagnetic correlations along rung bonds, as shown in Fig. 1.6(a). Here the gs is non-degenerate and it has finite triplet excitation gap. The properties of the CD phase are similar to the dimers that appear in a $J_1 - J_2$ model. The singlet dimers are formed along the legs for the CD phase, as shown in Fig. 1.6(b). At the MG point this phase has degenerate gs. The transition points between the RS and CD phases can be determined by computing dimer order parameter defined on leg l around site i by

$$D_{i,l} = < \mathbf{S}_{i,l} \cdot \mathbf{S}_{i+1,l} > - < \mathbf{S}_{i-1,l} \cdot \mathbf{S}_{i,l} > . \tag{1.8}$$

In the thermodynamic limit, the dimer order parameter is zero in the RS phase and finite in the CD phase. In the RS phase both commensurate and incommensurate nature of spin correlation can be noticed in smaller J_2/J_1 and larger J_2/J_1 limits, respectively. The phase diagram for the same model is extended for FM J_R in ref. [135]. They have found three kinds of phases; staggered dimer (SD) in small $|J_R|/J_1$ limit, and in large $|J_R|/J_1$ limit Haldane and NNN Haldane phases for small J_2/J_1 and large J_2/J_1, respectively. In the SD phase dimers along one leg is shifted by one bond with respect to the other leg as shown in Fig. 1.6(c). Two
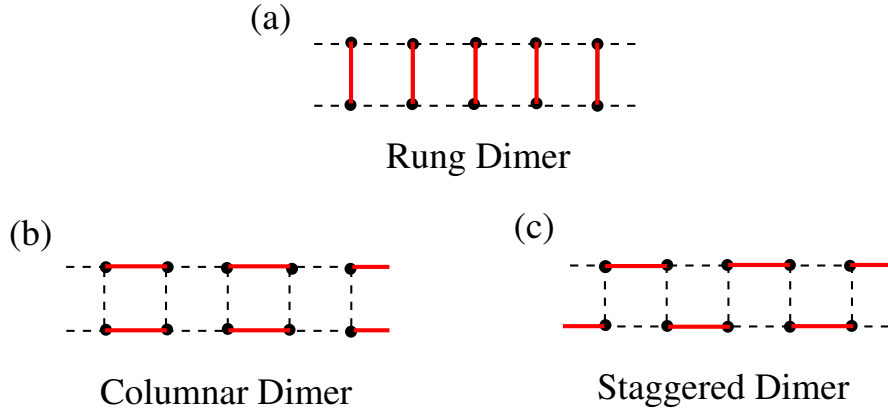
Figure 1.6: Some special types of Valance bond solid states: (a) Rung Dimer (b) Columnar Dimer and (c) Staggered Dimer are formed in a ladder. Dashed black lines represent legs and rungs of the ladder and thick red solid lines represent dimers.

spins on a rung remain parallel for both the Haldane phase and the NNN Haldane phase. The difference between these two phases is singlet dimers that are formed on alternative NN bonds and NNN bonds along the legs in the Haldane phase and the NNN Haldane phase, respectively. The influence of inter-chain coupling on the phase boundary between FM and incommensurate spiral gs in a coupled FM J_1 - AFM J_2 chains are investigated in ref. [137]. There are more types of ladder models which are investigated quite extensively, like ladders with alternative rung exchanges [138], with diagonal exchanges [139–141], with different interactions on two legs [142, 143] etc.

1.6 TWO DIMENSIONAL SPIN SYSTEMS

The two-dimensional magnets has been investigated over the last couple of decades with the inspiring initial work on 2D Heisenberg antiferromagnetic (HAF) square lattice by P. W. Anderson [86]. Though 2D systems lack exact solutions, some ideas about the gs and the excited state properties of these systems can be obtained by various analytical techniques like spin wave theory, renormalization group method, Schwinger boson mean field theory, some semi-anlytical techniques like series expansions, variational theory, and numerical techniques like exact diagonalization, quantum Monte Carlo etc. After rigorous studies on 2D HAF square lattice, it is now clear that the effect of quantum fluctuations is not strong enough to destroy the Néel long-range order in this lattice geometry [144]. However, the ordered state

disappears for any non-zero temperature as suggested by the Mermin Wagner theorem. P. W. Anderson and Fazekas first introduced the idea of resonating valence bond states, a new type of state for the 2D triangular lattice [145, 146], and this gs is very different from the classical three-sublattice Néel state where spins from different sublattices are in mutual angle of $120°$. Several works found that this lattice structure has LRO in the gs [147–150]. On the other hand, the gs in a 2D HAF kogome lattice is highly disordered due to the presence of strong quantum fluctuations [151, 152]. The HAF Honeycomb lattice are expected to have more quantum fluctuation than that in a HAF square lattice, but it still gives a finite Néel order parameter [153, 154]. The studies on a trellis lattice offer an opportunity to understand the effect of inter-ladder or inter-chain couplings [155, 156]. The presence of anisotropy or competition between different kinds of exchange couplings provides exotic phase diagrams for all these 2D lattices. Although there exist several theoretical and numerical studies on 2D lattices, the gs properties are far from being well understood in most of these lattices in various interaction limits due to the lack of appropriate theoretical framework and also efficient numerical methods to handle the large degrees of freedom involved in these 2D systems. As the 2D models are out of consideration for my thesis work, the detailed review on 2D lattices are not presented here.

The outline of the thesis is given in the following section.

1.6.1   *Outline of the thesis*

The thesis is organized in the following way.

In chapter 2, we describe the numerical methods i.e., exact diagonalization and density matrix renormalization group methods. These two numerical methods have been used to solve all the problems in this thesis.

In chapter 3, we propose a new DMRG algorithm which gives accurate results for 1D system with periodic boundary condition. We compare our results with recently developed matrix product state algorithm.

In chapter 4, we consider two-leg spin-1/2 ladder systems consisting of a ferromagnetic leg and an antiferromagnetic leg which interact through antiferromagnetic couplings with

each other. Two types of ladder geometries are studied here; zigzag and normal ladder. We predict the possible gs phases arising due to the frustration in these systems. We have also performed perturbation theory calculation at high rung interaction limit.

In chapter 5, we constructed the ground state phase diagram for a trellis ladder spin-1/2 model. The phase diagram is plotted based on pitch angle and correlation length obtained from spin-spin correlation. We have also fitted the experimental data of the trellis lattice compound CaV_2O_5 with our numerical data. We have found phase boundary both by linear spin wave analysis and DMRG calculations.

In chapter 6, a mixed spin ladder system made up of spin-1 and spin-1/2 legs is considered. We study the effect of inter-leg coupling on the energy gap, spin density and spin correlation of individual legs. The phase boundary between Ferrimagnetic to non-magnetic ground states is obtained in the presence of alternating dimerized zigzag bonds between two legs.

This thesis is concluded with necessary remarks and discussions in chapter 7.

NUMERICAL METHODS

The theoretical prediction of accurate solutions of a strongly correlated many body quantum system is one of the most challenging job in condensed matter physics. The many body problem is tractable analytically only in non-interacting or mean field limit. However, exact analytical solution is obtained by Bethe Ansatz method [91] for 1D isotropic Heisenberg model, whereas the 1D Hubbard model has been exactly solved by Lieb and Wu [22]. Most of the many body models are handled by approximated analytical methods like spin wave analysis [70], renormalization group method [72, 73], Schwinger boson mean field theory [71], field theoretical methods like bosonization [74], semi-classical non linear σ-model [61] etc. However, in some cases there are numerical methods which may give more reliable results than the analytical predictions. Nevertheless obtaining accurate solutions is quite challenging due the exponential growth of Hilbert space with the system size. If each individual site has m degrees of freedom then total number of degrees of freedom required is m^N for N sites. Therefore, the computational cost increases exponentially with increasing N.

For a spin-1/2 system, each site has two possible spin configurations; either $|\uparrow\rangle$ or $|\downarrow\rangle$, whereas each site on a fermionic system where both charge and spin degrees of freedom are involved, has four possible electronic configurations which are; empty site $|0\rangle$, singly occupied site $|\uparrow\rangle$ or $|\downarrow\rangle$ and doubly occupied site $|\uparrow\downarrow\rangle$. Hence, the degrees of freedom are 4^N and 2^N for fermionic system and spin-1/2 system, respectively, with size N. Exact diagonalization (ED) is the simplest method to obtain exact numerical results, but it is limited to small system size due to exponentially increasing dimension of Hamiltonian matrix with system size. To solve large system, various numerical algorithms like quantum Monte Carlo

(QMC) [78], numerical renormalization group (NRG) [75], density matrix renormalization group (DMRG) [76, 77] etc. are developed, and each technique has its own limitation based on the approximations considered in it. In this thesis, some quasi-1D spin ladder models are considered where ED is used to solve small system, and DMRG method for large system. Therefore, ED and DMRG methods are discussed briefly in this chapter.

2.1 EXACT DIAGONALIZATION METHOD

The eigenvalues and eigenvectors of a quantum many body model Hamiltonian can be obtained by exactly diagonalizing the Hamiltonian. ED method consists of three steps; 1) construction of the basis states 2) formation of Hamiltonian matrix in that basis states, and 3) diagonalization of the Hamiltonian matrix. If { $|\Psi_i\rangle$, $i = 1, n_b$ } is the basis set, then $\langle\Psi_i| H |\Psi_j\rangle = H_{ij}$ are matrix elements of the Hamiltonian. The dimension of Hamiltonian matrix is $n_b \times n_b$ for a system with basis size n_b. Most of the matrix elements of a Hamiltonian with short range interaction are zero. Hence only nonzero elements can be stored in sparse matrix form which requires storage only of order $O(n_b)$. Moreover, most of the Hamiltonians have symmetries which reduce the Hamiltonians to block diagonal forms. Now the individual blocks appeared in the matrix can be diagonalized independently at a much less computational cost. If Hamiltonian remains invariant after going through some symmetry transformation σ, then $[H, \sigma] = 0$. It means that H and σ have common eigenfunctions.

Both S^2 and S^z operators commute with Heisenberg Hamiltonian and have eigenvalues $S(S + 1)$ and m_s, respectively, where $m_s \in \{-NS, -NS + 1, ..., NS\}$ for a spin-S system with number of spins N. In these different S^z sectors the Hamiltonian Matrix is block diagonal. For a $S = 1/2$ spin system the number of basis states goes as $^NC_{N/2}$, $^NC_{N/2-1}$, $^NC_{N/2-2}$,...,and 1 for $m_s = 0, 1, 2, ...,$ and $N/2$, respectively. The frustrated spin systems are non-trivial due to the presence of large degeneracies in the ground state (gs) and low-lying exsited states. As a result the convergency of energy in the diagonalization process becomes slower or in some cases, energy does not even converge. The symmetry operations like translational, spin-parity, inversion etc. are used to separate out the degenerate states in the different symmetry subspaces. The translational operation moves each spin to the next spin position and Heisen-

berg Hamiltonian with periodic boundary condition remains invariant under this transformation. The spin-parity operator flips all the spins which keep the Hamiltonian invariant and it is valid only in $m_s = 0$ sector. The inversion symmetry corresponds to a rotation of the whole system by an angle π about an axis passing through 1st and $(N/2 + 1)$th spins of a system with periodic boundary condition. The matrix operation $\tilde{H} = U^\dagger H U$, where U is an unitary symmetry operator of size $n_b \times m$ ($n_b > m$), leads the Hamiltonian in different symmetry subspaces. After the rotation of Hilbert space in these symmetry subspaces the dimension of the Hamiltonian $\tilde{H}$ reduces to $m \times m$.

The computational cost required for the full digonalizaton of a Hamiltonian goes as $O_{(n_b^3)}$, and we can get full spectrum of a system with the size hardly up to $N \approx 24$ for a spin-1/2 system diagonalized using more than one symmetries. If we calculate the eigenvectors and eigenvalues only for the gs and a few number of low-lying excited states then the computational cost goes as $O_{(n_b^2)}$. The computational cost becomes worse for larger spin. Even for evaluating a few low-lying states of a matrix, a considerable computational effort is required. There are many algorithms like the Lanczos [157, 158], modified Lanczos [159] and Davidson methods [160, 161] to find some low-lying energy states. One of the most promising algorithm is Davidson algorithm for dealing with low-lying eigenstates of a large symmetric and sparse matrix. In this thesis, we have used an extension of the Davidson algorithm to solve non-symmetric matrix, and it is proposed by Retrrup [162]. The brief outline of the algorithm is given below.

Let us consider H is a given large sparse Hamiltonian matrix of order $n_b \times n_b$. We consider a set of l orthonormal guess vectors $\{\mathbf{v_i} : i = 1, ..., l\}$ and construct a small $l \times l$ matrix $h^{(l)}$, whose components are given by $h_{ij}^{(l)} = \langle \mathbf{v_i} | H | \mathbf{v_j} \rangle$. We diagonalize this small matrix using standard exact diagonalization routines,

$$h^{(l)} \mathbf{a}_k^{(l)} = \lambda_k \mathbf{a}_k^{(l)}, \qquad k = 1, ..., m. \tag{2.1}$$

Here $\mathbf{a}_k^{(l)}$ are the eigenvectors of $h^{(l)}$ with lowest m eigenvalues λ_k. Now we choose guess eigenvectors for the large matrix H, as the linear combination of $\mathbf{v_i}$ with components of $\mathbf{a}_k^{(l)}$ eigenvectors as coefficients.

$$\mathbf{C}_k^{(l)} = \sum_{i=1}^{l} a_k^{(l)}(i)\mathbf{v_i}, \tag{2.2}$$

where $a_k^{(l)}(i)$ is the ith component of the kth eigenvector of the small matrix $h^{(l)}$. Now we construct i^{th} component of correction vector $\mathbf{P}_k^{(l)}$ as

$$P_k^{(l)}(i) = \frac{R_k^{(l)}(i)}{\lambda_k^{(l)} - H_{ii}}, \tag{2.3}$$

with i^{th} component of the residual vector $\mathbf{R}_k^{(l)}$ for the kth eigenvalue, and the residual vector is given by

$$\mathbf{R}_k^{(l)} = (H - \lambda_k^{(l)}I)\mathbf{C}_k^{(l)}, \tag{2.4}$$

where I is the unit matrix. Now we expand the initial space $\{\mathbf{v_i} : i = 1, ..., l\}$ with a normalized vector $\mathbf{v}_{l+1}$ which is obtained from Gram-Schmidt orthogonalization of $\mathbf{P}_k^{(1)}$ to the set of vectors $\{\mathbf{v}_i : i = 1, ..., l\}$ i.e.,

$$\mathbf{v}'_{l+1} = \mathbf{P}_k^{(l)} - \sum_{i=1}^{l}(\mathbf{P}_k^{(l)}.\mathbf{v}_i)\mathbf{v}_i, \qquad \mathbf{v}_{l+1} = \frac{\mathbf{v}'_{l+1}}{||\mathbf{v}'_{l+1}||}, \tag{2.5}$$

The small matrix $h^{(l)}$ is now augmented to the matrix $h^{(l+1)}$ by adding new row and new column. Next, we repeated the procedure starting with solving the Eq. 2.1 with $l+1$ replacing l. The process is stopped until the dimensionality of the small matrix $h^{(l)}$ exceeds a threshold value and is restarted with the initial subspace spanned by the approximated m eigenvectors taken in Eq. 2.2. The iteration is finished when the eigenvalue converges within a chosen accuracy.

The computational cost in the above mentioned method goes as $O(n_b^2)$, therefore, it is difficult to diagonalize the Hamiltonian matrix for large system with ED. However, one can calculate gs and a few low-lying energy states of a spin-1/2 system with size up to $N \approx$

36 using underlying symmetries of the system. To solve larger systems many approximate numerical techniques are proposed, and among them DMRG method is the most suitable method to handle frustrated spin systems. In this thesis, we have studied frustrated spin ladders using DMRG method. Therefore, we will now discuss this method in brief.

2.2 DENSITY MATRIX RENORMALIZATION GROUP METHOD

The Density Matrix Renormalization Group (DMRG) method was introduced by Steve White in 1992 [76, 77]. It is mainly based on mainly exact diagonalization (ED) and numerical renormalization group (NRG) ideas. The lowest energy states are usually kept in real space RG method to produce an effective Hamiltonian of reduced dimension. This method achieved a great success in explaining Kondo problem [72, 73]. However, results of RG schemes in other many body problems such as Hubbard or Heisenberg models turned out to be poor. The DMRG keeps only the most probable states instead of the lowest energy states and ends up with diagonalizing the Hamiltonian constructed in truncated Hilbert space. This process starts with a small system and then gradually increases the system size by adding few new sites at every step. Each step involves the systematic truncation of irrelevant degrees of freedom. The detailed review on DMRG method is available in refs. [163–165].

This method is able to handle spin-1/2 1D and quasi 1D systems and provides very accurate gs energies and spin gaps for the same. A detailed study of spin correlation, spin gap, low energy spectrum, the presence of edge modes of a spin-1 chain has been performed using DMRG method in refs. [75, 166, 167]. Similar calculations have been executed for higher spin systems like $S = 3/2$, $S = 2$ Heisenberg chains [168, 169]. Several spin ladder models have been considered in refs. [122, 123]. The rigorous studies of the effect of frustrations in several spin systems e.g, zigzag spin chains have been done using this method [123, 170, 171]. The DMRG algorithm is also extended for 2D quantum systems but the result is poorer than that in 1D. Among the 2D systems, square, triangular, kagome lattices are examined using this algorithm [172, 173]. Not only for Heisenberg spin models this method is quite successful to solve low dimensional Hubbard model, t-J model, Pariser-Parr-Pople model [31, 174–176], 2D or 3D classical models and many others [177]. It is also used to calculate dynam-

ical properties, thermodynamic properties of low dimensional systems [178] and has been extended recently to solve time-dependent quantum systems [179].

The DMRG method consists of two algorithms; one is infinite-size DMRG algorithm which is followed by the other algorithm called finite-size DMRG algorithm. In Infinite-size DMRG algorithm, the system size is increased by adding new sites at each iteration until the desired length is reached. The algorithm of the infinite DMRG for a linear spin chain is described below.

We start with a small system size; let us say four sites as shown in Fig. 2.1(a). This system is divided into four blocks where first one site form left block L, last one site form right block R and there are one new left site l and one new right site r in between them. The full composite system is called superblock and its Hamiltonian can be written in the form $H = H_L \otimes H_l \otimes H_r \otimes H_R$. Now we can divide the superblock into system i and environment j. The system in composed of left block and left new site, whereas environment is composed of right new site and right block. Now we diagonalize H to get ground state wave function which can be written in the product basis form as

$$\Psi = \sum_{<ij>} C_{ij} |i\rangle |j\rangle. \tag{2.6}$$

Here $|i\rangle$ and $|j\rangle$ represent basis states of the system and environment, respectively. Now we form the density matrix of the system. The major contribution in the expectation value of any observable of the system comes from the most probable eigenstates of the density matrix of the system. Therefore we keep the eigenstates with largest eigenvalues of density matrix instead of keeping the eigenstates with lowest eigenenergies of the Hamiltonian in the system. The expectation value of any operator A acting on the system can be written as

$$\langle A \rangle = \langle \Psi | A | \Psi \rangle = \sum_{<iji'j'>} C_{ij}^\star C_{i'j'} \langle j | \langle i | A | i' \rangle | j' \rangle$$

$$= \sum_{<iji'>} C_{ij}^\star C_{i'j} \langle i | A | i' \rangle = \sum_{<ii'>} \rho_{ii'} \langle i | A | i' \rangle,$$

where

$$\rho_{ii'} = \sum_j C_{ij}^{\star} C_{i'j} \tag{2.7}$$

represents the elements of density matrix of the system [180]. In terms of density matrix ρ,

$$\langle A \rangle = Tr(\rho A) = \sum_{\alpha} \epsilon_{\alpha} \langle \alpha | A | \alpha \rangle, \tag{2.8}$$

where $|\alpha\rangle$ and ϵ_{α} are the eigenvector and eigenvalue of the matrix ρ. If ϵ_{α} for $\alpha > m$ is very small than summation over α in Eq. 2.8 can be kept only upto $\alpha = m$, which can give accurate expectation value. DMRG uses similar concept for renormalization.

Now ρ matrix is diagonalized and we keep m eigenstates with highest eigenvalues. These m number of states have highest weight in any information related to the system block. If the ρ matrix has dimension $M \times M$, then the reduced density matrix (ρ') has dimension $M \times m$. The reduction of dimension is necessary only when $M > m$. The summation over all the eigenvalues of the density matrix should be equal to unity. The accuracy of the calculation can be measured by truncation error which is given by the sum of all the eigenvalues of discarded eigenvectors of density matrix. If system and environment are symmetric to each other then we only need to calculate the density matrix of one block and do all the other operations only for one of them. The next step is to renormalize all operators involved in the system block to truncated density matrix basis space. The renormalized Hamiltonian and operators related to system block can be written in the form

$$\tilde{H}_i = \rho'^{\dagger} H_i \rho', \quad \tilde{O}_i = \rho'^{\dagger} O_i \rho', \tag{2.9}$$

where, H_i and O_i are the Hamiltonian and the operators of the system. The dimension of the remormalized Hamiltonian $\tilde{H}_i$ is reduced to $m \times m$. The renormalized Hamitonian $\tilde{H}_j$ and operators $\tilde{O}_j$ of environment block are same as $\tilde{H}_i$ and $\tilde{O}_j$, respectively. Now we add two new sites in between system and environment blocks as shown in Fig. 2.1(b), and the whole composite system forms the new superblock. Again we divide the new superblock in two symmetric blocks. If the Hilbert space dimension corresponding to each site is d then
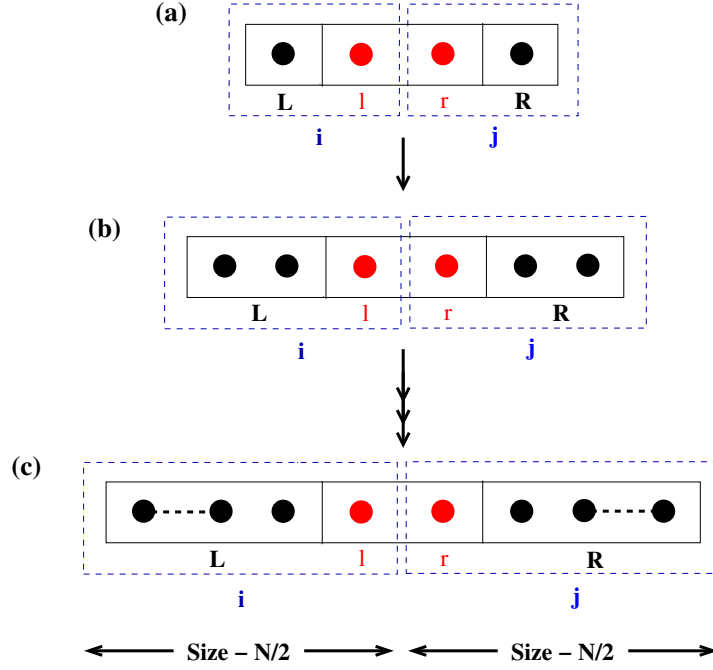
Figure 2.1: Schematic representation of the infinite DMRG algorithm steps for a 1D chain. The black and red filled circles are old and new sites, respectively. The black filled circles under a blue dashed box form left block (system block of previous step) or right block (environment block of previous step). The blue dashed boxes represent system and environment blocks.

the dimension of Hamiltonian of the new system block will be $d \times m$. The new system block Hamiltonian is obtained as

$$H'_i = \tilde{H}_i \otimes I_d + \tilde{S}^z_L \otimes S^z_l + \frac{1}{2}\left(\tilde{S}^+_L \otimes S^-_l + \tilde{S}^-_L \otimes S^+_l\right), \tag{2.10}$$

where I_d is unit matrix of dimension d, $\tilde{S}_L$ is spin matrix for the site situated at the right end of the left block or old system block and S_l represents the spin matrix for new site. The new environment block Hamiltonian H'_j is same as H'_i. Now combining the new system and environment blocks, we get the Hamiltonian for the new superblock as

$$\tilde{H} = H'_i \otimes I_{m \times d} + I_{m \times d} \otimes H'_j + I_m \otimes S^z_l \otimes S^z_r \otimes I_m$$
$$+ \frac{1}{2}I_m \otimes S^+_l \otimes S^-_r \otimes I_m + \frac{1}{2}I_m \otimes S^-_l \otimes S^+_r \otimes I_m, \tag{2.11}$$

where, S_r represents the spin matrix for the new site in environment block. Now we diagonalize the new superblock Hamiltonian and iterate all the steps of truncation until the desired length is achieved. Let us give a brief outline of the algorithm following the schematic Fig. 2.1.

1. We start with a superblock with four site.

2. Find the gs eigenenergy and eigenvector of the superblock.

3. From the obtained eigenvector the density matrix ρ of the system block is constructed following Eq. 2.7.

4. Diagonalize ρ and keep only the m number of eigenvectors with largest eigenvalues.

5. Renormalize all the operators and the Hamiltonian for the system block in truncated density matrix basis space using Eq. 2.9.

6. Add a new site to each block and construct the superblock Hamiltonian using the effective Hamiltonian and the operators of two blocks and two new sites as in Eq. 2.11.

7. Iterate all the steps (2) to (5) until the desired system size is achieved.

During the above mentioned process, all the operators related to all the left and right blocks are stored to be used in finite-size DMRG process. To get an optimized wave function and accurate system properties, we perform finite sweeps when the desired system size N is reached in infinte-size DMRG process. The system size remains fixed to N in finite DMRG algorithm. This process involves DMRG sweeps from left-to-right and right-to-left. The finite DMRG procedure is illustrated in the schematic Fig. 2.2 and summarized below.

1. Start with the diagonalized superblock obtained at the end of the infinite-size DMRG algorithm discussed above. This superblock has equal number of sites in each block as shown in Fig. 2.2(a).

2. The left to right sweep starts with adding one new site to the left block and removing one site from the right block to keep the system size fixed as shown in Fig. 2.2(b). Now old left block and the new site form the system block or new left block.
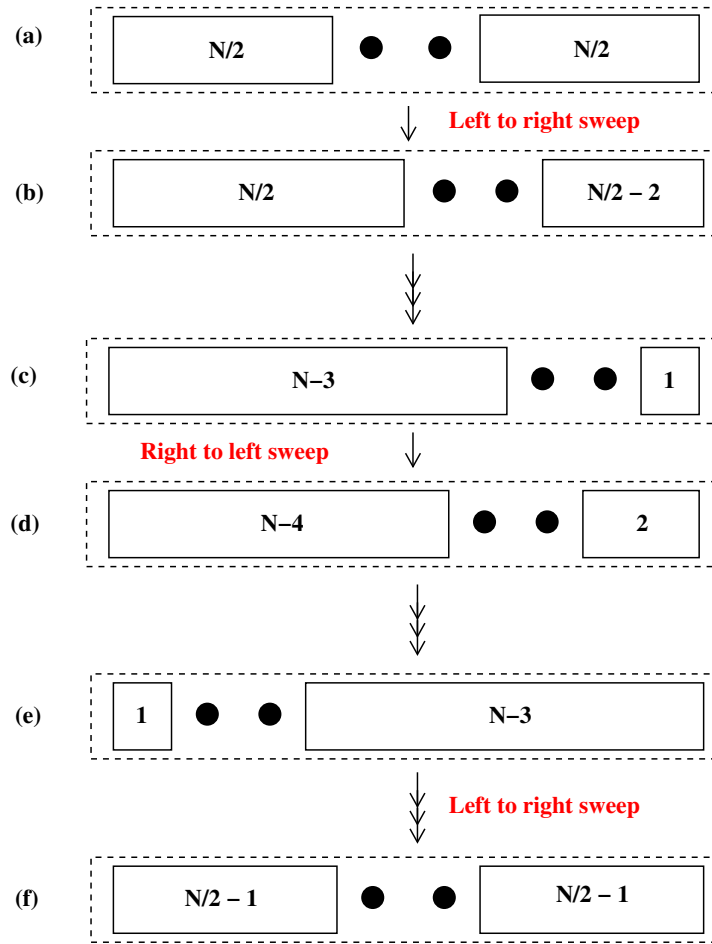
Figure 2.2: Schematic representation of the finite DMRG algorithm steps for a 1D chain. Dashed box dipicts the final system of size N coming from infinite DMRG algorithm. Filled black circles represent the new sites and solid boxes represent the left and right block of unequal lengths.

3. Diagonalize the super block Hamiltonian combining two new sites and two blocks and construct the reduced density matrix ρ' of the system block.

4. Renormalize all the operators and Hamiltonian of the system block in reduced density matrix basis space.

5. Again add one more new site to left block and shrink the right block. Repeat all steps until the right block is reduced to a single site as shown in Fig. 2.2(c).

6. Now the same process is done in right to left sweep by enlarging the right block by one site at each steps until the left block is reduced to one single site as shown in Fig. 2.2(d-e).

7. In the next step, we again start to add new sites to the left block and remove sites from the right block, and finally we reach a step where the left and the right block have the same size as shown in Fig. 2.2(f). This whole process is considered as one finite sweep.

To get optimized desired result, $5-10$ finite sweeps are sufficient in general.

The DMRG algorithm can give accurate results for a 1D systems with open boundary condition (OBC) and also does well for quasi-1D systems with OBC. However, this algorithm gives poor results for the system with periodic boundary condition (PBC). The PBC results are necessary to get rid of the boundary effects in the system. If the number of states required to get results with adequate accuracy is of the order $O(m^2)$ for OBC, then it requires the number of states of the order $O(m^4)$ for PBC to get results with same accuracy. The number of non zero elements in the Hamiltonian matrix becomes much higher in PBC due to the connection between old left and right blocks. The computational cost goes as $O(m^6)$ for PBC, whereas it is $O(m^3)$ for OBC. In conventional DMRG algorithm, the spin operators which form the superblock are involved in one time renomalization for OBC system, but in the case of PBC, at least two spin operators get renormalized multiple times. The multiple time renomalization reduces the accuracy drastically. In the first thesis work we proposed a new DMRG algorithm where new sites are added at both ends of a spin chain so that old-old block connections are removed to avoid multiple time renormalizations.

AN EFFICIENT DENSITY MATRIX RENORMALIZATION GROUP ALGORITHM FOR CHAINS WITH PERIODIC BOUNDARY CONDITION

3.1 INTRODUCTION

The quantum many body effect in the condensed matter gives rise to many exotic states such as superconductivity [181], multipolar phases [182, 183], valance bond state [184], vector chiral phase [182, 185] and topological superconductivity [186]. These effects are prominent in the one dimensional (1D) electronic systems due to the confinement of electrons. The confinement of electrons and the competition between the electron-electron repulsion and the kinetic energies of electrons produce many interesting phases like spin density wave (SDW), dimer or the bond order wave phase and charge density wave (CDW) phase in one dimensional systems [187–189]. Although, these quantum many body effects in the system are crucial for exotic phases, dealing with these systems is a challenging job because of the large degrees of freedom. The degrees of freedom increases as 2^N or 4^N for a spin-1/2 system or a fermionic system respectively.

In most of the cases, the exact solutions for these systems with a large degrees of freedom are almost impossible. Therefore, during the last three decades many numerical techniques have been developed e.g., Quantum Monte Carlo (QMC) [78], Density Functional Theory (DFT) [190], Renormalization group (RG) [191] and density matrix renormalization group (DMRG) method [76, 77]. The DMRG is a state of the art numerical technique for 1D systems with open boundary condition (OBC). However, the numerical effort to maintain the

accuracy for PBC systems becomes exponential [192, 193]. It is well known that periodic boundary condition (PBC) is essential to get rid of boundary effect of a finite open chain and also to preserve the inversion symmetry in the systems [194].

The DMRG technique is based on the systematic truncation of irrelevant degrees of freedom and has been reviewed extensively in the Ref. [192, 193]. In 1D system with OBC, the number of relevant degrees of freedom is small [192, 193]. Let us consider that for a given accuracy of the OBC system, m_{obc} number of eigenvector state of the density matrix is required, then the conventional DMRG for the PBC system requires O(m_{obc}^2) [195]. In the conventional DMRG, computational effort for the OBC systems with sparse matrices goes as O(m_{obc}^3), whereas, it goes as O(m_{obc}^6) for the PBC system [196]. The accuracy of energies for the PBC systems calculated from the conventional DMRG decreases significantly, and there is a long bond in the system which connects both the ends.

The accuracy of operators decreases with the number of renormalization, especially the raising/creation $S^+/a+$ and lowering/annihilation S^-/a^- operator of spin/fermionic systems. The conventional DMRG is solved in S^z basis, therefore the exact S^z operator remain diagonal and multiple times renormalization deteriorate the accuracy slowly, but $S^+/a+$ and S^-/a^- are off diagonal in this exact basis, therefore, the multiple time renormalization of these operators decrease the accuracy of the operators. Similar type of accuracy problem occurs for multiple time renormalized a^+ and a^- in the fermionic systems. In fact, it has been noted that accuracy of energy of a system with PBC significantly increases if the superblock is constructed with very few times renormalized operators [189]. To avoid multiple renormalization new sites are added at both the ends of the chain in such a way that only second time renormalized operators are used to construct the superblock. In this algorithm there is a connectivity between the old-old sites and their operators are renormalized; and this connectivity spoils the sparsity of the superblock Hamiltonian [189].

In this chapter[1] a new DMRG algorithm is proposed, which can be implemented upon the existing conventional DMRG code in a few hours and gives accurate results which are comparable to that of MPS algorithm. In fact this algorithm can be implemented for two

---

1 The work reported here is based on the paper "An Efficient Density Matrix Renormalization Group Algorithm for Chains with Periodic Boundary Condition", Dayasindhu Dey, Debasmita Maiti and Manoranjan Kumar, Papers in Physics **8**, 080006 (2016).

legged ladders without much effort [197]. We have studied the spectrum of density matrix of the system block, ground state energy and correlation functions of a Heisenberg anti-ferromagnetic Hamiltonian for spin-1/2 and spin-1 on a 1D chain with PBC.

This chapter is divided into five sections. The model Hamiltonian is discussed in Sec. 3.2. The new algorithm and the comparative studies of algorithm are done in Sec. 3.3. The accuracy of various quantities is studied in the Sec. 3.4. In Sec. 3.5 results and algorithm are discussed.

3.2 MODEL HAMILTONIAN

Let us consider a strongly correlated electronic system where Coulomb repulsion is dominant, therefore the charge degree of freedom gets localized, for example, Hubbard model in large U limit in a half filled band. In this limit the system becomes insulating, but the electrons can still exchange their spin. The Heisenberg model is one of the most celebrated model in this limit, and only the spin degrees of freedom are active in the model. The Heisenberg model Hamiltonian can be written as

$$H = \sum_{\langle ij \rangle} J_{ij} \mathbf{S}_i \cdot \mathbf{S}_j \tag{3.1}$$

where, J_{ij} is the anti-ferromagnetic exchange interaction between nearest neighbor spin. In the rest of the chapter J_{ij} is set to be 1.

3.3 COMPARISON OF ALGORITHMS

A ground state wavefunction calculated from the conventional DMRG can be represented in terms of the matrix product state (MPS) as shown by Ostlund and Rommer [198]. The wavefunction can be written as

$$|\psi\rangle = \sum_{n_1,n_2,\dots,n_L} \mathrm{tr}(A^1_{n_1} A^2_{n_2} \dots A^L_{n_L})|n_1, n_2, \dots, n_L\rangle, \tag{3.2}$$

where, $A^k_{n_k}$ are a set of matrices of dimension $m \times m$ for site k and with n_k degrees of freedom. The wave function $|\psi\rangle$ can be accurately found if m is sufficiently large. The expectation value of an operator O_k in the gs [196, 199] can be written as

$$\langle O_k \rangle = \text{tr} \left(\sum_{n_k, n'_k} \langle n_k | O_k | n'_k \rangle A^k_{n_k} \otimes A^k_{n'_k} \right), \tag{3.3}$$

where n_k is the local degrees of freedom of site k. The matrix A can be evaluated by using the following equations

$$H_k |\psi_k\rangle = \lambda N_k |\psi_k\rangle, \tag{3.4}$$

$$N^k = E^{k+1}_1 E^k_1 \ldots E^L_1 E^1_1 \ldots E^{k-1}_1, \tag{3.5}$$

where

$$E^k_1 = \sum_{n_k, n'_k} \langle n_k | 1 | n'_k \rangle A^k_{n_k} \otimes A^k_{n'_k}. \tag{3.6}$$

Here H_k is the effective Hamiltonian of kth site and λ is the expectation value of energy. The A matrices are evaluated at this point and the matrices are rearranged to keep the algorithm stable. The H_k and N can be calculated recursively while evaluating A of one site at a time [196]. Here, N matrices are ill conditioned and require storing approximately L^2 matrices as well as multiplication of L^2 matrices of $m \times m$ size [196] at each step. The evaluation of A and N are done for all the sites and backward and forward sweep for all the sites are executed similar to the finite system DMRG. The mathematical operations of matrices of dimension $m^2 \times m^2$ to represent the Hamiltonian cost $\sim (o)m^6$, but the special form of these matrices reduces the cost by a factor of m. Therefore, this algorithm scales as $\sim (o)m^5$ [196].

The above algorithm is extended by Verstraete et. al., for translational invariant systems [200]. Only two types of matrices A^1 and A^2 are considered [200]. Product of the two matrices can be repeated to compute N. In this algorithm only two matrices A^1 and A^2 are updated and

optimized to get the gs properties. This algorithm scales as (o)m^3, although it does not work for finite system, or systems with impurity etc. Pippan et. al. introduced another MPS based efficient algorithm for translational invariant PBC systems [196]. In the old version of MPS most of the computation cost goes in constructing the product of $m^2 \times m^2$ matrices E defined in the Eq. (3.6). The new MPS algorithm overcomes this problem by performing a SVD of the product of sufficiently large ($l \gg 1$) number of $m^2 \times m^2$ transfer matrices[196, 201]. The singular values, in general, decay very fast; therefore, only $p \, (\ll m^2)$ among m^2 singular values are significant [201]. Thus the computational cost now is reduced to (o) $p \times m^3$ [196]. However one requires $p \sim m$ to reach adequate numerical accuracy of physical measures as pointed out in the Ref. [201].

Although, the above technique is efficient and accurate, there are various reason for developing the new algorithm. First, the modified MPS works efficiently for system where the singular values of product of matrices decay exponentially and this algorithm scales as (o) pm^3 where p can vary linearly with m. Second, the implementation of the MPS based numerical technique is quite different from the conventional DMRG, and the MPS algorithm should be written from scratch. Third, many conventional numerical techniques like dynamical correction vector [202] or continued fraction [203], implementation of symmetries like parity or inversion symmetries is difficult. In this chapter we will explain a new algorithm which is very similar to the conventional DMRG technique, and also show that the new algorithm can give accuracy comparable to that of MPS based techniques. This algorithm is applied for $S = 1/2$ and $S = 1$ chains with PBC. But first, let us try to understand the algorithm before discussing the results.

In this algorithm, we will try to avoid the multiple renormalization of operators, whereas the other parts of the algorithm remain the same as the conventional DMRG. Before going to the new algorithm let us recap the conventional DMRG.

1. Start with a superblock of four sites consisting of one site for both the left and the right block and two new sites.

2. Get desired eigenvalues and eigenvectors of the superblock and construct the density matrix ρ of system which consists of the left or the right block and a new site.

3. Now construct an effective ρ' with m number of eigenvectors of ρ corresponding to m largest eigenvalues. The effective system Hamiltonian and all operators in the truncated basis are constructed using the following equations,

$$\tilde{H} = \rho'^{\dagger} H \rho'; \qquad \tilde{O} = \rho'^{\dagger} O \rho' \tag{3.7}$$

4. Superblock is constructed using the effective Hamiltonian and operators of the system block and two new sites.

5. Repeat all the steps from 2 till the desired system size is reached. The full process is called infinite DMRG.

As mentioned earlier, the conventional algorithm is excellent for 1D open chain as superblock is constructed with only one time renormalized operators. However, for PBC system one needs a long bond; therefore, at least two operators of superblocks are renormalized multiple times. In the new algorithm the multiple time renormalization of operator is avoided and the algorithm goes as

1. Start with a superblock with four blocks consisting of a left and a right block and two new site blocks. The blocks are shown in Fig. 3.1 as filled circles and may have more than one site. Here we have considered only one site in each block. New blocks may also have more than one site and are shown as open circles. In this chapter new blocks have one site in a chain or two for a ladder like structure with PBC [194].

2. Get the eigenvalues and eigenvectors of the superblock and construct the density matrix ρ of the system which consists of the left or the right block and two new blocks. The left system block is shown inside the box in Fig. 3.1a.

3. Now construct an effective ρ' with m number of eigenvectors of ρ corresponding to m largest eigenvalues of the density matrix. The effective system Hamiltonian and operators in the truncated basis are calculated using Eq. (3.7).

4. The superblock is constructed using the effective Hamiltonian and operators of system blocks and two new sites.
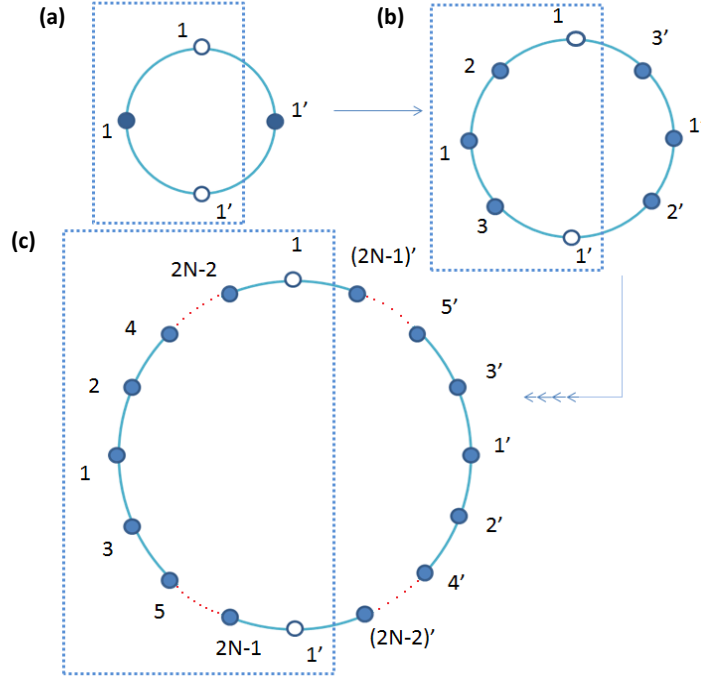
Figure 3.1: Pictorial representation of the new DMRG algorithm with only one site in the new block. (a) One start with two blocks left and right represented by filled circles and two new sites blocks represented as open circles. The dotted box represents the system block for the next step. (b) Superblock of the next DMRG step is shown. (c) The Final step of infinite DMRG of $N = 4N$ system size is shown with $2N - 1$ number of sites in each of the left and the right blocks and two new sites.

5. Now go to step 2 and the processes 2 - 5 are repeated till the desired system size is reached.

We notice that the superblock Hamiltonian is constructed using the effective Hamiltonian of blocks and operator which are renormalized once. Therefore, the massive truncation because of long bond is avoided in this algorithm. Bonds in the superblock are only between new-new sites or new-old sites. For construction of Hamiltonian matrix of old-new site bond, new site operator is highly sparse; however old sites renormalized operators are highly dense. The old-old sites interaction in the conventional algorithm generates a large number of non-zero matrix elements in the superblock Hamiltonian matrix and the diagonalization of dense matrix goes as m^4. But, in the new algorithm, old-new sites interaction in the superblock generates only a sparse Hamiltonian matrix, and its digonalization scales as m^3.
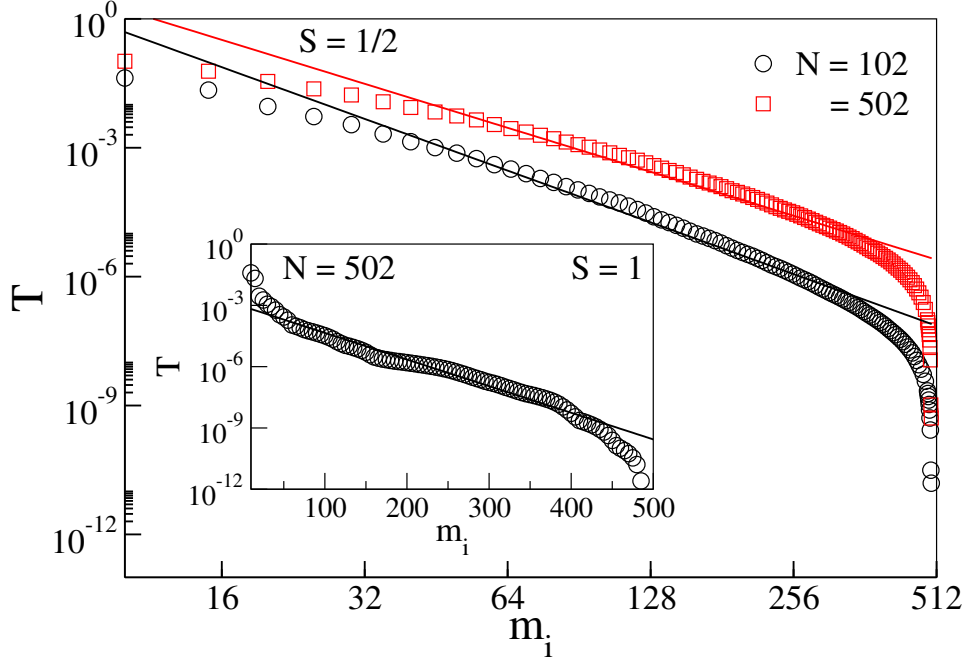
Figure 3.2: Truncation error T of the density matrix for spin-1/2 chain (main). The inset shows the truncation error for the $S = 1$ chain. For $S = 1/2$ the truncation error follows power law decay whereas it follows exponential decay for $S = 1$ system.

3.4 RESULTS

We consider spin-1/2 and spin-1 chains with PBC of length up to $N = 500$ to check the accuracy of results for the Heisenberg Hamiltonian. In this part we study the truncation error of density matrix T, error in relative ground state energy $\frac{\Delta E}{|E_0|}$ and dependence of correlation function $C(r)$ on m. The correlation function $C(r)$ is defined as

$$C(r) = \mathbf{S}_0 \cdot \mathbf{S}_r, \tag{3.8}$$

where $\mathbf{S}_0$ corresponds to the reference spin and $\mathbf{S}_r$ is the spin at a distance r from the reference spin. The relative ground state energy can be defined as $\Delta E/|E_0|$, where $\Delta E = E(m) - E_0$ with E_0 be the most accurate value for $S = 1$ chain [196] and $E_0 = E(m = 1200)$ for $S = 1/2$ chain.

As discussed earlier, the DMRG is based on the systematic truncation of the irrelevant degrees of freedom and the eigenvalues of the density matrix represents the importance of
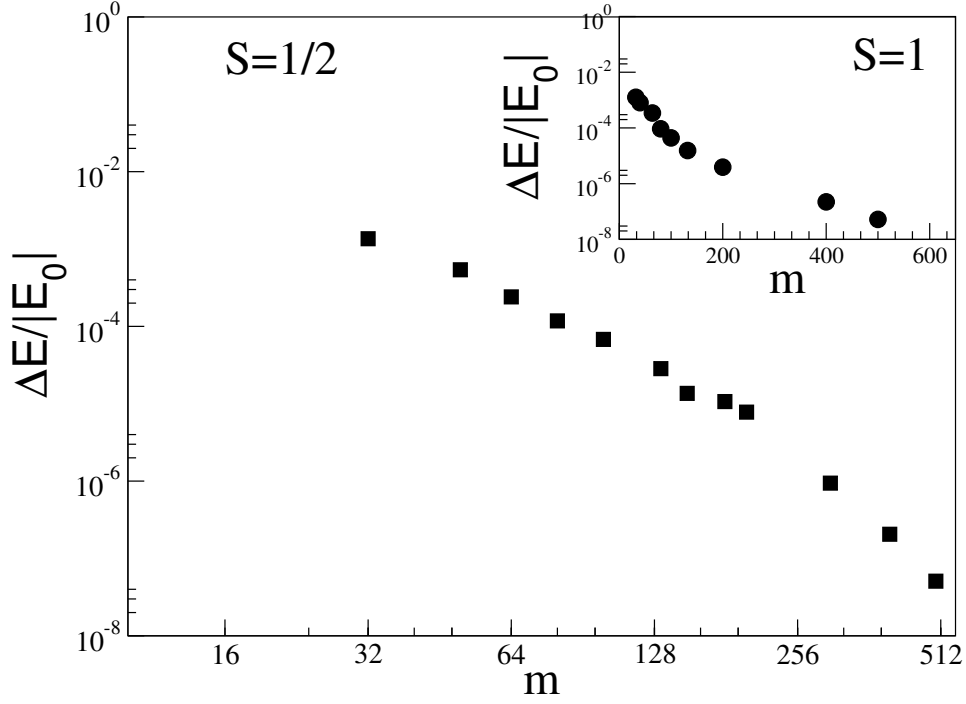
Figure 3.3: Energy accuracy $\Delta E/|E_0|$ for spin half chain with PBC (main) which shows a power law behavior with m. The inset shows the energy accuracy for spin one chain with PBC which shows exponential behavior with m.

the respective states. In the DMRG only selected states corresponding to highest eigenvalues are kept and rest of other states are thrown. We define truncation error T as

$$T = 1 - \sum_{i=1}^{m} \lambda_i \qquad (3.9)$$

where λ_i are eigenvalues of density matrix of the system block arranged in descending order. In the main Fig. 3.2, T is shown as function of m for $S = 1/2$ and the inset shows the same for $S = 1$ system with N=102 and 502. We notice that $m \sim 350$ for $S = 1/2$ and $m \sim 300$ for $S = 1$ are sufficient to achieve $T = 10^{-9}$. In the main Fig. 3.2 T vs m in log-log plot show a linear behavior i.e., T for both system size of $N = 102$ and 502 for $S = 1/2$ follows a power law $T \propto m_i^\alpha$ with $\alpha = 4.0$ and 3.4 respectively. The m dependence of T for $S = 1$ ring is shown in the inset of Fig. 3.2. The truncation error T in this case decays exponentially i.e., $T \propto \exp(-\beta m_i)$ with $\beta = 0.03$ for both $N = 102$ and 502.

The relative error in energies $\Delta E/|E_0|$ for $S = 1/2$ and 1 with $N = 102$ spins are shown in Fig. 3.3 main and inset respectively. The exact energies of spin-1 system is $E_0/N \sim$ 1.4014840386 and this value is obtained by using conventional DMRG with $m = 2000$ and
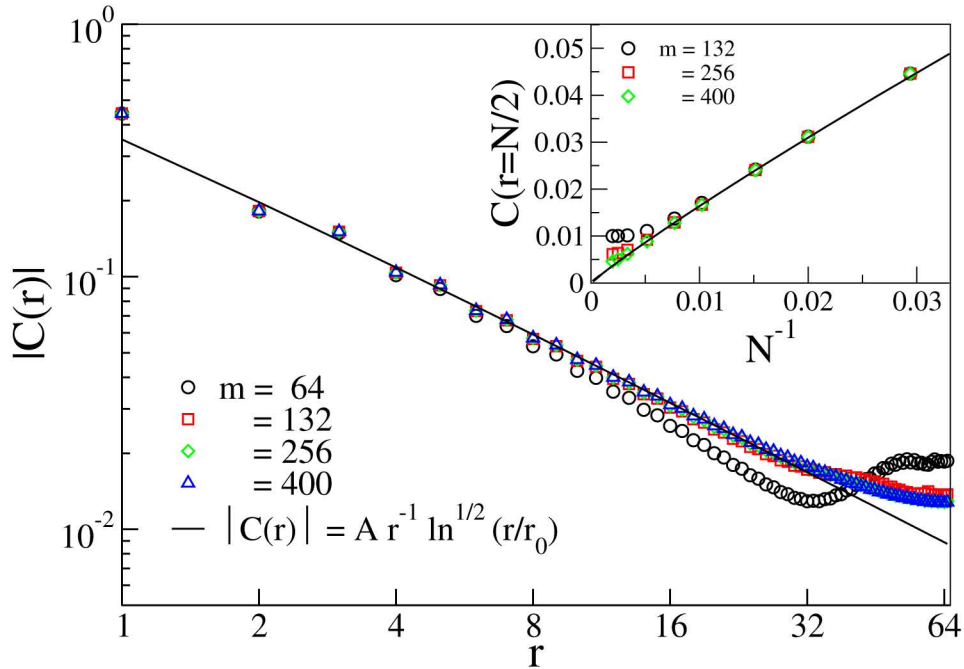
Figure 3.4: The main figure shows the variation of $|C(r)|$ (defined in Eq. 3.8) as a function of r for different m. The solid curve in the main figure is the logarithmic correction formula: $Ar^{-1}\ln^{1/2}(r/r_0)$ with $A = 0.22$ and $r_0 = 0.08$. [116, 204] The inset shows the variation of $C(N/2)$ with the inverse of N for different m. The solid curve is the form: $A(N/2)^{-1}\ln^{1/2}(N/2r_0)$ with $A = 0.323$ and $r_0 = 0.08$.

up to $N = 100$ site chain [196]. Extrapolation of energies with m is done to obtain the above value [196]. We notice that $-\frac{\Delta E}{E_0}$ for $S = 1/2$ systems goes to 10^{-6} for $m = 256$ where as, it goes to 10^{-8} for $m \approx 500$ as shown in the main Fig. 3.3. Although the similar accuracy of the energy can be achieved with $m = 100$ in MPS approach, the scaling is $\sim m^4$ rather than $\sim m^3$ in our algorithm. For $S = 1$ accuracy of 10^{-8} can be reached with $m \sim 450$ as shown in the inset of Fig. 3.3.

The dependence of accuracy of correlation function $|C(r)|$ of $S = 1/2$ for $N = 130$ as a function of m is shown in the main Fig. 3.4. We notice that $m = 256$ is sufficient to achieve an accuracy of $\sim 10^{-4}$. We also notice that $|C(r)| \propto r^{-1}$ with the well known logarithmic correction specially for smaller r [204]. We have fitted the correlations with the well known form $|C(r)| = Ar^{-1}\ln^{1/2}(r/r_0)$ with $A = 0.22$ and $r_0 = 0.08$ [116]. Deviation in function for large r is the artifact of finite systems. In our algorithm two sites are added symmetrically and the new sites are added $N/2$ sites apart, consequently the distance between two new sites is $N/2$. Therefore, the new-new sites correlation function is $C(N/2)$ and is plotted with N^{-1} in the inset of Fig 3.4. We observe that $m = 256$ is sufficient for $N \sim 200$ to

achieve sufficient numerical accuracy. The curve behaves almost linearly with the logarithmic correction: $|C(N/2)| = 2AN^{-1}\ln^{1/2}(N/2r_0)$ with $A = 0.323$ and $r_0 = 0.08$.

3.5 SUMMARY

The DMRG is a state of the art numerical technique for solving the 1D quantum many body systems with open boundary condition. However, the accuracy of the 1D PBC system is rather poor. The MPS approach gives very accurate results but the computational cost goes as (o) m^5 [200]. Later this algorithm was modified and the computational cost of the modified algorithm goes as (o) $p \times m^3$ where p in general varies linearly with m [201] but p can go as m^2 in case of long range order in the system. The computational cost of the algorithm presented in this chapter scales as (O) m^3 because of the sparse superblock Hamiltonian and is very similar to the conventional DMRG. To achieve this goal we avoid the multiple times renormalization of the operators which are used to construct the superblock. This algorithm can readily be used to solve general 1D and quasi-1D systems e.g., J_1–J_2 model, two legged ladder. The new algorithm can be implemented with ease using the conventional DMRG code.

Our calculation suggests that most of quantities e.g., ground state energies, energy gaps and correlation function can accurately be calculated by keeping $m \sim 400$. The superfluity stiffness [205] and dynamical structure factors using the correction vector technique [202] or continued fraction method [203], can be calculated with this algorithm. The symmetries e.g., spin parity, electron-hole, inversion can easily be implemented in this algorithm [202]. This algorithm is used by us in calculating accurate static structure factors and correlation function for $J_1 - J_2$ model for a spin-1/2 ring geometry [194].

<div style="text-align: right; font-size: 3em;">4</div>

FRUSTRATED SPIN-1/2 LADDER WITH FERRO- AND ANTIFERROMAGNETIC LEGS

4.1 INTRODUCTION

The theoretical studies of magnetic spin-1/2 ladder systems have been an active area of research because of the existence of interesting phases like dimer [206], spiral phase [102], different ordered phases [207], magnetization plateau [208] etc. The spin-1/2 ladder model systems show a rich quantum phase diagrams in various interaction coupling limit. The Heisenberg antiferromagnetic (HAF) spin-1/2 normal ladder is realized in $SrCu_2O_3$ [42], $(VO)_2P_2O_7$ etc. [45, 209], whereas zigzag ladder, which is considered as the chain with nearest and next nearest neighbor interactions, has been realized in $(N_2H_5)CuCl_3$ [210], $LiCuSbO_4$ [39], $LiSbVO_4$ [38], Li_2CuZrO_4 [41] etc. The AF normal ladder system is a spin liquid with a spin gap and short range spin correlation. It was conjectured that the spin gap decreases smoothly as rung exchange interaction decreases [124, 206, 211] and reduces to zero only when rung interaction strength approaches to zero. The rung interaction induces the singlet dimer formation between the two nearest spin-1/2 on different legs [45, 211]. Ladders with ferromagnetic legs/rungs and antiferromagnetic rungs/legs are also well studied and show interesting phases [46, 47, 132, 212–214]. However, the AF zigzag ladder is completely different from normal ladder. The zigzag ladder in the weak rung coupling limit $J_1/J_2 < 0.44$ behaves like two independent HAF spin-1/2 chains [102, 103, 215], and shows gapped spiral phase for $0.44 < J_1/J_2 < 2$. It is gapped system with dimer configuration for $2 < J_1/J_2 < 4.148$ [100, 102, 103, 215, 216].

In this chapter[1] we consider spin ladders which have ferromagnetic (F) spin exchange interactions along one of the legs, and antiferromagnetic (AF) interactions on the other leg; and spins on these two legs are interacting through AF interaction. The focus of this chapter is to study some universal theoretical aspects such as the existence of exotic phases in the ground state (GS) and low-lying excitations in this system. We show that the ferromagnetic-antiferromagnetic (F-AF) ladders pose quasi-long range behavior in incommensurate regime, and frustration can be induced even for very small rung coupling limit.

These two legged ladders can represent the interface of the two layered magnetic spin-1/2 system consisting of an antiferromagnetic and a ferromagnetic layer where the two layers interact with direct or indirect antiferromagnetic exchange. Similar interfaces are studied by Suhl *et al.* [217] and Hong *et al.* [218]. We further simplify the model by considering only a inter-facial line of spins in the interface of both the layers. We consider two possibilities of arrangement of inter-facial spins; first, when spins are directly facing each-other as in normal ladder (NL), and second, where spins on one leg is shifted by half of the lattice unit forming a zigzag ladder (ZL). The spin arrangements of NL and ZL are shown in the Fig. 5.1(a) and (b). These systems are interesting because both the ladders are frustrated irrespective to the nature of rung interactions.

These spin-1/2 NL or ZL can also give some preliminary information about the phases at the interface of bilayer F-AF magnetic thin films. The inter-facial properties of the F-AF thin film materials [219, 220] remain a subject of active research till date. At low temperature (below Néel temperature and Curie temperature), the spins on both the layers remain ordered. This leads to an exchange bias at the interface. Many theoretical models based on microstructure have been proposed to explain the exchange bias field phenomenon [219–223] at the interface of these F-AF layers, e.g., discrete micromagnetics models [224–231], continuum micromagnetics models [232–234], and many others [217, 235, 236]. Suhl [217] considered only the interfacial spins similar to our model and pointed out, the spins at the antiferromagnetic side of the interface is in the mean field of the ferromagnetic spins. This

---

[1] The work reported here is based on the paper "Frustrated spin-1/2 ladder with ferro- and antiferromagnetic legs", Debasmita Maiti, Dayasindhu Dey and Manoranjan Kumar, Journal of Magnetism and Magnetic Materials **446**, 170 (2018).
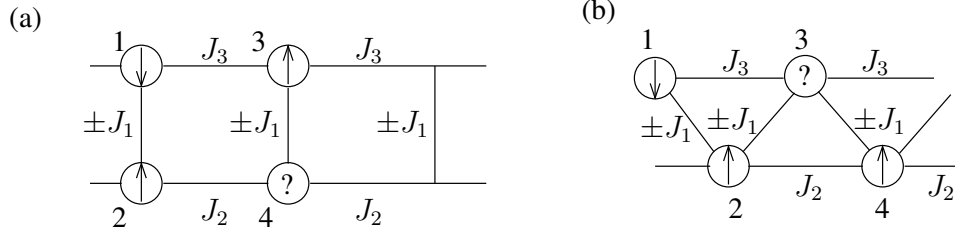
Figure 4.1: (a) and (b) show the normal and the zigzag arrangements of the interfaces. The arrows show the spin arrangement and the question mark represents the frustrated spin.

happens because the Néel temperature is lower than the Curie temperature, and the spins on the ferromagnetic side is more robust.

This chapter is divided into four sections. In Sec. 4.2, the model Hamiltonian is introduced and the numerical methods are explained. The numerical results for both the ladders are given in Sec. 4.3 and the effective model Hamiltonian is constructed in Sec. 4.4. All the results are discussed and summarized in Sec. 4.5.

4.2 MODEL HAMILTONIAN AND NUMERICAL METHOD

We consider a 2-leg ladder (either NL or ZL) of F and AF legs. We further consider the half-filled insulating case where the electrons are completely localized, but spins can interact with its nearest neighbors. Thus we can write an isotropic Heisenberg spin-1/2 model Hamiltonian for the system shown in Figs. 4.1 (a) and (b) as

$$H = H_{\text{rung}} + H_{\text{leg}}, \tag{4.1}$$

where

$$
\begin{aligned}
H_{\text{leg}} &= \sum_{i=1}^{N/2-1} J_2 \, \mathbf{S}_{2i} \cdot \mathbf{S}_{2i+2} + J_3 \, \mathbf{S}_{2i-1} \cdot \mathbf{S}_{2i+1}, \\
H_{\text{rung}}^{\text{NL}} &= J_1 \sum_{i=1}^{N/2} \mathbf{S}_{2i-1} \cdot \mathbf{S}_{2i}, \\
H_{\text{rung}}^{\text{ZL}} &= J_1 \sum_{i=1}^{N-1} \mathbf{S}_i \cdot \mathbf{S}_{i+1}.
\end{aligned}
\tag{4.2}
$$

Here the rung Hamiltonian for the NL and ZL are written as $H_{\text{rung}}^{\text{NL}}$ and $H_{\text{rung}}^{\text{ZL}}$, respectively. The nearest neighbor AF interaction J_3 is along the upper leg, and nearest neighbor F interaction J_2 is along the lower leg. J_1 is interaction along the rung of the systems as shown in Fig. 4.1(a) and Fig. 4.1(b) for the NL and the ZL, respectively. The interactions along legs are set to $J_2 = -1$ and $J_3 = 1$, however, rung interaction ($J_1 = \alpha$) is a variable quantity. To understand the GS properties of these systems as a function of α, we solve the Hamiltonian in Eq. (4.1) numerically.

We use the exact diagonalization (ED) method for small systems and Density matrix renormalization group (DMRG) method to handle the large degrees of freedom for large systems. The DMRG is based on the systematic truncation of irrelevant degrees of freedom at every step of growth of the chain [76, 164, 192]. We have used recently developed DMRG method where four new sites are added at every DMRG steps [171]. We have also used the recently developed DMRG for periodic boundary condition (PBC) when the system is under PBC [237]. The eigenvectors corresponding to m largest eigenvalues of the density matrix of the system in the GS of Hamiltonian in Eq. (4.1) are kept to construct the effective density matrix. We have kept m up to 500 to keep the truncation error less than 10^{-10}. We have used system sizes up to $N = 200$ to minimize the finite size effect.

4.3 NUMERICAL RESULTS

In this section, we analyze the GS of both the ZL and the NL for various rung interaction (α) limits. Here we consider only the antiferromagnetic inter-chain interaction i.e., $\alpha > 0$. In the small α ($\ll 1$) limit, the NL and the ZL behave like decoupled chains. In this phase the F leg remains in ferromagnetic state, whereas other leg possesses antiferromagnetic arrangement of spins. However, in thermodynamic limit the decoupled phase exists only for $\alpha \sim 0$. On further increase in α, the competition between the F and the AF interactions forces the F leg to reduce its total magnetization. There is an incommensurate spin density wave (SDW) phase for parameter space $0.07 < \alpha < 1.14$ in the NL and $0.04 < \alpha < 1.06$ for the ZL with $N = 200$ spins. In thermodynamic limit, the lower limit of α value for SDW phase tends to zero. In the large α limit of the NL, the two nearest neighbor spins from different legs
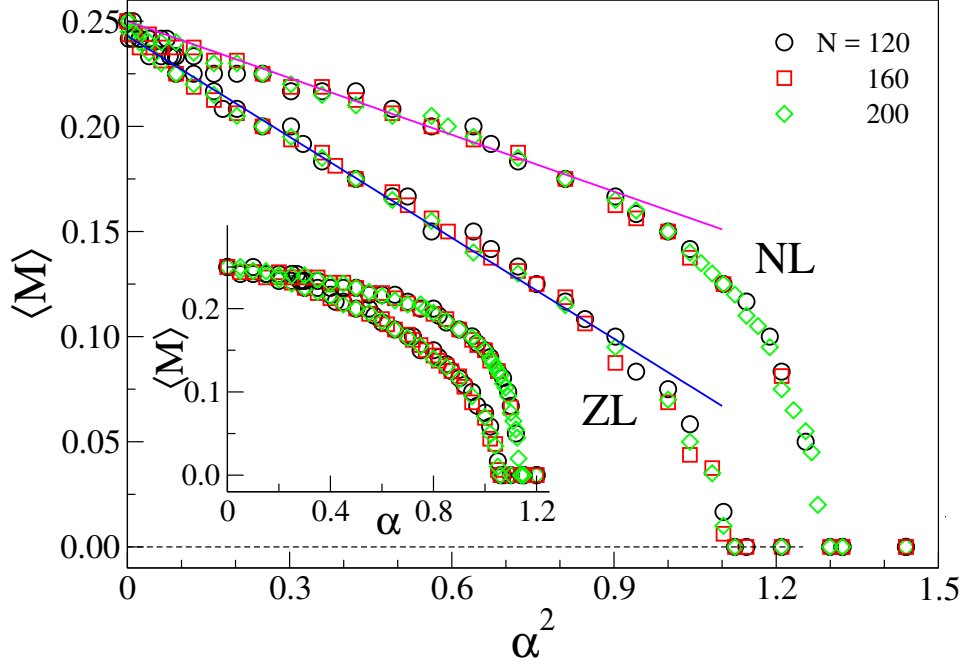
Figure 4.2: The ground state magnetization $\langle M \rangle$ with inter chain coupling interaction α for both the NL and the ZL. The main figure plots $\langle M \rangle$ vs. α^2; the straight line fits for $\alpha < 0.9$ i.e., $\alpha^2 < 0.8$ reveals that $\langle M \rangle \propto \alpha^2$ in this regime. The inset shows the $\langle M \rangle$ - α curve.

form a singlet dimer. However, the ZL behaves like a single spin-1/2 chain of N spins where each leg contains $N/2$ spins. To verify the above phases, total magnetization $\langle M \rangle$ in GS, correlation functions $C(r)$, and the spin densities ρ_r for both the systems are analyzed.

4.3.1 *Magnetization*

For small inter-chain antiferromagnetic coupling ($\alpha \ll 1$), two legs of the ladder behave as decoupled chains, and the system has its ground state magnetization $\langle M \rangle = \frac{\sum_{i=1}^{N} S_i^z}{N} = \frac{1}{4}$. All of the magnetization contribution comes from the F leg. The magnetization $\langle M \rangle$ decreases continuously with α, and $\langle M \rangle$ goes finally to zero for large α. The $\langle M \rangle$ as a function of α^2 is shown in Fig. 4.2 (main) for three system sizes $N = 120, 160$, and 200 of both the NL and the ZL systems, and the inset show the $\langle M \rangle - \alpha$ curve. We notice there are step like behavior in $\langle M \rangle - \alpha$ plot in finite system, but width of steps decreases with system size N. However, $\langle M \rangle - \alpha$ curve should be continuous in the thermodynamic limit. We notice that the NL shows slower change in $\langle M \rangle - \alpha$ as compared to the ZL.

45

The transition from incommensurate SDW phase to spin fluid phase at $\alpha = \alpha_c = 1.06$ is relatively faster in the ZL compared to the transition from incommensurate SDW to dimer phase at $\alpha = \alpha_c = 1.14$ in the NL, and the $\langle M \rangle$ vanishes at the transition point $\alpha = \alpha_c$. In fact our analytical perturbation calculation for the NL in Sec. 5.4 also suggests that the contribution from interaction along the legs are zero at large α limit. In this limit the NL system of N spins behaves as a collection of $\frac{N}{2}$ number of independent singlet dimers. The continuous variation in the ZL near the transition point can be attributed to delocalized nature of the system. In this limit J_1 dominates, and this system behaves like a HAF spin-1/2 chain with weak and alternate AF and F next nearest neighbor interaction. The ferromagnetic interaction J_2 stabilize the AF arrangement of spins, whereas AF interaction J_3 frustrates the system.

To understand the spin arrangement and correlation between the spins, spin correlations and spin densities are studied.

4.3.2 *Spin-spin correlations*

Longitudinal spin-spin correlations are defined as

$$C(r) = \langle S_i^z S_{i+r}^z \rangle \tag{4.3}$$

where S_i^z and S_{i+r}^z are the z-component of spin operators at reference site i and at a distance r from the reference site i, respectively. Our reference site is at the AF leg in this subsection. We have also defined spin density fluctuation as

$$C^{\mathrm{F}}(r) = \langle S_i^z S_{i+r}^z \rangle - \langle S_i^z \rangle \langle S_{i+r}^z \rangle. \tag{4.4}$$

We find three types of correlations for both the ladder systems in different parameter regimes as shown in Fig. 4.3. Black circles represent correlations with spins located on AF leg, whereas squares represent the correlations with the spins on F leg. $C(r)$ for three different phases are shown in Figs. 4.3(a)–(c) for the NL and Figs. 4.3(d)–(f) for the ZL with N=200. For $\alpha = 0.05$, the spins on different legs are uncorrelated, and the spins on the AF
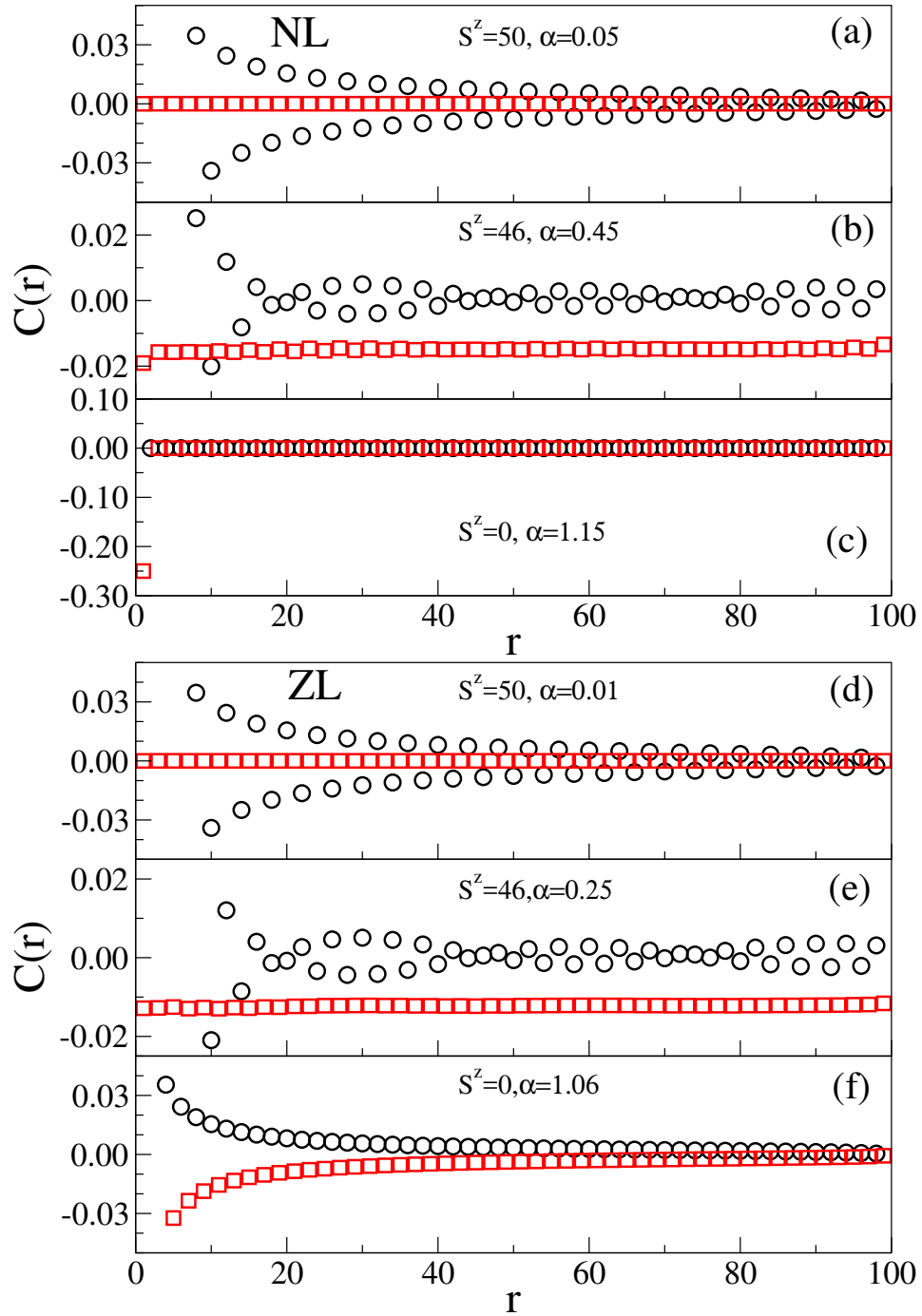
Figure 4.3: The longitudinal spin-spin correlations $C(r)$ are plotted for N=200 considering the reference spin on the AF leg. Here circles represent $C(r)$ with the spins of the AF leg whereas squares represent $C(r)$ with the spins of the F leg. Different values of α are chosen to show the (a) decoupled phase, (b) incommensurate SDW phase, (c) dimer phase for $\alpha = 0.05$, 0.45, 1.15 respectively in the NL, and (d) decoupled phase, (e) incommensurate SDW phase, (f) spin-fluid phase for $\alpha = 0.01$, 0.25, 1.06 respectively in the ZL.

leg show quasi-long-range order, as shown in Fig. 4.3(a). The similar behavior is found in the ZL for $\alpha = 0.01$ as shown in Fig. 4.3(d). The incommensurate phase in the NL is observed for $0.07 < \alpha < 1.14$ and in the ZL for $0.04 < \alpha < 1.06$. We choose $\alpha = 0.45$ for the NL and $\alpha = 0.25$ for the ZL to make sure that we have same S^z value in both types of ladder. At large distance r, the value of $C(r)$ for both the NL and the ZL is finite as shown in Fig. 4.3(b) for NL and Fig. 4.3(e) for ZL. However, $C^F(r)$ decays algebraically for the AF and the F leg separately where we consider the reference spin on the AF and the F leg, respectively.

At large α limit ($\alpha \geq 1.16$), the behavior of the two ladders become completely different. In NL the $C(r)$ have non-zero value only up to $r = 1$, as shown in Fig. 4.3(c). In the large α (≥ 1.06) limit the ZL behaves like a single antiferromagnetic Heisenberg chain and the $C(r)$ decays following a power law ($\propto r^{-\gamma}$) where spins from AF and F leg situated alternatively with distance r. The $C(r)$ in this regime is shown in Fig. 4.3(f) for $\alpha = 1.06$.

The incommensurate SDW phases for the NL and the ZL are similar to that in the HAF spin-1/2 chain in a magnetic field; therefore, $C(r)$ in the F and the AF legs are analyzed separately for both the NL and the ZL. $C^F(r)$ for the F leg in both the systems are vanishingly small. To understand it better, we plot $C^F(r)$ for the AF leg in Figs. 4.4(a) and (b) for the NL and the ZL, respectively, for same α ($= 0.2$) and $N = 200$. We find that $C^F(r)$ in AF leg for both the systems follow the relation

$$C^F(r) \propto (-1)^r \, r^{-\gamma} \, \sin\left(\frac{\pi(r+c)}{\beta}\right) \tag{4.5}$$

Here β is proportional to wavelength of the SDW, γ represents the power law coefficient, and $\frac{\pi c}{\beta}$ is a phase shift. In Fig. 4.4(a) and Fig. 4.4(b) solid lines are the fitted curves where the symbols indicate numerically calculated values of $C^F(r)$. β depends on the value of α. In the main Fig. 4.4(a), $C^F(r)$ for $\alpha = 0.2$ for the NL is shown, and the values are fitted using Eq. (4.5) with the values $\beta = 25$ and $\gamma = 1.5$. Fig. 4.4(b) shows the same for the ZL and the fitted parameter values are $\beta = 17$ and $\gamma = 1.25$. The insets of Fig. 4.4(a) and Fig. 4.4(b) are the zoomed $C^F(r)$ and these show that Eq. (4.5) fits very well even for large distances. The variation of β with α is discussed in the subsections 4.3.3 and 4.3.4. The $C^F(r)$ on the F leg have values of order of $10^{-5} - 10^{-6}$; therefore, it is difficult to exactly fit the $C^F(r)$ values on the F leg.
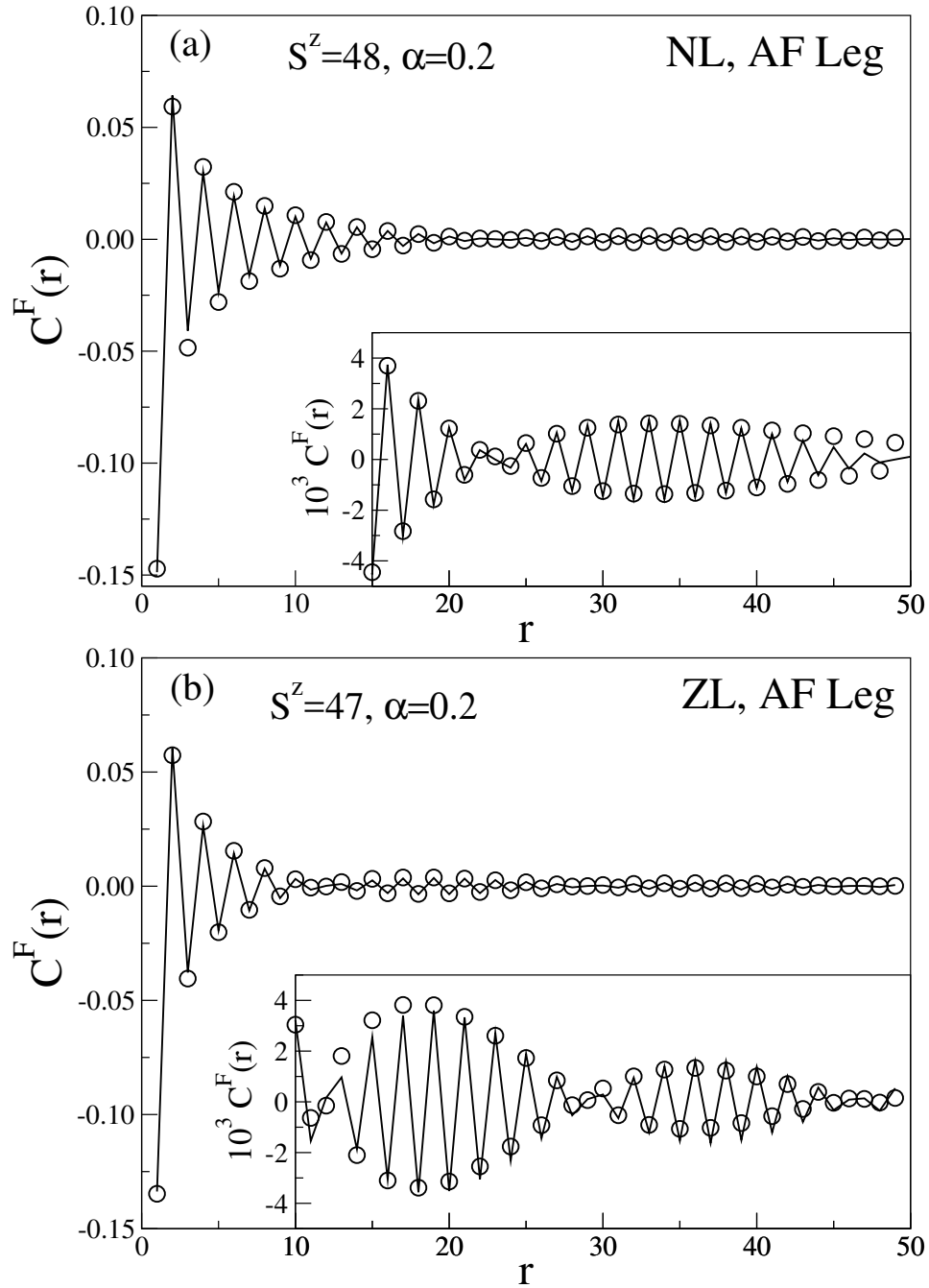
Figure 4.4: Spin density fluctuations $C^F(r)$ for the spins on the AF leg for (a) NL and (b) ZL. The reference spin is on the AF leg. The points are the ground state $C^F(r)$ calculated using DMRG for $N = 200$, $\alpha = 0.2$ for both the ladders. Calculated $C^F(r)$ are fitted using Eq. (4.5) and the solid lines represent the fitted curves. The insets are the zoomed $C^F(r)$ plot.
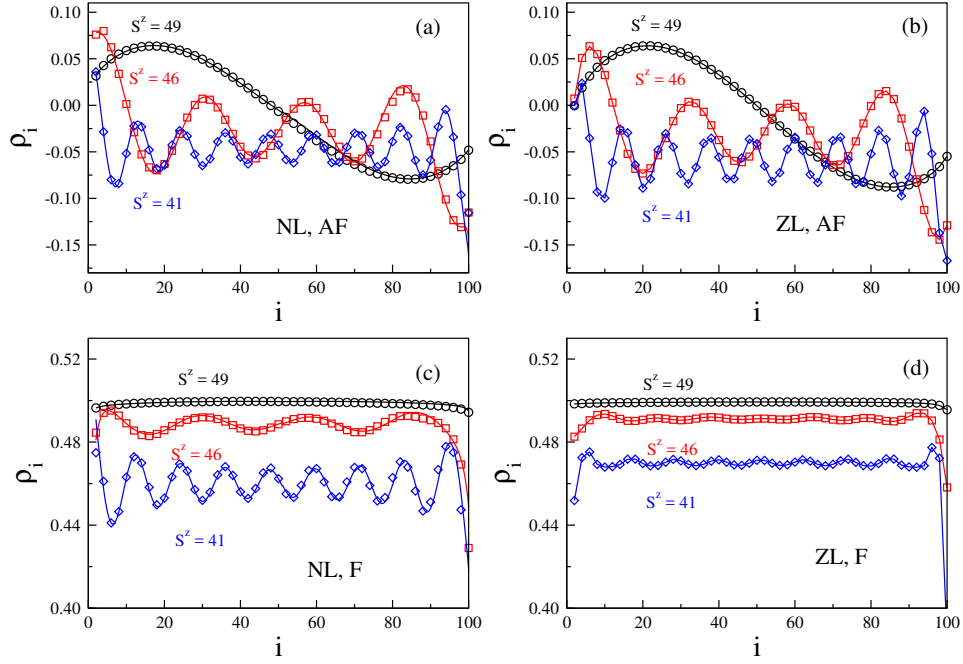
Figure 4.5: Spin densities for alternate sites on the AF leg and the F leg of the NL and the ZL for $S^z = 49$, 46 and 41. (a) and (c) depict the spin densities on AF leg and F leg of NL for $\alpha = 0.1, 0.45, 0.75$ respectively; (b) and (d) show the spin densities on the AF leg and F leg for ZL for $\alpha = 0.1, 0.25, 0.45$ respectively.

4.3.3 Spin density

The distribution of the spin density on different legs is important, especially in the higher magnetic states. The spin densities on the odd (even) sites correspond to the spin densities on the AF (F) leg. In Figs. 4.5(a) and (b), the spin densities of alternate sites in the AF leg are shown for the NL and the ZL respectively. For small α, three S^z sectors are considered at different α. The incommensurate spin density (ρ_i) for $S^z = 49$, 46, and 41 for $\alpha = 0.1, 0.45$, and 0.75 in the AF leg of the NL are shown in Fig. 4.5(a). ρ_i for same values of S^z for $\alpha = 0.1, 0.25$, and 0.45 in the AF leg of the ZL system are shown in Fig. 4.5(b). In these systems the incommensurate SDW phase shows the similar behavior for a given S^z except at the boundary of the system. ρ_i in the F leg for both the NL and the ZL also show incommensurate SDW as shown in Figs. 4.5(c) and (d), respectively. However, the incommensurate SDW is more prominent in smaller S^z. The edge spin densities of the F leg in the NL is much smaller than the ZL system. The spin density modulation in the F leg is very small for $\alpha \rightarrow 0$; however, the amplitude of the modulations increase with α. For a given S^z incommensurate
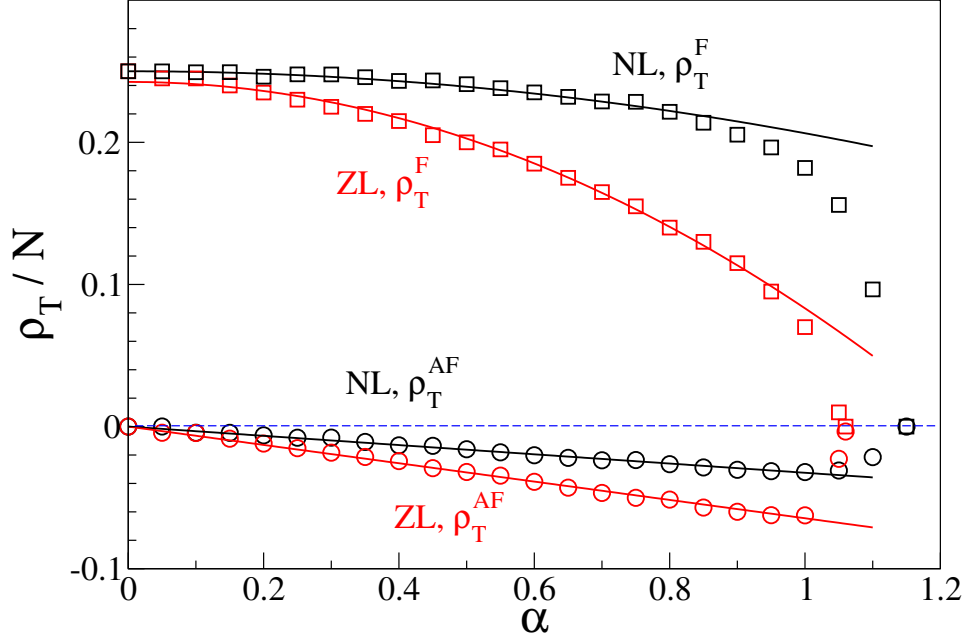
Figure 4.6: Total spin density on the AF leg and the F leg for both NL and ZL for different values of α. For $\alpha < 0.9$ in the F leg $\rho_T^F \propto \alpha^2$ while in the AF leg $\rho_T^{AF} \propto \alpha$.

SDW in ZL has smaller amplitude than that in NL, but both have similar β. For large $\alpha < \alpha_c$, the periodicity of the AF and the F legs are the same. The total spin density, on each leg of the system, ρ_T is shown as a function of α in Fig. 4.6. The circle and square of same color represent ρ_T for the AF and the F leg, respectively, however black and red symbols represent the NL and the ZL, respectively. The ρ_T value in the AF leg is zero in decoupled limit, and it varies linearly with α with negative slope in both the systems for $\alpha < 0.9$. However, for $\alpha > 0.9$, ρ_T increases rapidly, and goes to zero at the transition point (α_c). In the F leg of both systems, ρ_T decreases monotonically with α^2 for $\alpha < 0.9$; ρ_T decreases rapidly to zero near the transition point $\alpha_c = 1.14$ (1.06) for the NL (the ZL).

If we ignore some points near the edges, the spin densities in Fig. 4.5 can be fitted with the equation which is proportional to $\sin\left(\frac{\pi(r+c)}{\beta}\right)$ part in Eq. (4.5). For the same value of α, ρ_i and $C^F(r)$ have same β for a particular system. The lowest density amplitudes at the edges is due to the boundary effect. The AF leg has highest density at the edge and induces highest fluctuation in the F leg. The incommensurate SDW has well defined pitch angle.
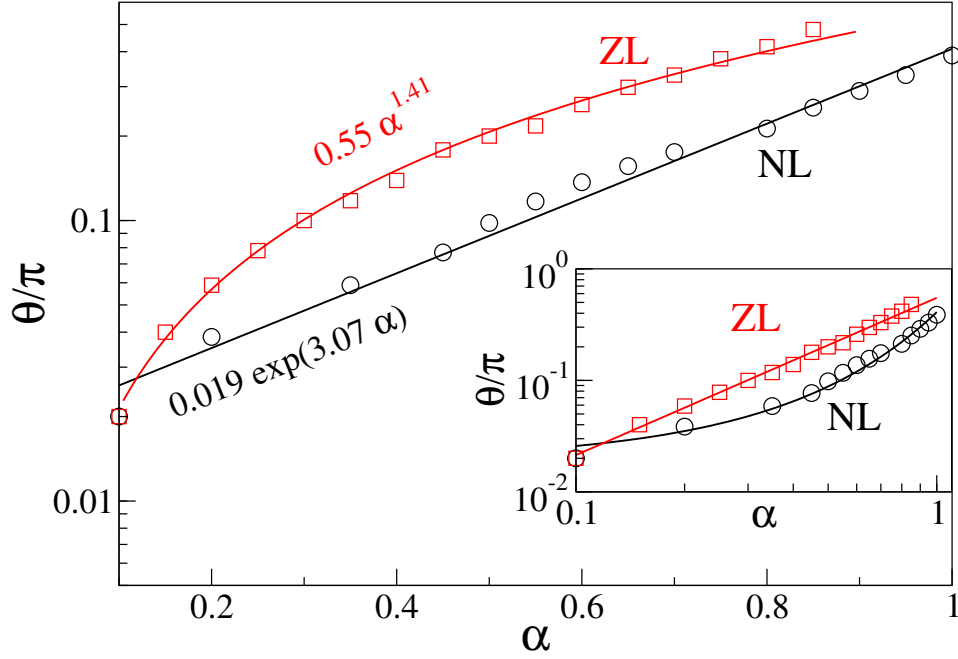
Figure 4.7: The pitch angle (θ) for different values of α in both the NL and the ZL in log-linear scale (main figure) and in log-log scale (inset). The solid lines are the exponential fit (for NL) and the power law fit (for ZL). The actual fitted formulae are given on the plot near the curves.

4.3.4 *Pitch angle*

We notice that accurate calculation of the pitch angle (θ) from $C^{\text{F}}(r)$ becomes extremely difficult because of power law nature of $C^{\text{F}}(r)$. However, θ can be directly calculated from the spin density calculations. Now let us consider the length of the AF chain is l for which the total angle change between i^{th} and $i + l^{\text{th}}$ spin is 2π. The length l is the wavelength of the incommensurate SDW. Therefore θ can be defined as $2\pi/l$. The pitch angle θ in the AF leg as a function of α is plotted in Fig. 4.7 for the NL with black circle and for the ZL with red squares. The main figure shows the log-linear plot. The pitch angle for the NL follows exponential decay as shown in the main Fig. 4.7. The line represents the fitted curve with $0.019 \exp(3.07\alpha)$. The convention of symbols in the inset is the same as in the main figure. The inset of Fig. 4.7 shows the log-log plot of θ/π vs. α, which is fitted with $0.55\,\alpha^{1.41}$ for the ZL.

4.3.5 *Large α limit*

In the large $\alpha > 1.14$ limit, the NL behaves as dimer of two nearest neighbor spins at different leg of ladder. The $C(r)$ for $\alpha = 1.15$ is very short ranged and is non-zero only for nearest neighbor spins as shown in Fig. 4.3(c). The GS energy is exactly equal to $-\frac{3}{8}N\alpha$. The AF 2-leg ladder has a short range order and has finite lowest energy gap (spin gap) $\Delta = -3J_1/4$ in the perfect dimer limit. This energy is equivalent to breaking a singlet bond. The short range correlation in NL and gaped excitation are explained in the analytical Sec. 4.4.

In this limit the ZL system behaves as a single chain of N spins with nearest neighbor exchange interaction J_1. It is well known that the GS of spin-1/2 HAF chain is a spin fluid state and this phase can be characterized by the algebraic decay of spin-spin correlations and the gapless energy excitation. The transition point from the incommensurate SDW phase to the spin fluid in the ZL is at $\alpha \approx 1.06$.

4.4 EFFECTIVE HAMILTONIAN FOR NL

In large inter-chain coupling limit the NL shows dimer phase as already mentioned in Section 4.3.5. To understand the dimer phase we treat the NL analytically in this section. Our aim is to find an effective Hamiltonian for the NL in the strong coupling limit i.e., for $\alpha \gg 1$. There is a very sharp critical α for NL and the system has singlet GS for $\alpha > \alpha_c$.

In the strong rung coupling limit the system can be approximated as a collection of $N/2$ rungs. The Hamiltonian then becomes $H_{\text{rung}}^{\text{NL}}$ (see Eq. (4.2)). The GS of this Hamiltonian is $2^{N/2}$ fold degenerate. Each of $N/2$ rungs can be either in the state $|S_0\rangle$ or $|T_1\rangle$ with energies $E(S_0) = -3J_1/4$ and $E(T_1) = J_1/4$. H_{leg} lifts the degeneracy and leads to an effective Hamiltonian that can be derived by standard many-body perturbation theory [238]. Following the same procedure mentioned in [239], we can write the spin operators in terms of the pseudo-

spin-1/2 operators. Let us introduce pseudo spin-1/2 operators to be acted on the states $|S_0\rangle_i$ and $|T_1\rangle_i$ of rung i following

$$
\begin{aligned}
\tau_i^z |S_0\rangle_i &= -\frac{1}{2}|S_0\rangle_i & \tau_i^z |T_1\rangle_i &= \frac{1}{2}|T_1\rangle_i \\
\tau_i^+ |S_0\rangle_i &= |T_1\rangle_i & \tau_i^+ |T_1\rangle_i &= 0 \\
\tau_i^- |S_0\rangle_i &= 0 & \tau_i^- |T_1\rangle_i &= |S_0\rangle_i
\end{aligned}
\tag{4.6}
$$

One can express the original operators in Eq. (4.2) in terms of the pseudo-spin operators. This can be done by inspection and are given by:

$$
\begin{aligned}
S_{2i-1}^+ &= -\frac{1}{\sqrt{2}}\tau_i^+ & S_{2i+1}^+ &= \frac{1}{\sqrt{2}}\tau_i^+ \\
S_{2i-1}^- &= -\frac{1}{\sqrt{2}}\tau_i^- & S_{2i+1}^- &= \frac{1}{\sqrt{2}}\tau_i^- \\
S_{2i-1}^z &= \frac{1}{2}\left(\tau_i^z + \frac{1}{2}\right) & S_{2i+1}^z &= \frac{1}{2}\left(\tau_i^z + \frac{1}{2}\right)
\end{aligned}
\tag{4.7}
$$

Substituting these expressions into the Hamiltonian we get the effective Hamiltonian as:

$$
\begin{aligned}
H &= H_0 + J_{xy}^{\text{eff}} \sum_{i=1}^{N/2} \frac{1}{2}\left(\tau_i^+ \tau_{i+1}^- + \tau_i^- \tau_{i+1}^+\right) \\
&\quad + J_z^{\text{eff}} \sum_{i=1}^{N/2} \tau_i^z \tau_{i+1}^z + h_{\text{eff}} \sum_{i=1}^{N/2} \tau_i^z + C_0
\end{aligned}
\tag{4.8}
$$

where $J_{xy}^{\text{eff}} = \frac{J_3+J_2}{2}$, $J_z^{\text{eff}} = \frac{J_3+J_2}{4}$, $h_{\text{eff}} = \frac{J_3+J_2}{4}$, and $C_0 = \frac{J_3+J_2}{4}$. For the AF-F ladder $J_3 = -J_2 = J$, therefore at strong coupling limit $H = H_0$. The critical rung interactions are given in the Appendix.

4.5 DISCUSSION AND CONCLUSIONS

In this chapter we studied F-AF ladder models with an antiferromagnetic leg and a ferromagnetic leg coupled through antiferromagnetic rungs. Two types (NL and the ZL) of ladders are considered (see Fig. 4.1). It is clear from Figs. 4.1(a) and (b) that irrespective of the struc-

ture both NL and ZL are frustrated in nature. Our calculation suggests that both NL and ZL show incommensurate SDW phase for $0 < \alpha < \alpha_c$ in the thermodynamic limit.

We show that the ZL exhibits some similarities with the NL in the low α limit, but have remarkable differences in the large α limit. In small and intermediate α limit both ladders exhibit incommensurate SDWs. In large α limit the ZL behaves like single HAF chain and the NL shows an exact dimer phase. The pitch angle in the incommensurate SDW phase of the ZL show algebraic variation, whereas it changes exponentially in the NL. The spin density fluctuation $C^{\mathrm{F}}(r)$ follows the power law in both legs for both type of ladders as shown in Fig. 4.4; this behavior is similar as partially magnetized HAF chain. Most of HAF ladder [45, 211] or frustrated ladder [123, 215, 216] shows exponential behavior of correlation function in the spiral phase. The critical value α_c for incommensurate SDW to singlet dimer transition in NL is almost independent of system size, and can be explained by analytical calculation of perturbation theory of this system. The finite size effect on α_c in ZL is also weak.

For $\alpha < 0.9$ in both the ladders $\langle M \rangle \propto \alpha^2$ as shown in Fig. 4.2. $\langle M \rangle$ decreases rapidly to zero for $\alpha > 0.9$. Interestingly for both the ladders in $\alpha < 0.9$ regime, the total spin density on the F leg $\rho_T^F \propto \alpha^2$ whereas on the AF leg $\rho_T^F \propto \alpha$ for $\alpha < 0.9$ as shown in Fig. 4.6. The spin density ρ_T^{AF} at AF-leg of both the systems is always negative, and ρ_T^{AF} for the ZL have higher magnitude than the NL contrary to the ρ_T^F.

In the mean field limit this model can be approximated as a partially magnetized HAF chain, at least in small coupling limit. Here the F-leg act as a uniform external magnetic field on the AF-leg. Using the Heisenberg Hamiltonian with anisotropy constant, Suhl and Schuller explained the effective bias field $H_{\mathrm{eff}} \propto J_c^2$ in Eq. (12) of [217], where J_c is the exchange interaction strength between two layers. However as shown in Fig. 4.2, $\langle M \rangle \propto \alpha^2$ in both the systems for $\alpha < 0.9$. Assuming the magnetization in these systems is proportional to field (h), we obtain $h \propto \alpha^2$. T. M. Hong suggested in [218] that in low temperature limit $h \propto J_c$. Our calculation agrees very well with the calculations in [217]

In a recently published paper by Sekiguchi and Hida [240], a spin ladder model similar to our NL system has been considered. They have shown the J_2, J_3 dependencies of α_c using nonlinear σ model and perturbation theory. Their ED calculations show that their is a

phase transition from Lieb-Mattis ferrimagnetic to partial ferrimagnetic phase. However, our extended system calculation shows the absence of the Lieb-Mattis ferrimagnet.

In conclusion, we consider F-AF two-legged spin-1/2 ladders with antiferromagnetic rungs. In the finite $\alpha < 1.0$ regime we notice the incommensurate SDW phase in both the ladders. We also notice that the NL behaves like a collection of independent dimers for $\alpha > 1.14$, whereas the ZL behaves like a single spin-1/2 chain for $\alpha > 1.06$. The magnetization on the F leg varies as J_1^2, whereas it varies linearly with J_1 on AF leg.

APPENDIX

4.A CRITICAL RUNG INTERACTION

According to the numerical analysis we find a sharp transition from the $S_G > 0$ to $S_G = 0$ at some critical value of α for both the ladders. This critical value is independent of the system size. Let us consider a toy model of four spins as shown in Fig. 4.1(a). The eigenvalues in the $^z S = 0$ sector are $\frac{1}{4}(-2J_1 + J_2 + J_3)$, $\frac{1}{4}(2J_1 + J_2 + J_3)$, $-\frac{1}{4}\left(J_2 + J_3 + 2\sqrt{(J_2 - J_3)^2 + J_1^2}\right)$, $-\frac{1}{4}\left(J_2 + J_3 - 2\sqrt{(J_2 - J_3)^2 + J_1^2}\right)$, $-\frac{1}{4}\left(2J_1 + J_2 + J_3 + 2\sqrt{(-J_1 + J_2 + J_3)^2 + 3J_1^2}\right)$, and $-\frac{1}{4}\left(2J_1 + J_2 + J_3 - 2\sqrt{(-J_1 + J_2 + J_3)^2 + 3J_1^2}\right)$. On the other side, the eigenvalues in the $S^z = 1$ sector are $\frac{1}{4}(-2J_1 + J_2 + J_3)$, $\frac{1}{4}(2J_1 + J_2 + J_3)$, $-\frac{1}{4}\left(J_2 + J_3 + 2\sqrt{(J_2 - J_3)^2 + J_1^2}\right)$, $-\frac{1}{4}\left(J_2 + J_3 - 2\sqrt{(J_2 - J_3)^2 + J_1^2}\right)$. The interactions are set to $J_2 = -1$ and $J_3 = 1$, and $J_1 = \alpha$ is a variable. This leads to the lowest two eigenvalues: $E_0(S^z = 0) = -\frac{3}{2}\alpha$ and $E_0(S^z = 1) = -\frac{1}{2}\sqrt{4 + \alpha^2}$. As we consider the $\alpha > 0$ case only, the critical value $\alpha_c = \frac{1}{\sqrt{2}}$ for this toy model.

QUANTUM PHASE DIAGRAM OF A FRUSTRATED SPIN-1/2 SYSTEM ON A TRELLIS LADDER

5.1 INTRODUCTION

In the last couple of decades frustrated low dimensional quantum magnets have been intensively explored in search of various exotic phases like spin fluid with quasi-long-range order (QLRO) [97, 98, 102, 103, 123, 216], spin dimer with short-range order (SRO) [98, 99, 123, 206, 241], vector chiral [242, 243], multipolar phases [242–245] etc. These phases arise in presence of some specific types of spin exchange interactions which may enhance the quantum fluctuations in low-dimensional frustrated systems like one dimensional (1D) spin chains realized in materials, $LiCuVO_4$ [38], Li_2CuZrO_4 [41], Li_2CuSbO_4 [39], $(N_2H_5)CuCl_3$ [210] etc., and quasi-1D spin ladders manifested in form of $SrCu_2O_3$ [42], $(VO)_2P_2O_7$ [45, 209] etc. Frustrated twisted ladders are also realized in materials like $Ba_3Cu_3In_4O_{12}$ and $Ba_3Cu_3Sc_4O_{12}$ [46, 213, 246, 247]. Majority of the 1D frustrated magnetic systems mentioned above are modelled by simple J_1-J_2 chain [97, 99, 102, 103, 123, 216]. This model can explain the gapless spin fluid [97, 216], gapped dimer [99, 123], gapped non-collinear [102, 103, 123, 216] and decoupled phases [170].

In fact many of these 1D systems like $LiCuVO_4$ [38], Li_2CuZrO_4 [41] show three dimensional ordering at low temperature; therefore, interchain couplings are considered to understand the interesting physics below the three dimensional ordering temperature. However, there are materials with effective spin interactions confined to quasi-1D ladder like structure e.g., $SrCu_2O_3$ [42], $(VO)_2P_2O_7$ [45, 209], CaV_2O_5, MgV_2O_5 [58, 59] etc. These systems have
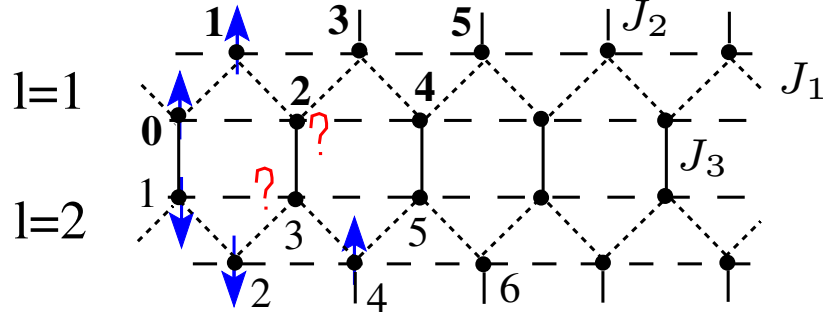
Figure 5.1: Two coupled zigzag ladders form trellis ladder. The extended lines show the extension of trellis ladder to a 2D trellis lattice structure. The arrows represent arrangement of spins and question marks represent frustrated spins. The reference site is labeled by '0' and the distances of other sites along same ladder are shown in bold numbers, and normal numbers represent the distances on other ladder. l represents the zigzag ladder indices.

antiferromagnetic (AFM) spin exchange interactions along both legs and rungs, and there is also a weak interaction between two adjacent ladders. The ground state (gs) of these systems is a gapped SRO phase [206].

The 1D $J_1 - J_2$ system, in large J_2 limit, is called zigzag ladder [216], where two chains are coupled through zigzag bonds, for example LiCuVO$_4$ [38]. The isolated ladders like zigzag and normal ladders have been extensively studied [123, 132, 206, 212]; however, the effect of interladder coupling on these ladders is rarely studied. Networks of the coupled zigzag ladders can form a trellis lattice like structure as shown in Fig. 5.1. The trellis lattice is composed of a number of zigzag ladders coupled through normal rung bonds; alternatively, we can assume coupled normal ladders interacting through zigzag like bond interactions. In this lattice spin exchange interaction strengths J_2 and J_3 are along leg and rung of a normal ladder, respectively, and J_1 is zigzag bond interaction strength between two ladders as shown in Fig. 5.1.

In this chapter [1] we consider only two coupled zigzag ladders and call it *trellis ladder* because of its geometry. We also impose periodic boundary condition along the width to mimic the trellis lattice. In various interaction limits, two coupled zigzag ladders can behave like a two-leg honeycomb ladder as considered in ref. [135], where both J_1 and J_2 are AFM, but J_3 can be either ferromagnetic (FM) or AFM. This system shows two types of Haldane

---

1 The work reported here is based on the papers "Melting of ferromagnetic order on a trellis ladder", Debasmita Maiti and Manoranjan Kumar, Journal of Magnetism and Magnetic Materials **486**, 165266 (2019) and "Quantum phase diagram of a frustrated spin-1/2 system on a Trellis Ladder", Debasmita Maiti and Manoranjan Kumar, arXiv:1907.04709 [cond-mat.str-el].
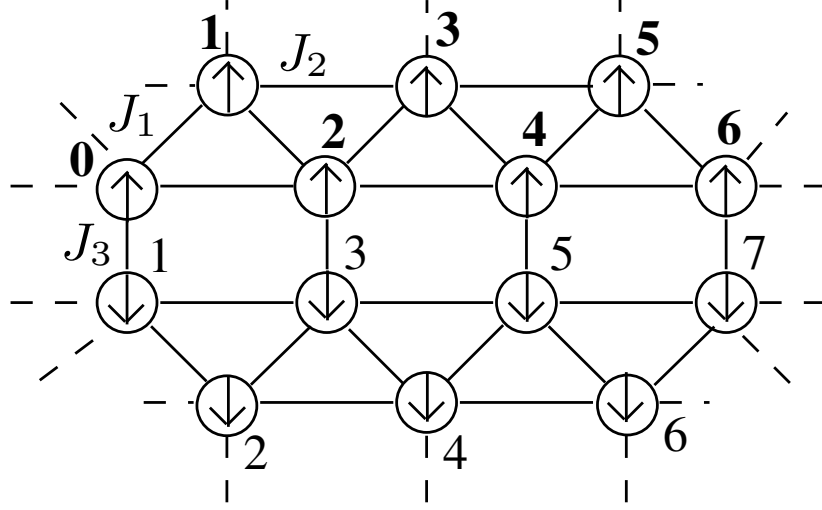
Figure 5.2: The spin arrangement in collinear striped short range ordered phase.

phase for the FM J_3, columnar dimer and rung singlet phases in presence of the AFM J_3. Normand *et al.* have considered a similar coupled ladders with all three AFM J_1, J_2 and J_3 interactions. For large J_2/J_1 they have noticed dimerized gs, whereas non-collinear (NC) long-range order (LRO) for large J_3 (J_2'). They have found Néel LRO phase in the small $J_2 < 0.4$ limit [155]. Zinke *et al.* have shown the effect of interchain coupling on NC gs of $J_1 - J_2$ model [137], in a two dimensional geometry. The effect of interladder coupling on spin gap and magnon dispersion is calculated using perturbation theory by Miyahara *et al.* [156]. They also try to model the magnetic susceptibility of $SrCu_2O_3$ and CaV_2O_5 using quantum Monte Carlo and mean field type scaling methods [156]. However, the system with FM J_1, and AFM J_2 and J_3 has not been studied in the ladder system. In this chapter, we consider a spin-1/2 trellis ladder structure, which is composed of two zigzag ladders with FM J_1 and AFM J_2, and they are coupled by AFM J_3 as shown in Fig. 5.1. Our main focus of this chapter is to construct the quantum phase diagram (QPD) and also understand the effect of rung interaction J_3 on the various exotic phases of zigzag ladder [102]. We notice that in small $J_2/|J_1|$ limit, gs has collinear striped (CS) SRO on each zigzag ladder; however, spins on one zigzag ladder are aligned antiferromagnetically with respect to the spins on the other zigzag ladder. The NC spin order sets in for moderate value of J_2. The presence of QLRO in NC regime at small J_3/J_2 limit is a striking effect of the J_3. In large J_3 limit, rung dimer is the dominant gs.

This chapter is divided into four sections. In section 5.2 the model Hamiltonian and numerical method are explained. The numerical results are given in section 5.3. Linear spin wave analysis and experimental data fitting of CaV_2O_5 are given in section 5.4 and section 5.5, respectively. All the results are discussed and summarized in Section 5.6.

5.2 MODEL HAMILTONIAN AND NUMERICAL METHOD

A four-legged spin-1/2 ladder made of two coupled zigzag ladders is considered as shown in Fig. 5.1. The exchange interactions between spins along the legs and rungs are AFM in nature. The diagonal exchange interactions J_1 in a zigzag ladder are FM. We can write an isotropic Heisenberg spin-1/2 model Hamiltonian for the trellis ladder system as

$$H = \sum_{l=1,2} \sum_{i=1}^{N/2} J_1\, \mathbf{S_{l,i}} \cdot \mathbf{S_{l,i+1}} + J_2\, \mathbf{S_{l,i}} \cdot \mathbf{S_{l,i+2}}$$
$$+ J_3\, \mathbf{S_{1,i}} \cdot \mathbf{S_{2,i}} + HS_i^z, \tag{5.1}$$

where $l = 1, 2$ are the zigzag ladder indices. $\mathbf{S_{l,i}}$ is the spin operator at site i on zigzag ladder l. We consider $J_1 = -1$, and J_2 and J_3 are variable AFM exchange interaction strengths. We use periodic boundary condition along the rungs, whereas it is open along the legs of the system.

We use density matrix renormalization group (DMRG) method to handle the large degrees of freedom in our system. This method is a state of art numerical technique for 1D or quasi-1D system, and it is based on the systematic truncation of irrelevant degrees of freedom [76, 164, 192]. We use recently developed DMRG method where four new sites are added at every DMRG step [171]. This method while constructing superblock, avoids the old-old operator multiplication which leads to the generation of large number of non-zero but small matrix elements in superblock Hamiltonian. The number of eigenvectors m corresponding to the largest eigenvalues of the density matrix, is kept for the renormalization of operators and Hamiltonian of the system block. We have kept m up to 400 to restrict the truncation error less than 10^{-10}. We have used system sizes up to $N = 300$ to minimize the finite size effect.

We first present an outline of the QPD which is constructed based on various quantities like correlation function $C(r)$, pitch angle θ and bond order $C(r = 1)$. A detailed numerical and analytical calculations is discussed in the following subsections. For $J_1 = 0$, this system is composed of two isolated normal ladders, and two isolated zigzag ladders for $J_3 = 0$. In $J_1 = 0$ limit, gs shows the formation of singlet dimers along the rungs on the normal ladder [206]. On the other hand, for $J_3 = 0$ the system shows various phases arising due to the presence of frustration in each zigzag ladder, at different exchange coupling limits. For $J_2/|J_1| < 0.25$, the gs of an isolated zigzag ladder has ferromagnetically ordered spins and gapless excitations. In the intermediate parameter regime, $0.25 < J_2/|J_1| < 0.67$, NC order arises in this system with a small finite spin gap [102, 103, 215, 216]. The system behaves like two decoupled AFM chains exhibiting QLRO in spin-spin correlation and gapless excitations in $J_2/|J_1| > 0.67$ limit [103]. We notice that if two zigzag ladders start interacting with each other through rung coupling J_3, it immediately opens a spin gap in the system. In section 5.4 we discuss the linear spin wave analysis of this model. At the end, we apply this model to fit magnetic susceptibility and magnetization of CaV_2O_5 in large J_3 limit. We also predict the specific heat curve at high temperature which can be verified experimentally.

5.3.1 *Quantum Phase Diagram*

The QPD of the Hamiltonian in Eq. 5.1 is shown in $J_2/|J_1|$ and $J_3/|J_1|$ parameter space. The resulting phase diagram in Fig. 5.3 shows two distinct phases: the CS(SRO) and NC spin order. In small J_3 and $J_2 < 0.25$ limit, individual zigzag ladder retains the FM arrangement of spins; however, the spins on two different zigzag ladders are aligned antiparallelly with respect to each other. Therefore, the gs of the whole system has effective multiplicity $S^z = 0$. The spin-spin correlation decays exponentially along each zigzag chain. This phase can be called as CS (SRO) phase. As we increase J_3, the correlation length ξ decreases. The details of this phase have been discussed in the ref. [248]. At higher J_3 value, even for $J_2 < 0.25$, NC phase emerges but with small amplitude and ξ in spin spin correlation. For $J_2 > 0.25$, spiral
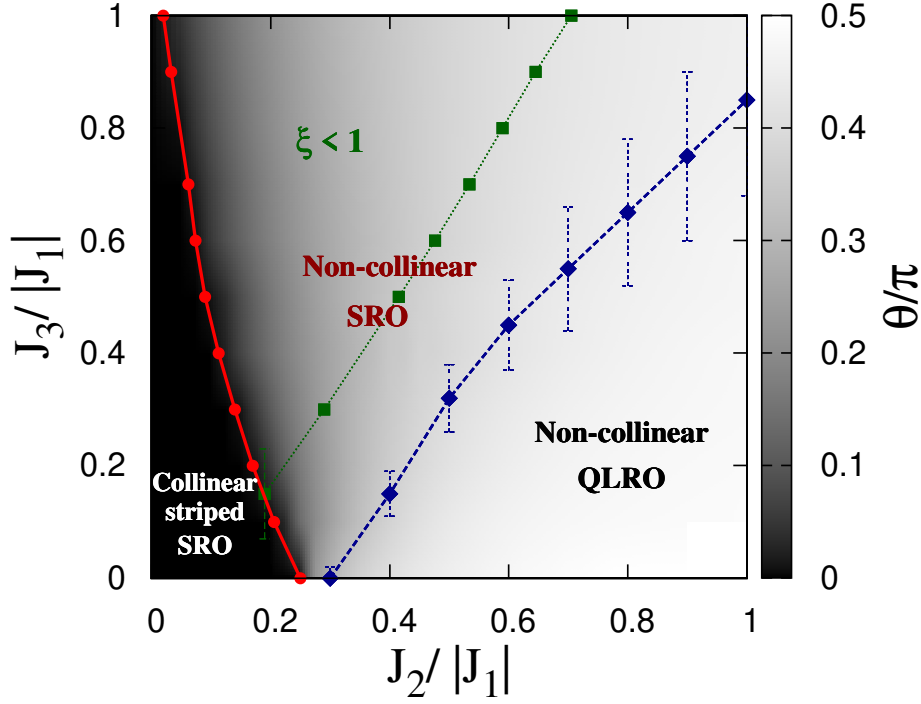
Figure 5.3: The QPD of the model Hamiltonian in Eq. 5.1 for $H = 0$: red solid line with circles represents the boundary between CS(SRO) and NC(SRO) phases. The green dotted line with square symbols in NC(SRO) regime represents the boundary line with $\xi \approx 1$. NC(QLRO) phase lies below the blue dashed line with diamonds. The color gradient represents the pitch angle θ distribution in the $J_2 - J_3$ parameter space.

arrangement of spins becomes more prominent for lower J_3. In the NC regime, C(r) is either QLRO (decay following power law) called as NC(QLRO), or SRO (exponentially decaying) called as NC(SRO) for the small or large J_3, respectively. The θ vanishes at the boundary between CS(SRO) and NC(SRO) phases. In Fig. 5.3, color gradient represents θ distribution in the parameter space. The red solid line with circles represents the boundary between CS(SRO) and NC(SRO) phases in the gs. The region above the green dotted line with square symbols represents the SRO phase where spin correlation length is confined to its neighbor i.e., $\xi \leq 1$. In the large J_3 limit, the correlation strength along rung dominates, and it tends to form singlet dimers along the rungs. The dimer phase is characterized by large energy gap, and the spin correlation is confined within the nearest neighbors ($\xi \leq 1$). Interestingly, for large J_2/J_3 limit the gs is in unique NC(QLRO) phase. To best of our knowledge, QLRO phase exits with pitch angle $\theta = \pi$ or $\frac{\pi}{2}$ [102, 103], whereas this system shows QLRO
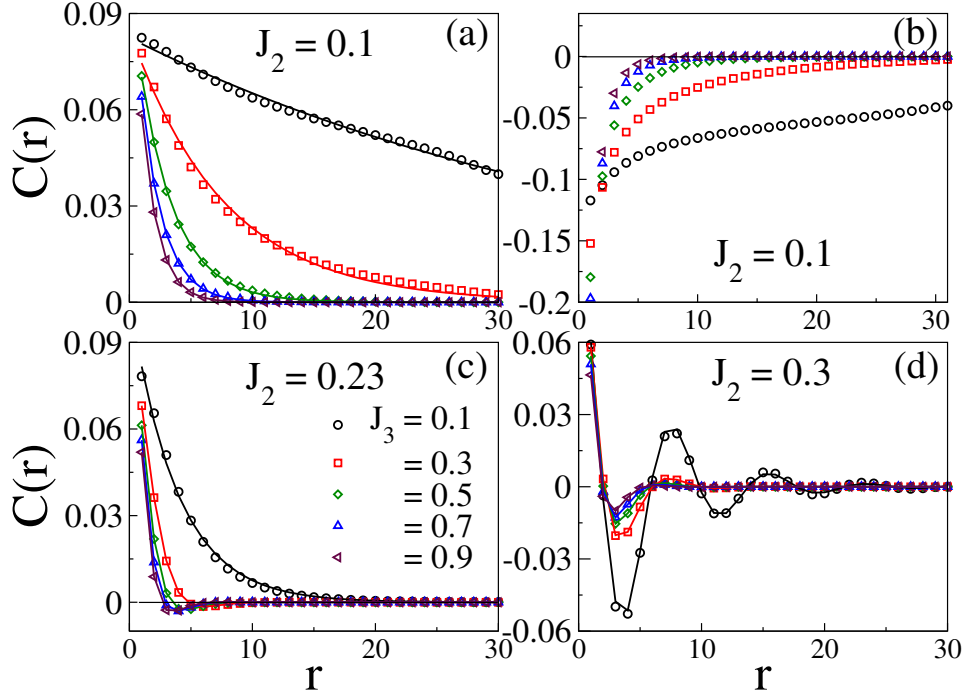
Figure 5.4: The longitudinal spin-spin correlation $C(r)$ are shown along the zigzag leg with the reference spin situated on same zigzag ladder in (a), whereas $C(r)$ on the other zigzag leg is shown in (b) for $J_2 = 0.1$ and five values of $J_3 = 0.1, 0.3, 0.5, 0.7$ and 0.9 with $N = 122$. In (c) and (d), $C(r)$ in the same zigzag leg are shown for $J_2 = 0.23$ and 0.3 with same five values of J_3. The solid lines represent respective exponential fits.

even with $\theta < \frac{\pi}{2}$. NC(QLRO) phase lies below the blue dashed line with diamond symbols. The phase boundary between NC(SRO) and NC(QLRO) phases has large error bar due to the inability to distinguish between the power law and exponential nature of $C(r)$ in this parameter regime. To verify these different phases $C(r)$, θ, ξ and $C(r = 1)$ are studied in detail in the next subsections.

5.3.2 *Spin-spin correlation C(r)*

We calculate the longitudinal spin-spin correlation $C(r) = < S_0^z S_r^z >$, where S_0^z and S_r^z are the z-component of the spin operators at the reference site 0 chosen at the middle of a zigzag chain and the site r at a distance r from 0th spin, respectively. In Fig. 5.1, the distance r is shown along the same zigzag ladder with bold numerics with respect to the reference site 0, whereas, normal numerics represent distances on the other zigzag leg. We note that in $J_2/|J_1| < \frac{1}{4}$ limit, all the spins are aligned parallelly on individual zigzag ladder and have
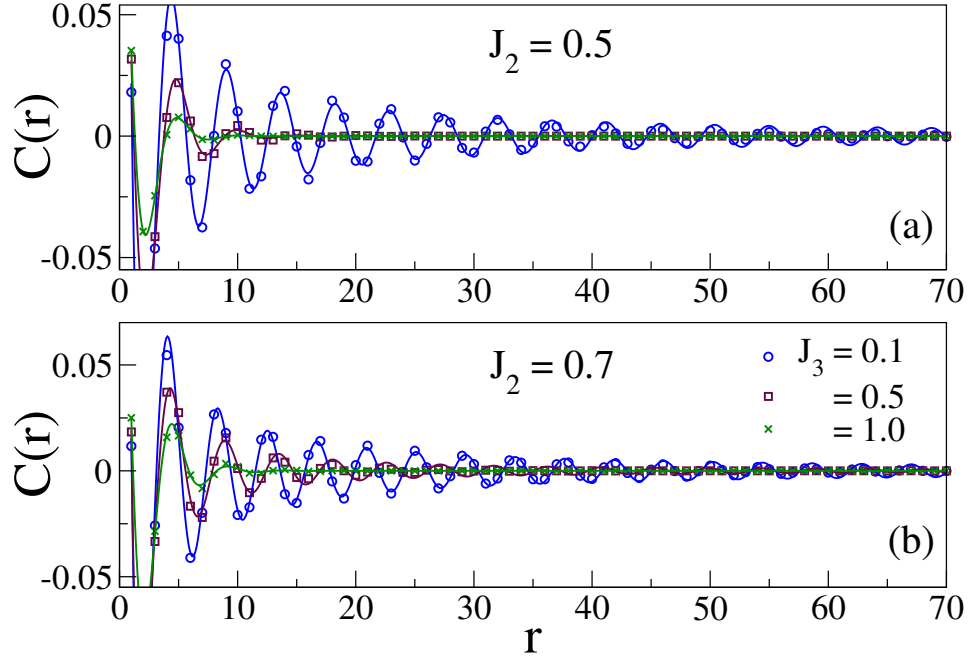
Figure 5.5: For three values of $J_3 = 0.1, 0.5$ and 1.0 with $N = 298$, $C(r)$ are shown in (a) and (b) for $J_2 = 0.5$ and 0.7, respectively. The solid curves represent respective sinusoidal fits with algebraic or exponential decay.

short range longitudinal correlation for finite J_3. $C(r)$ follows an exponential behavior as shown in the Fig. 5.4(a) for $J_2 = 0.1$, and $J_3 = 0.1, 0.3, 0.5, 0.7$ and 0.9. We notice that each zigzag ladder shows collinear arrangement of spins as $C(r) > 0$, but it decays exponentially with r i.e.,

$$C(r) \propto \exp\left(\frac{-r}{\xi}\right). \tag{5.2}$$

The fitting curve represents an exponential function with correlation length ξ. Fig. 5.4(b) shows the $C(r)$ of the same reference spin with the spins on the other zigzag leg. The negative values suggest anti-parallel arrangement of spins relative to the reference spin leg. This behavior of $C(r)$ confirms the stripe nature of spin arrangement on each zigzag ladder. Therefore, we call it collinear striped phase. The spin arrangement in CS(SRO) phase is shown in Fig. 5.2. On further increase in J_2, $C(r)$ starts to oscillate at higher J_3 even at the limit $J_2 < 0.25$. For $J_2 = 0.23$, C(r) is shown in Fig. 5.4(c) for the same set of J_3 values. We

note that NC(SRO) arises for $J_3 \geq 0.3$. While C(r) for $J_3 = 0.1$ is fitted by Eq. 5.2, C(r) for other J_3 can be fitted with the equation below,

$$C(r) \propto \exp\left(\frac{-r}{\xi}\right)\sin\left(\theta r + c\right).$$ (5.3)

The NC order can be easily noticed at lower J_3 for $J_2 > 0.25$. For $J_2 = 0.3$, C(r) is shown in Fig. 5.4(d) and fitted by Eq. 5.3. We note that ξ decreases with J_3. For moderate J_2, the NC phase follows SRO behavior, whereas it shows QLRO in the gs for higher $J_2 > 0.45$ but for small J_3. The transition between NC(SRO) to NC(QLRO) seems continuous, and hence it is difficult to find an accurate phase boundary. In QLRO regime C(r) is fitted with sinusoidal power law function written as

$$C(r) \propto r^{-\kappa}\sin\left(\theta r + c\right).$$ (5.4)

In Fig. 5.5(a) and (b), $C(r)$ are plotted for $J_2 = 0.5$ and 0.7, respectively, with $J_3 = 0.1, 0.5$ and 1.0. For $J_2 = 0.5$, and $J_3 = 0.1$, C(r) fits with power law in Eq. 5.4 where $\kappa \approx 1$, whereas C(r) follows exponential decay at $J_3 = 0.5$ and 1.0 with $\xi = 2.29$ and 1.56, respectively. For $J_2 = 0.7$, and $J_3 = 0.1$ and 0.5, C(r) decays algebraically with $\kappa = 1.15$ and 1.37, respectively, but exponentially for $J_3 = 1.0$ with $\xi = 1.99$. We notice that the width of the NC(QLRO) region increases with J_2.

5.3.3 *Pitch angle θ*

In the NC phase we calculate pitch angle θ from the fitting parameter in Eq. 5.3 and Eq. 5.4. θ/π is plotted as a function of J_2 for various values of J_3, as shown in Fig. 5.6. θ/π versus J_2 curves are fitted with function $\theta/\pi = a[1 - e^{b(J_2 - J_2^c)}]$, where a, b and J_2^c are the fitting parameters. J_2^c is the phase boundary point between CS(SRO) and NC(SRO) phases for a given J_2 and J_3. θ increases from 0 to $\pi/2$ with J_2. The $\theta \approx \pi/2$ region is confined to high J_2/J_3 limit. The variation of θ is represented by color gradient in the phase diagram in Fig. 5.3.
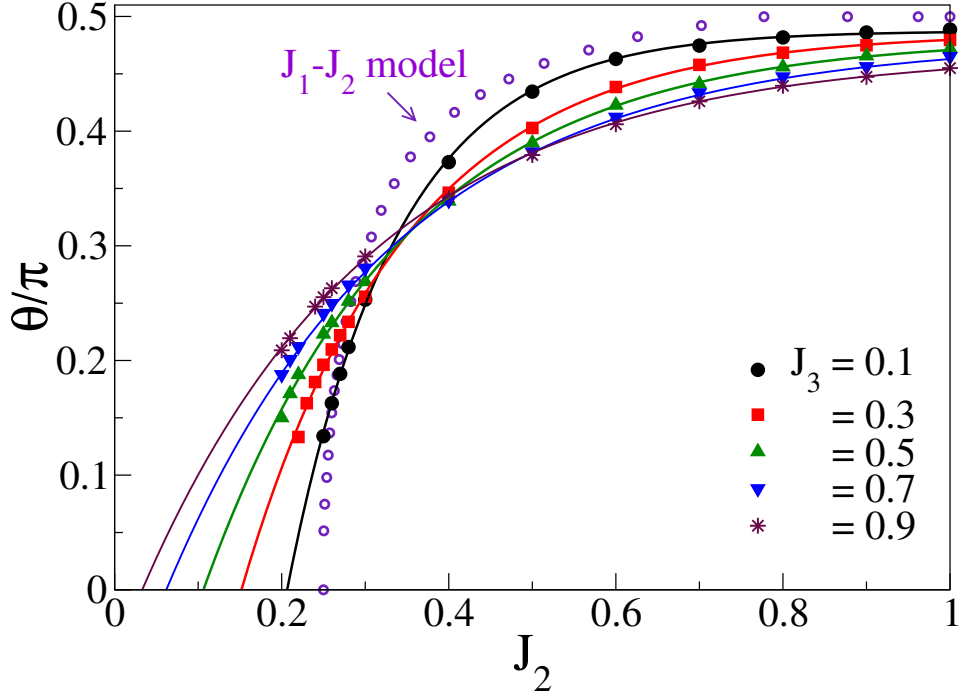
Figure 5.6: The variation of pitch angle θ with J_2 are shown for five values of $J_3 = 0.1, 0.3, 0.5, 0.7$ and 0.9. The open circles represent θ for $J_1 - J_2$ spin-1/2 model on a zigzag ladder with FM J_1 and AFM J_2.

5.3.4 Correlation length ξ

The correlation length ξ extracted from fitting Eq. 5.2 and Eq. 5.3 is a measure of correlation length in CS(SRO) and NC(SRO) phase, respectively. In CS(SRO) phase, ξ follows an algebraic decay with J_3 for a given J_2, as shown in the Fig. 5.7. At $J_2 = 0.15$, ξ is approximately 28.5 for $J_3 = 0.1$, however it decrease to 1.58 for $J_3 = 0.6$. ξ becomes less than 1 for $J_3 > 0.9$ for $J_2 = 0.15$, and in this parameter regime the system is completely dimerized along the rung. In NC(SRO) regime ξ are plotted as function of J_2 for $J_3 = 0.5, 0.6, 0.7, 0.8, 0.9$ in Fig. 5.8. The correlation length can be fitted by $\xi = c + dJ_2$, where c and d are the fitting parameters. We note that ξ increases with J_2/J_3. Higher value of J_2 needs more strength in J_3 to keep the same correlation length in NC(SRO) phase. Surprisingly, this behavior is completely opposite in the case of CS(SRO) phase, where higher J_2 requires lower J_3 to sustain the same correlation length. When $\xi \leq 1$, dominant correlation strengths become confined within the three nearest neighbors among which the rung bond correlation is dominant over other two bond strengths. In fact $\xi \leq 1$ represents the correlation length within nearest neighbor distance;
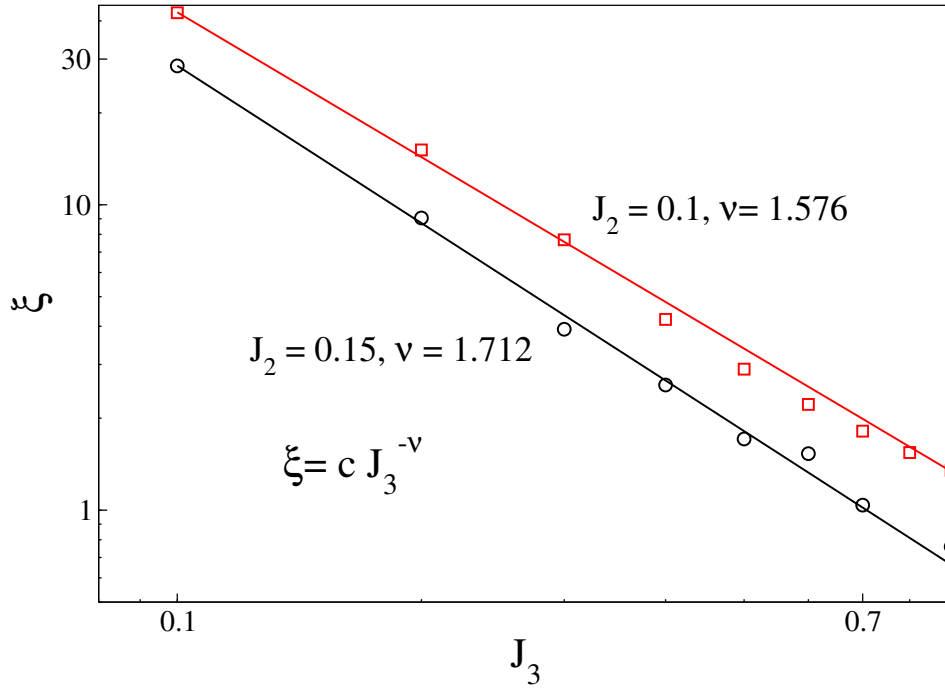
Figure 5.7: In CS(SRO) phase, the correlation length ξ vs. J_3 plots for $J_2 = 0.1$ and 0.15 in log-log scale. The solid lines represent respective power law fits.
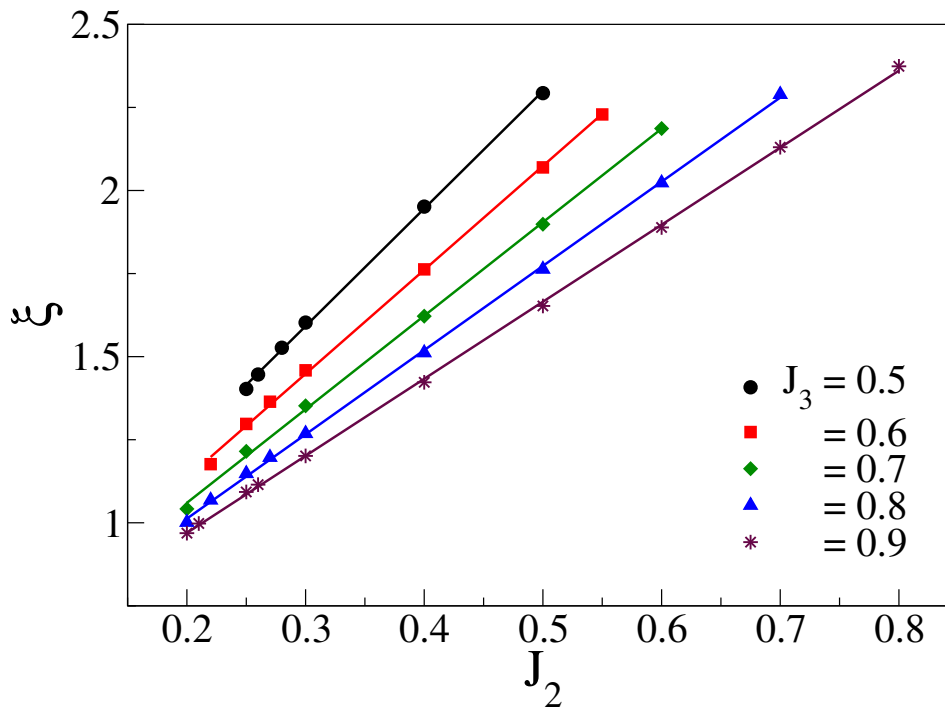
Figure 5.8: In NC(SRO) phase $\xi - J_2$ curves are shown for five values of $J_3 = 0.5, 0.6, 0.7, 0.8$ and 0.9. The solid lines represent respective linear fits.
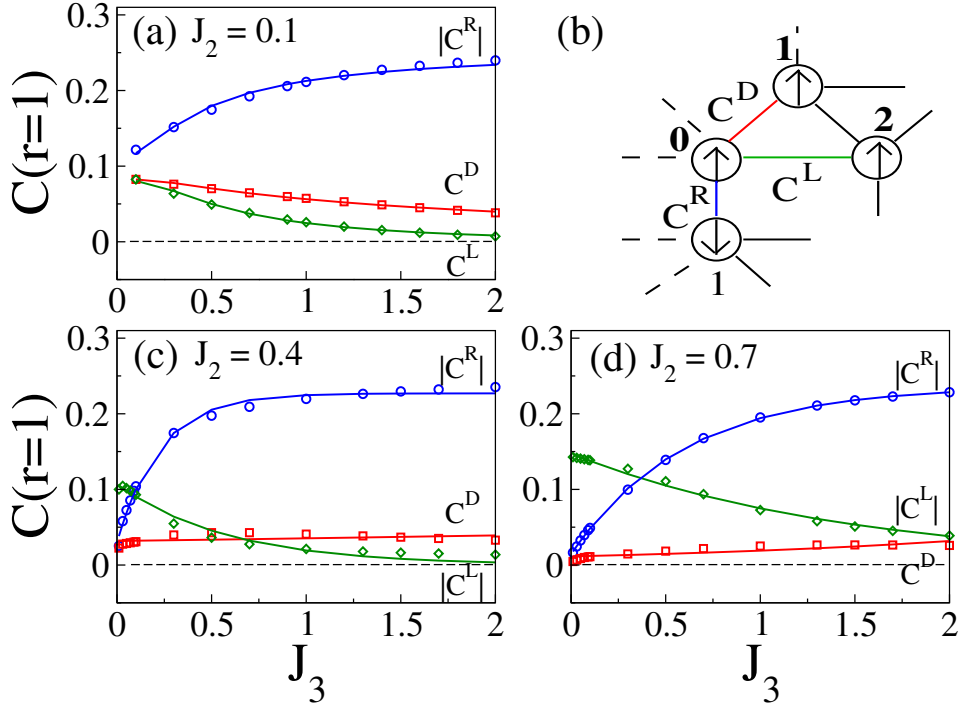
Figure 5.9: Nearest neighbor correlation function $C(r = 1)$ at the mid of zigzag ladder is shown. The $C(r = 1)$ along the rung (C^R, circle), diagonal direction (C^D, square), and leg (C^L, diamond) are shown in the schematic in (b). $C(r = 1) - J_3$ plots are shown for $J_2 = 0.1, 0.4$ and 0.7 in (a), (c) and (d), respectively. The lines represent respective exponential fits.

as per our convention of distance, both $r = 1$ and $r = 2$ are the nearest neighbors to the reference spin. In this limit, the system behaves like a collection of singlet rung dimers. The varying strength of nearest neighbor bond correlations depending on J_2 and J_3 are discussed in the next subsection.

5.3.5 *Nearest neighbor bond correlation $C(r = 1)$*

It is quite interesting to see the relative strength of nearest neighbor $C(r = 1)$ or longitudinal bond order in the parameter space. The magnitude of $C(r = 1)$ along the rung $|C^R|$, along the leg $|C^L|$, and along the zigzag leg C^D are shown for $J_2/|J_1| = 0.1, 0.4$, and 0.7 in Fig. 5.9(a), (c) and (d), respectively. The bonds along three directions are shown in the schematic Fig. 5.9(b). We notice that C^D and C^L have positive values for CS(SRO) phase whereas, C^L becomes negative for NC phase. In the NC phase $|C^L|$ is dominant for small J_3, but $|C^R|$ dominates for $J_3 > 0.08$ and 0.38 for $J_2 = 0.4$ and 0.7, respectively. The effect of J_3 on C^D is weak, and
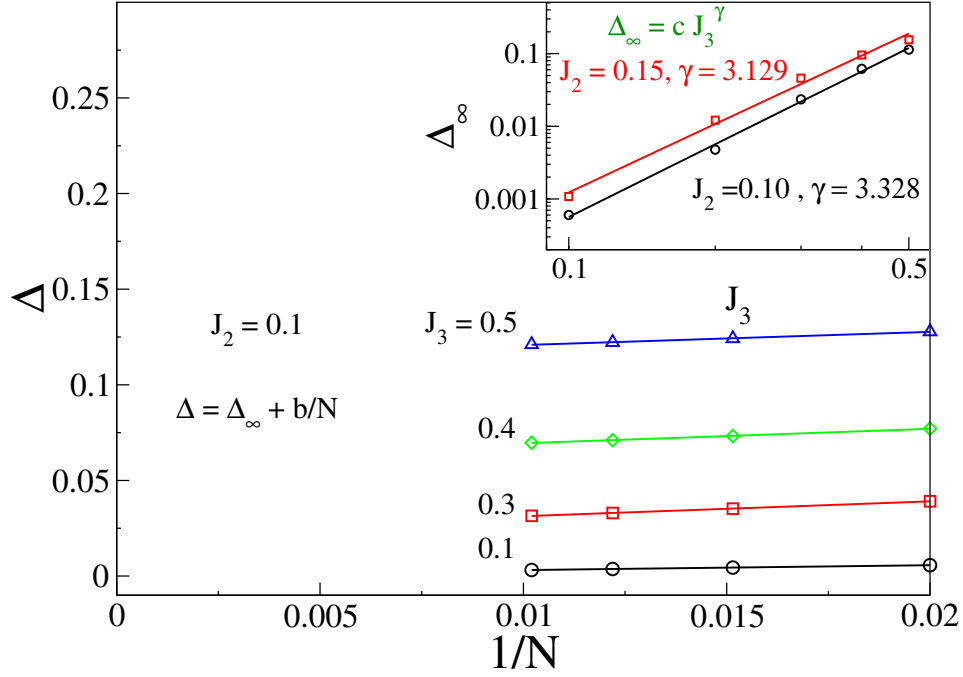
Figure 5.10: The extrapolation of spin-gap Δ with respect to system size N for different $J_3 = 0.1, 0.3, 0.4$ and 0.5 at $J_2 = 0.1$. The solid lines are the fitted curves. In the inset, the spin gap in thermodynamic limit, Δ_∞ vs. J_3 plots for $J_2 = 0.1$ and 0.15 are shown in log-log scale.

also the magnitude of C^D is small. Therefore, we can safely conclude that major contributions of energy come from $|C^R|$ and $|C^L|$ in NC phase. $|C^R|$ increases exponentially with J_3 and saturates to a value which is nearly equal to 0.25.

5.3.6 Spin gap

The correlation function $C(r)$ of the system shows the short range spin order in CS(SRO) phase. Therefore, we explore the excitation energy gap or spin gap in this phase. The rung interaction dominates other interactions; thus we expect the opening of the spin gap Δ. We calculate Δ for various $J_3 = 0.1, 0.3, 0.4$ and 0.5 at $J_2 = 0.1$. The main Fig. 5.10 shows the extrapolation of the spin gap Δ, from which we obtain the spin gap Δ_∞ in the thermodynamic limit. Δ_∞ increases algebraically with J_3, as shown in the inset of Fig. 5.10 for $J_2 = 0.1$ and 0.15. The algebraic exponent γ for $J_2 = 0.1$ and 0.15 are 3.33 and 3.13, respectively. We notice that γ decreases with increasing J_2. This may be due to the delocalization of magnon along the leg of zigzag ladder.

In the CS(SRO) phase spins on the same zigzag ladder are arranged ferromagnetically, whereas spins from different zigzag ladders are arranged antiferromagnetically to each other. We perform the linear spin wave analysis of the Hamiltonian for this phase. We use the Holstein-Primakoff transformation to the Hamiltonian in Eq. 5.1. The details of the calculation are given in appendix A.

The Hamiltonian can be written in terms of bosonic operators a_j, b_j, a_j^+ and b_j^+, where a_j/a_j^+ and b_j/b_j^+ correspond to spin up and spin down operators or spins on leg $l = 1$ and $l = 2$, respectively. We consider only up to quadratic terms. After Fourier transformation, the resultant Hamiltonian can be written as

$$
H = (2J_1 + 2J_2 - J_3)Ns^2 + \sum_k s[(2J_1(\cos k - 1)
$$
$$
+2J_2(\cos 2k - 1) + J_3)(a_k^+ a_k + b_k^+ b_k)
$$
$$
+J_3(a_k^+ b_{-k}^+ + a_k b_{-k})].
\tag{5.5}
$$

The above Hamiltonian can be transformed to diagonal form using the Bogoliubov transformation i.e.,

$$
a_k = uc_k - vd_k^+,
$$
$$
b_{-k}^+ = -vc_k + ud_k^+,
\tag{5.6}
$$

where $u^2 - v^2 = 1$, $u^2 + v^2 = \frac{J_k}{\sqrt{J_k^2 - J_3^2}}$ and $2uv = \frac{J_3}{\sqrt{J_k^2 - J_3^2}}$, and $J_k = 2J_1(\cos k - 1) + 2J_2(\cos 2k - 1) + J_3$. Applying Bogoliubov transformation, we get

$$
H = (2J_1 + 2J_2 - J_3)Ns^2
$$
$$
+ \sum_k \omega_k(c_k^+ c_k + d_k^+ d_k + 1),
\tag{5.7}
$$
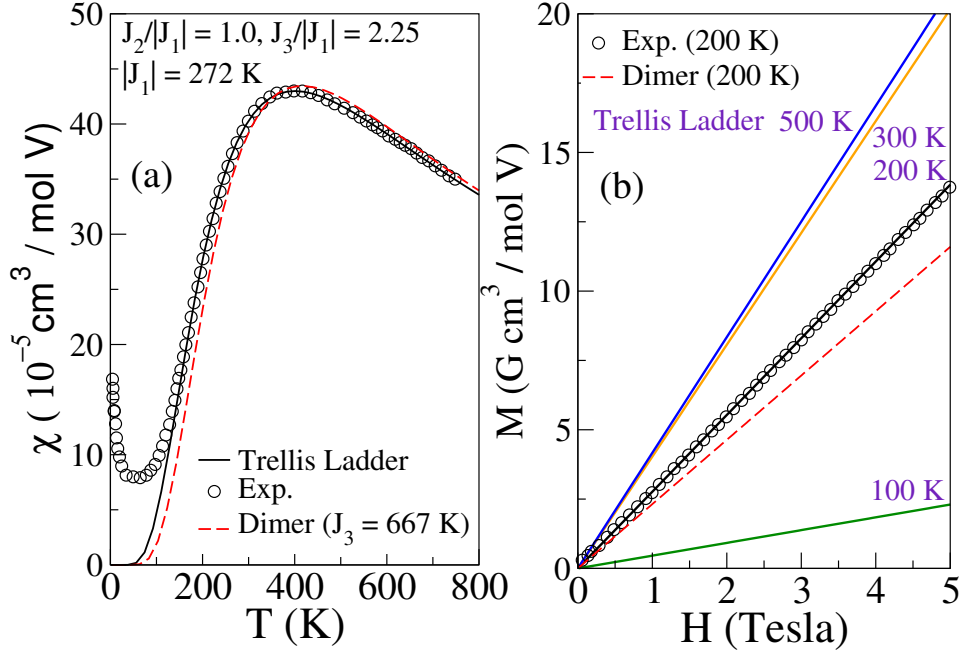
Figure 5.11: (a) Magnetic susceptibility χ as a function of temperature T for CaV$_2$O$_5$ sample 1 [249] is shown by the circles. Solid curve represents the fitted curve obtained by the trellis ladder model and dashed curve represents the fitted curve using dimer model. (b) Circles represent Magnetization M versus applied magnetic field H curve at $T = 200$ K for CaV$_2$O$_5$ sample 2 [249]. The black solid line is the fit using our model and dashed line represents the fit for a perfect dimer system at $T = 200K$. The fitting parameters are same as used to fit $\chi - T$ curve. The other $M - H$ plots for $T = 100K, 300K$ and $500K$ are shown by the solid lines using the model in Eq. 5.1.

where $\omega_k = S(\sqrt{J_k^2 - J_3^2})$.

The gs energy per bond is given by

$$\epsilon = (J_1 + J_2 - \frac{J_3}{2})S(S+1)$$
$$+ \sum_k \frac{s}{2\pi} \int_0^\pi \sqrt{J_k^2 - J_3^2}dk \qquad (5.8)$$

The ϵ can be minimized using $\frac{d\omega_k}{dk} = 0$ and we find these conditions; $\cos k = \frac{-J_1}{4J_2}$ and $\cos k = \frac{-J_1}{4J_2} \pm \frac{\sqrt{(J_1+4J_2)^2 - 4J_2J_3}}{4J_2}$. The second condition $J_3 \leq \frac{(J_1+4J_2)^2}{4J_2}$ for any real value of $\cos k$, gives the phase boundary between CS(SRO) and NC(SRO) phases. This boundary is similar to that found by DMRG calculation.
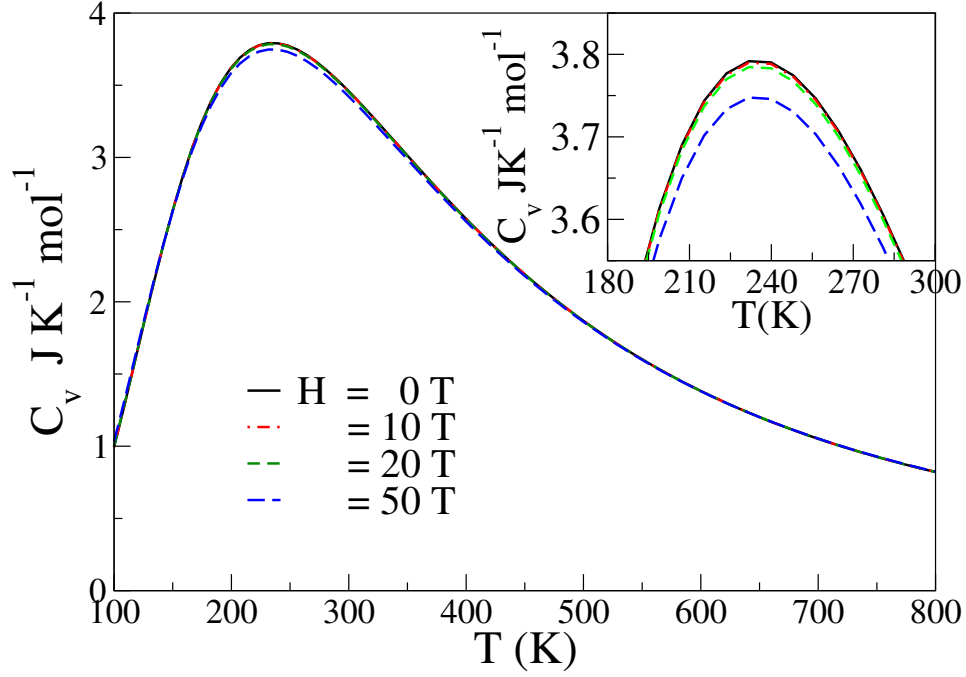
Figure 5.12: Specific heat $C_v(T)$ are plotted as function of T with $J_2/|J_1| = 1.0$, $J_3/|J_1| = 2.25$ and $|J_1| = 272K$ for $H = 0$, 10, 20 and 50 Tesla. The zoomed $C_v(T)$ near the peak are shown in the inset.

5.5 FITTING EXPERIMENTAL DATA OF CAV₂O₅

There are many vanadate compounds like CaV_2O_5, MgV_2O_5, NaV_2O_5 etc., which are suspected to behave effectively like two leg ladders coupled by zigzag bonds forming trellis lattice like structure. Among these materials the interladder coupling (J_1) in CaV_2O_5 is expected to be ferromagnetic. The LDA+U calculations performed by Korotin *et al.* [59] give an estimation of the J_1, J_2, and J_3 exchange interaction strengths as $-28K$, $122K$ and $608K$, respectively. In this compound, V^{4+} ions have one electron in d-orbital and behave like spin-1/2 ions. The experimental magnetic susceptibility $\chi(T)$ is taken from sample 1 and magnetization $M(H)$ is taken from sample 2 of ref. [249] which are represented by circles in Fig. 5.11(a) and (b), respectively. The dimer model fitting of susceptibility data deviates significantly from the experimentally observed data. The experimental data is shown as circle and dimer fit is shown by red dashed line in Fig. 5.11(a). The model Hamiltonian in Eq. 5.1 is used with $J_1 = -272K$, $J_2 = 272K$ and $J_3 = 612K$ to fit the experimental data of $M(H)$ and $\chi(T)$. The fitting curve of $\chi(T)$ shown by black solid curve is in excellent agreement with experimental data for $T > 160K$. As shown in Fig. 5.11(b) $M - H$ curve fitted with dimer

model shown by red dashed line is quite off at high H, whereas our model gives excellent fitting, as shown by the black solid line at $T = 200K$. We predict $M - H$ curve at other three different $T = 100, 300$ and $500K$. We notice the enhancement of M as a function of T, which is quite unusual. This behavior of $M - H$ curve can be understood in terms of large singlet-triplet gap. A moderate temperature enhances the possibility to reach higher magnetic state for a given field H.

We also predict the magnitude of specific heat C_v as a function of T for four values of magnetic field $H = 0, 2, 5, 10$ Tesla as shown in Fig.5.12. The C_v has broad peak at $T \approx 235K$. The effect of magnetic field H is small. The C_v decreases with H, but the suppression of C_v is visible only near the peak. Initially CaV_2O_5 was assumed to be only a dimer system with singlet-triplet energy gap $660K$ [250]. We use the model Hamiltonian in Eq. 5.1, and our fittings of $\chi(T)$ and $M(H)$ with same model parameters suggest that J_1 and J_2 are only 1/2 of J_3. It is found that our predicted values of J_1 and J_2 are significantly different from the predicted values in ref. [59], whereas the value of J_3 is similar with their calculated value by LDA+U method.

5.6 DISCUSSION AND CONCLUSIONS

In this chapter we have studied the isotropic Heisenberg spin-1/2 model, given in Eq. 5.1, on the trellis ladder. The QPD of this model is constructed. The phase boundaries of the QPD are calculated based on the correlation function $C(r)$, pitch angle θ and correlation length ξ using the DMRG method. Our linear spin wave analysis of this model predicts phase boundary of CS(SRO) and NC(SRO) phases, and it is quite consistent with our DMRG results. We also use this model to fit $\chi - T$ and $M - H$ data of CaV_2O_5, and understand the temperature T dependence of $M - H$ curves and magnetic field H dependence of $C_v - T$ curves.

In fact our lattice system can also be mapped to a two coupled $J_1 - J_2$ Heisenberg spin-1/2 chains. Zinke *et al.* studied the effect of interchain coupling J_3 on non-collinear phase in a coupled 2D array of $J_1 - J_2$ spin chains using the coupled cluster theory [137]. They

showed that the collinear to non-collinear transition point J_2^c increases with J_3. However, our model shows that the critical value J_2^c decreases with J_3. This inconsistency may be because of the confined geometry or ladder structure in our case. The J_2^c value at phase boundary of CS(SRO) and NC(SRO) phases decreases with J_3, and it can also be shown by linear spin wave analysis. As shown in Fig. 5.6, the variation of θ for $J_2 > 0.3$ decreases with J_3 and this trend is consistent with literature [137], and this may happen because of the deconfinement of quasi-particle along rung of the model. In Fig. 5.3 of QPD the majority of the parameter space is SRO phase; however, for small value of J_3/J_2, an incommensurate (QLRO) phase appears, which is quite unique in this ladder system. The $J_1 - J_2$ spin-1/2 zigzag model in similar parameter space shows either incommensurate (SRO) or decoupled phase [102, 123]. The QLRO in the system may be induced because of dominant effective anti-ferromagnetic interaction along the leg.

We apply this model to understand the magnetic properties of the CaV_2O_5, and have reliable fitting of the experimental data [249]. We apply a criterion of simultaneous fitting of both experimental $\chi - T$ and $M - H$ curves. Our best fit suggests that $J_2/|J_1|$ is close to 1, and J_1 is approximately $-272K$. For a given H, $M - H$ for this system increases with T, whereas in general magnetization decreases with increasing temperature. We notice that in a highly gapped system, higher T allows the system to access the higher magnetic states easily; therefore, it is much easier to magnetize this system at moderate temperature for a given H. Our calculated singlet-triplet energy gap is $459K$, whereas dimer model predicts it as $660K$. The modelling of $\chi(T)$ of CaV_2O_5 was done by Miyahara $et\ al.$ using QMC method, and they showed that small J_1 does not effect the magnetic $\chi(T)$, as shown in Fig.6 of ref. [156]. They estimated the value of $J_1 = 45K$, $J_2 = 67K$ and $J_3 = 672K$. Johnston $et\ al.$ treated this system as collection of dimers, and extracted the value of $J_3 = 667K$ with small J_1 and J_2 [249]. Korotin $et\ al.$ also calculated the value of $J_1 = -28K$, $J_2 = 122K$ and $J_3 = 608K$; however, their calculation also assumes other types of interactions [59]. Our simultaneous fitting of experimental $\chi - T$ and $M - H$ data also suggests it as dominant dimer with $J_3 = 612K$, but -J_1 and J_2 are only about half in magnitude of the J_3.

In summary, we study the QPD of model Hamiltonian in Eq. 5.1 on the trellis ladder. We show that J_3 plays an important role to localize the system. This system shows interesting

CS(SRO) and NC(QLRO) phases which is rare in ladder like structures. This model Hamiltonian is used to fit the experimental magnetic properties of CaV_2O_5 and we also show that the interaction J_1 and J_2 are much larger than earlier predicted values, and J_1 is ferromagnetic in nature. In many zigzag ladder systems like $LiCuVO_4$ [38], Li_2CuZrO_4 [41], Li_2CuSbO_4 [39] etc., where three dimensional ordering occurs at low T, this model can be applied to understand the effect of interladder coupling in the system. We have also predicted the $M - H$ and $C_v - T$ curve which can be verified experimentally.

For up spins the Holstein-Primakoff transformations take the form

$$S^z_{Aj} = s - a^+_j a_j,$$
$$S^+_{Aj} = \sqrt{(2s - a^+_j a_j)}a_j,$$
$$S^-_{Aj} = a^+_j \sqrt{(2s - a^+_j a_j)}, \tag{5.9}$$

For the down spin

$$S^z_{Bj} = -s + b^+_j b_j,$$
$$S^+_{Bj} = a^+_j \sqrt{(2s - a^+_j a_j)},$$
$$S^-_{Bj} = \sqrt{(2s - a^+_j a_j)}a_j, \tag{5.10}$$

We use the linear approximation at classical limit

$$S^z_{Aj} = s - a^+_j a_j,$$
$$S^+_{Aj} = \sqrt{2s}a_j,$$
$$S^-_{Aj} = \sqrt{2s}a^+_j, \tag{5.11}$$

for spin up, and for spin down

$$S^z_{Bj} = s - b^+_j b_j,$$
$$S^+_{Bj} = \sqrt{2s}b^+_j,$$
$$S^-_{Bj} = \sqrt{2s}b_j. \tag{5.12}$$

In terms of bosonic operators, the Hamiltonian takes the form up to quadratic order as

$$H = (2J_1 + 2J_2 - J_3)Ns^2 + \sum_j s[[J_1(a_j^+ a_{j+1} + b_j^+ b_{j+1})$$

$$+ J_2(a_j^+ a_{j+2} + b_j^+ b_{j+2}) + J_3 a_j b_j + h.c.]$$

$$- (J_1 + J_2)(a_j^+ a_j + b_j^+ b_j) - J_1(a_{j+1}^+ a_{j+1} + b_{j+1}^+ b_{j+1})$$

$$+ J_2(a_{j+2}^+ a_{j+2} + b_{j+2}^+ b_{j+2}) + J_3(a_j^+ a_j + b_j^+ b_j)]. \tag{5.13}$$

Fourier transforms of the bosonic operators are,

$$a_j = \sum_k \exp\{(-ikj)\} a_k,$$

$$a_j^+ = \sum_k \exp\{(ikj)\} a_k^+. \tag{5.14}$$

GROUND STATE PROPERTIES OF MIXED-SPIN(1,1/2) LADDER

6.1 INTRODUCTION

Many of spin-1/2 compounds like $CuCl_2.2N(C_5D_5)$ [35], $KCuF_3$ [36], $KCuGaF_6$ [37] and spin-1 compounds like $CsNiCl_3$ [62], $Ni(C_2H_8N_2)_2NO_2(ClO_4)$ [64], $Ni(C_5H_{14}N_2)_2N_3(PF_6)$ [65] etc. can be modelled by a simple Heisenberg model with nearest neighbor (NN) antiferromagnetic (AFM) exchange interaction. Bethe and Hulthén noted that the exact ground state (gs) of the one-dimensional (1D) spin-1/2 chain with NN AFM exchange interaction is a gapless state [91, 94]. In this model the spin correlation follows an algebraic decay with logarithmic corrections [95]. However, the spin-1 chain with NN AFM exchange interaction has a gapped gs. In fact, Haldane conjectured on the basis of field theoretical studies that the gs of integer-S chains are gapped, whereas the gs of half-integer-S chains are gapless [61]. A linear $S = 1$ chain has small correlation length $\xi \approx 6$ lattice unit [75]. The wave function of the gs of the $S = 1$ chain can be written in terms of valence bond solid (VBS) state [117]. This system possesses localized edge modes of spin-1/2, and the density matrix renormalization group (DMRG) studies of finite chains have confirmed the presence of edge states in integer-S chains [75].

We consider a two legged zigzag ladder system comprising spin-1 and spin-1/2 legs. Spins on each leg are interacting with AFM exchange interaction; however, these two legs interact with each other through a zigzag like exchange interaction J_1 which can be either ferro- or antiferromagnetic in nature. The zigzag bonds can be dimerized with amplitude δ, and the spin-1 and spin-1/2 leg can have their exchange strength J_2x and $J_2(1 - x)$, respectively, as
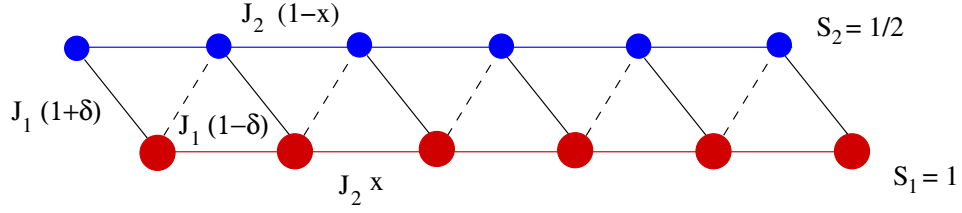
Figure 6.1: Mixed spin ladder with alternate bond interaction is shown. The dimerization δ is along the zigzag bond. The exchange interaction strengths in spin-1 and 1/2 legs are $J_2 x$ and $J_2(1-x)$, respectively.

shown in Fig. 6.1. As mentioned above an individual spin-1 chain behave very differently from a spin-1/2 chain, but the gs properties of this combined system are still not well understood. Note that this system can be treated as mixed spin chain in large J_1 limit.

The studies of mixed spin chains containing two kinds of spins sitting next to each other have attracted much attention due to recently synthesized chain materials like $NiCu(pba)(H_2 O)_3 2H_2 O$ with $(S_1, S_2) = (1, 1/2)$, $ACu(pbaOH)(H_2 O)_3 nH_2 O$, where $A \equiv Ni, Co, Fe, Mn$ with $(S_1, S_2) = (1, 1/2), (3/2, 1/2), (2, 1/2), (5/2, 1/2)$, respectively [251]. According to Lieb-Mattis theorem [119], the mixed spin chains exhibit a ferrimagnetic gs with total spin $S = (N/2)(S_1 - S_2)$, where $N/2$ is the total number of unit cells. A number of studies on mixed Heisenberg chains have been done quite extensively. The linear spin wave theory (LSWT) and density matrix renormalization group (DMRG) calculations show that the correlation length in spin correlation reduces to $\xi \approx 1.44$ for a mixed spin chain with $S_1 = 1$ and $S_2 = 1/2$ [120]. The inclusion of next nearest neighbor (NNN) interaction and bond alternating NN interaction makes the physics more interesting. The frustration induced due to the NNN interaction in a mixed spin chain provides quantum phase transition from ferrimagnetic to non-magnetic state as predicted by Ivanov *et al.* using LSWT and DMRG calculations [121]. In this chapter, we have shown the effect of the parameters δ and x on ferrimagnetic to non-magnetic phase transition point.

When $\delta = 1$, the zigzag ladder shown in Fig. 6.1 reduces to a mixed spin normal ladder. The ladder with $S_1 = 1$ and $S_2 = 1/2$ legs behaves effectively like $S = 3/2$ Heisenberg chain for strong ferromagnetic (FM) rung coupling, whereas the equivalence of this system with antiferromagnetic rung coupling is not clear yet [252]. The phase diagram of this mixed spin ladder has been constructed with both columnar bond alternation and staggered bond alternation along the legs by Languri et al. [253]. We have studied the effect of FM or AFM

rung coupling (provided $\delta = 1$) on the energy gap, spin density and spin correlation of individual legs.

This chapter is organized in four sections. In Sec. 6.2, we present the Hamiltonian and numerical method. The results are explained in Sec. 6.3. An conclusion has been drawn in Sec. 6.4.

6.2 MODEL HAMILTONIAN AND NUMERICAL METHOD

We consider a 1D dimerized spin ladder made of spin $S_1 = 1$ and $S_2 = 1/2$ chains. The zigzag (NN) interactions are $J_1(1 + \delta)$ and $J_1(1 - \delta)$ for odd and even bonds, respectively. The interaction between the spins on spin-1 leg is $J_2 x$ and on spin-1/2 leg is $J_2(1 - x)$, respectively. The system is represented schematically in Fig. 6.1. A general model Hamiltonian for this system can be written as

$$H = J_1 \sum_{i,\nu}(1 + 2\nu\delta)\mathbf{S}_{1,i} \cdot \mathbf{S}_{2,i+\nu} + J_1 x \sum_{i,\nu}\mathbf{S}_{1,i} \cdot \mathbf{S}_{1,i+1} + J_2(1 - x)\sum_{i,\nu}\mathbf{S}_{2,i} \cdot \mathbf{S}_{2,i+1}, \qquad (6.1)$$

where $\nu = \pm 1/2$.

When $J_2 = 0$ the model becomes a simple ferrimagnetic chain with NN interaction $J_1 = J$ for $\delta = 0$, and a dimerized ferrimagnetic chain with NN alternate interaction $J_1(1 \pm \delta)$ for non-zero δ. When $x = 1/2$ and $\delta = 1$, the system reduces to a mixed spin normal ladder system. We have considered two cases: (I) When $x = 1/2$ and $\delta = 1$, we study the influence of both FM and AFM rung coupling J_1 on the energy gap, spin density and spin correlation on individual legs. In this limit we define a parameter $\alpha = 4|J_1|/J_2$. (II) For various values of x and δ, we find the critical point of $\alpha' = J_2/J_1$, where ferrimagnetic to non-magnetic phase transition occurs. All the calculations in this chapter is based on the DMRG method. We have used $m = 300$ to get accurate results.

As we discussed earlier, the individual spin-1 and spin-1/2 chains have quite distinct behaviors, and now we consider a situation where spin-1 and -1/2 spin chains are coupled with each other with either FM or AFM interaction. In this system, we can ask following questions: 1) what happens to quasi-long range order and gapless excitation of spin-1/2 chains ? 2) What happens to short range correlation and edge states in spin-1 ? 3) How do the gaps of the system change with the inter-chain interaction? Is the VBS theory still valid ? 4) What happens to ferrimagnetic to non-magnetic phase transition point for a mixed spin chain with NNN interaction when we consider dimerized NN bonds? To answer these questions we first calculate various gaps, spin densities and spin correlation. Initially, we keep $x = 1/2$ and $\delta = 1$.

6.3.1 *Energy Gaps*

In the decoupled or small α limit the energy gap is similar to the sum over the energy gaps of the two separate spin-1 and spin-1/2 AFM chains. Now according to Haldane's conjecture spin-1 chain has finite energy gap, while spin-1/2 chain has gapless excitation. There are also spin-1/2 edge modes in spin-1 chain with open boundary condition (OBC). The singlet-triplet gap in spin-1 open boundary chain vanishes in the thermodynamic limit. Therefore, to understand the effect of α, a study of energy gaps with system size is important.

Now let us first focus on the energy gaps when J_1 is AFM. We calculate the low lying spin excitation energy gaps for different interaction strength between α. We calculate low spin excitation gaps defined as

$$\Gamma_n(\alpha, N) = E_0(\alpha, N, S^z = n) - E_0(\alpha, N, S^z = 0).$$ (6.2)

E_0 is the lowest energy state in a given $S^z = n$ sector. In the decoupled limit i.e., for $\alpha = 0$, we get two separate spin-1/2 and spin-1 chains. Therefore, the gs is a singlet state and the total energy is equal to the sum of the gs energies of individual spin-1/2 and spin-1 chains.

Table 6.1: Values of various exponent and constants are evaluated from the fitting of the $\Gamma_1(\alpha, N)$ shown in Fig. 6.2(a) using Eq. 6.3

α	A	ξ	B	γ
0.02	0.719	5.638	0.141	0.992
0.04	0.765	5.163	0.068	0.410
0.06	0.821	4.457	0.136	0.422
0.08	0.981	3.633	0.245	0.485
0.20	0	–	0.800	0.642
0.30	0	–	1.13	0.704
0.40	0	–	1.39	0.744

At $S_z = 1$ sector the lowest energy will be the sum of the gs energy $E_0(S_z = 0)$ of spin-1/2 chain and the $E_0(S_z = 1)$ of spin-1 chain in the thermodynamic limit. At the $S^z = 2$ sector the lowest energy arises from $E_0(S^z = 1)$ of both the chains. The energy gap $\Gamma_1(0, N)$, defined in Eq. 6.2, decays exponentially with system size for spin-1 OBC chain as shown in Fig. 6.2(a). The exponentially decaying energy gap is a signature of the presence of the edge modes. On the other hand, $\Gamma_1(0, N)$ decays following power law with system size for a spin-1/2 chain. Hence, the nature of energy gaps with system size will have contribution from both the in spin-1/2 and spin-1 chains and we expect,

$$\Gamma_2(0, N) = A \exp(-(N/2)/\xi) + B/(N/2)^\gamma. \tag{6.3}$$

The energy gaps $\Gamma_1(\alpha, N)$ and $\Gamma_2(\alpha, N)$ for AFM J_1 are shown in Fig. 6.2(a) and (b), respectively. For reference we have also put the lowest excitation for $S = 1$ and $1/2$ spin chains. In Fig. 6.2(a) the exponential part dominates for small α. All curves for $\alpha > 0.3$ follow power law decay. For different α the values of coefficients A, B, ξ, γ are shown in the Table 6.1. In Fig. 6.2(b), power law dominates in $\Gamma_2(\alpha, N)$ even for small α.

Now let us study the low spin excitation energy gap $\Gamma_1(\alpha, N)$ for FM J_1. For very small α (i.e., in the decoupled limit) the energy gaps have contribution from both the legs, therefore, the energy gaps follow the Eq. 6.3. Fig. 6.3 shows energy gaps for different values of FM α. For $\alpha > 0.3$ the energy gaps follow a power law decay. Moreover, for very large α, $\Gamma_1(\alpha, N)$ behaves similar to that in a $S = 3/2$ chain scaled by factor 0.6. Fig. 6.3(b) shows the energy gap $\Gamma_2(\alpha, N)$ with FM α. In this case the effect of the spin-1 leg i.e., the contribution of the
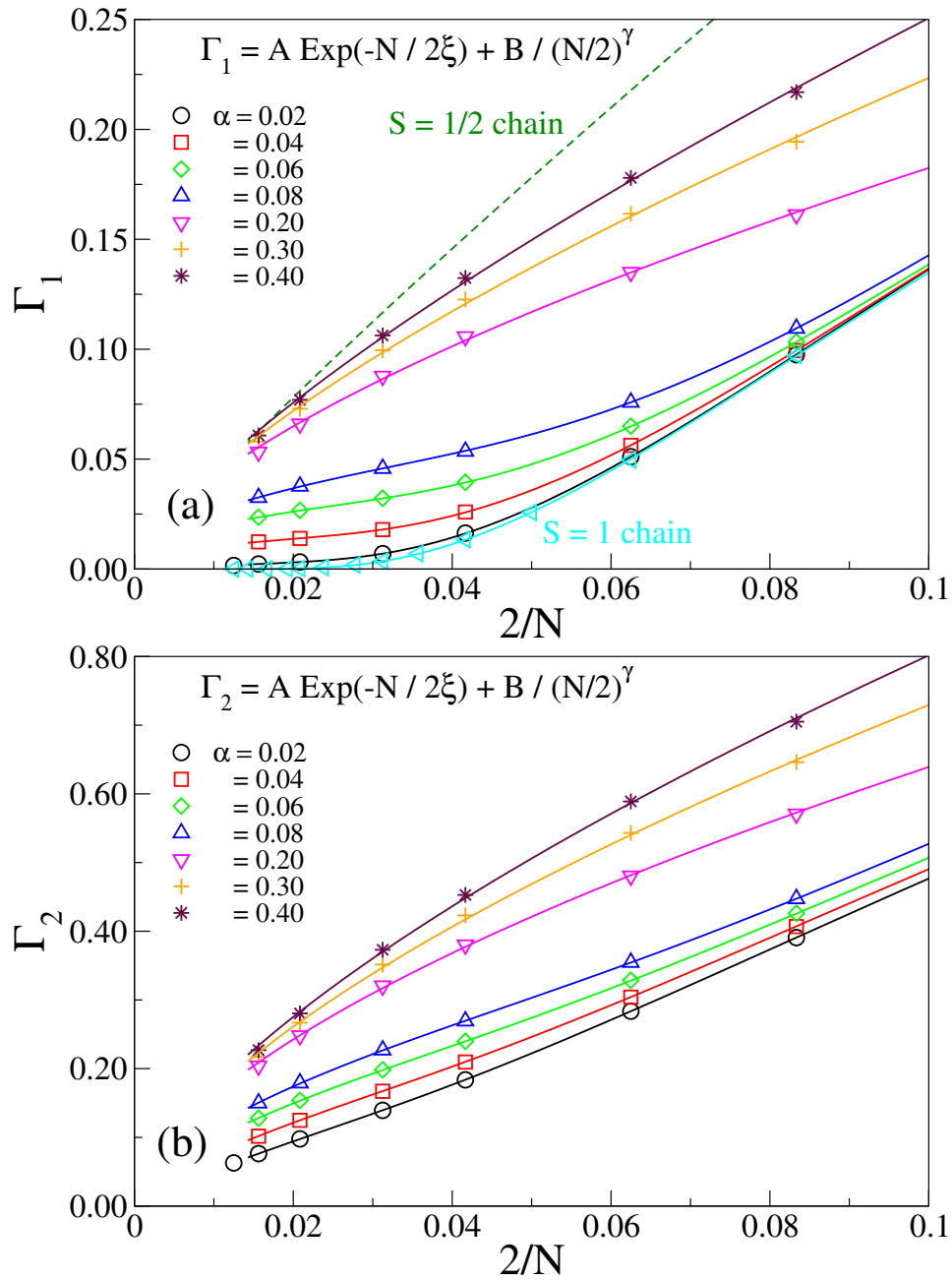
Figure 6.2: (a) The upper panel shows the energy gap $\Gamma_1(\alpha, N)$ for different α, for AFM J_1. (b) The lower panel shows the energy gap $\Gamma_2(\alpha, N)$ for different α, for AFM J_1. For small $\alpha (< 0.1)$ the exponential part is appreciable. For $\alpha > 0.1$ the gaps follow only power law decay.
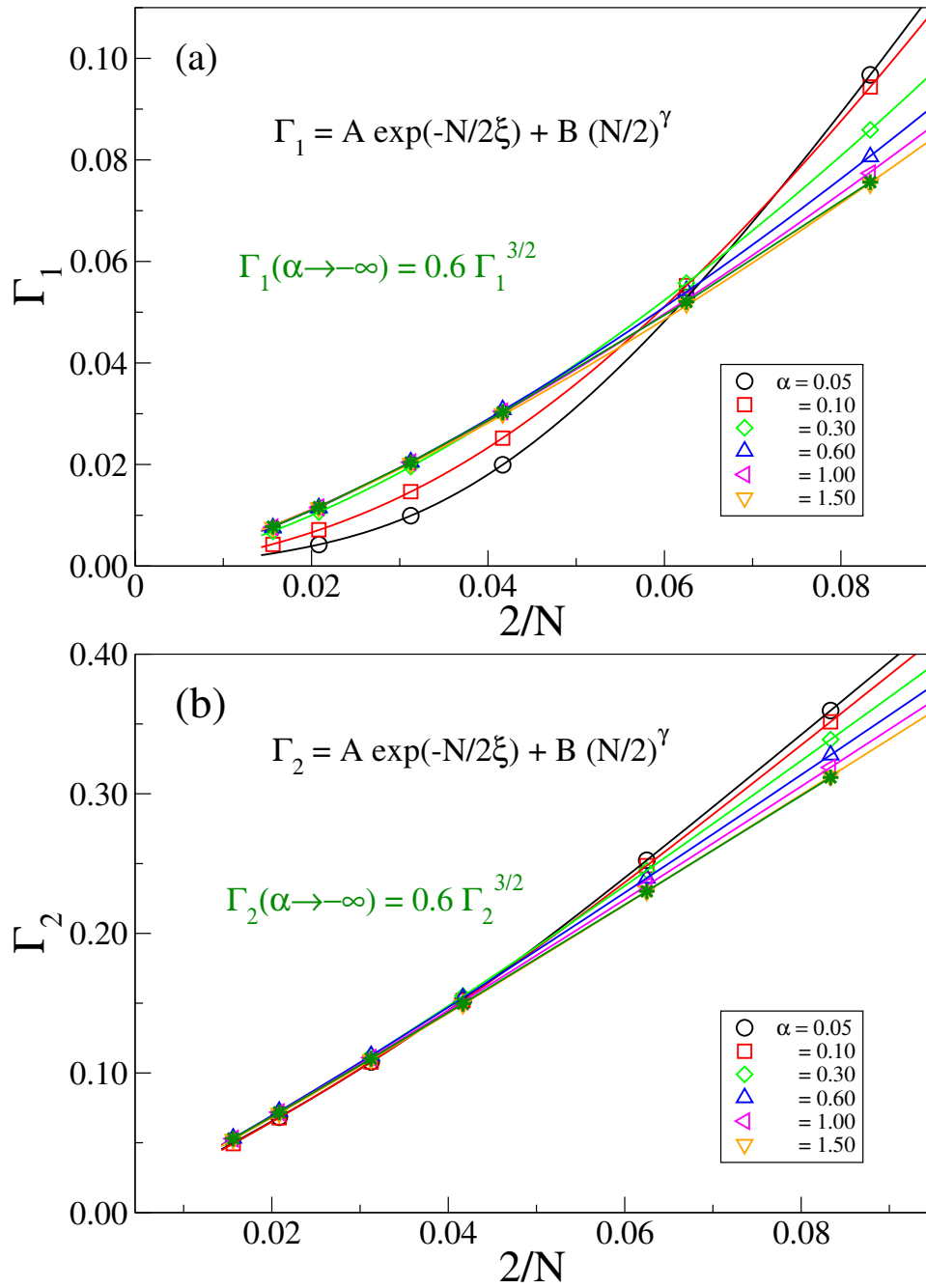
Figure 6.3: (a) The upper panel shows the energy gap $\Gamma_1(\alpha, N)$ for different α for FM J_1. (b) The lower panel shows the energy gap $\Gamma_2(\alpha, N)$ for different α for FM J_1.

exponential behavior to the energy gap is small even for $\alpha \to 0$. At very large α the energy gap $\Gamma_2(\alpha, N)$ follows the same behavior as that in a $S = 3/2$ chain, where we need to scale $\Gamma_2(\alpha, N)$ of the $S = 3/2$ chain by a factor 0.6. Next, we study the spin densities at each legs to understand how the system behaves with different coupling.

6.3.2 *Spin densities*

The spin densities at each site r is defined as

$$\rho(r) = \langle S_r^z \rangle. \tag{6.4}$$

There are two rungs at the middle of the ladder with even number of rungs. One of the middle rung is considered as the reference for the spin-density calculations. We plot the spin densities in the $S^z = 1$ sector on each leg separately. Fig. 6.4(a) and (b) show spin densities on the spin-1 and spin-1/2 leg of the system, respectively, for the AFM J_1. From Fig. 6.4(a), it is clear that the spin densities at very small $\alpha(= 0.02)$ coincide with the spin densities of a spin-1 HAF chain, and it shows the presence of the edge states. With an increase in α the edge states slowly die out and the behavior of the spin densities become similar to that of a spin-1/2 HAF chain scaled by a factor of 1.6, for very large α.

Now let us consider the system with FM J_1. We notice that spin densities for $\alpha > 0.3$ have similar profile for all larger α. In Fig. 6.5(a) and (b) the spin densities are shown for $S_z = 1$ sector. The spin densities in each leg behaves very similar to the spin-3/2 chain.

6.3.3 *Spin-spin correction*

The spin-spin correlation at a distance r with respect to a reference spin is defined as

$$C(r) = \langle S_0^z S_{i+r}^z \rangle, \tag{6.5}$$

In the spin-1/2 chain $C(r)$ follows a power law decay with distance r with a logarithmic correction, while in the spin-1 chain $C(r)$ follows an exponential decay with r. We first
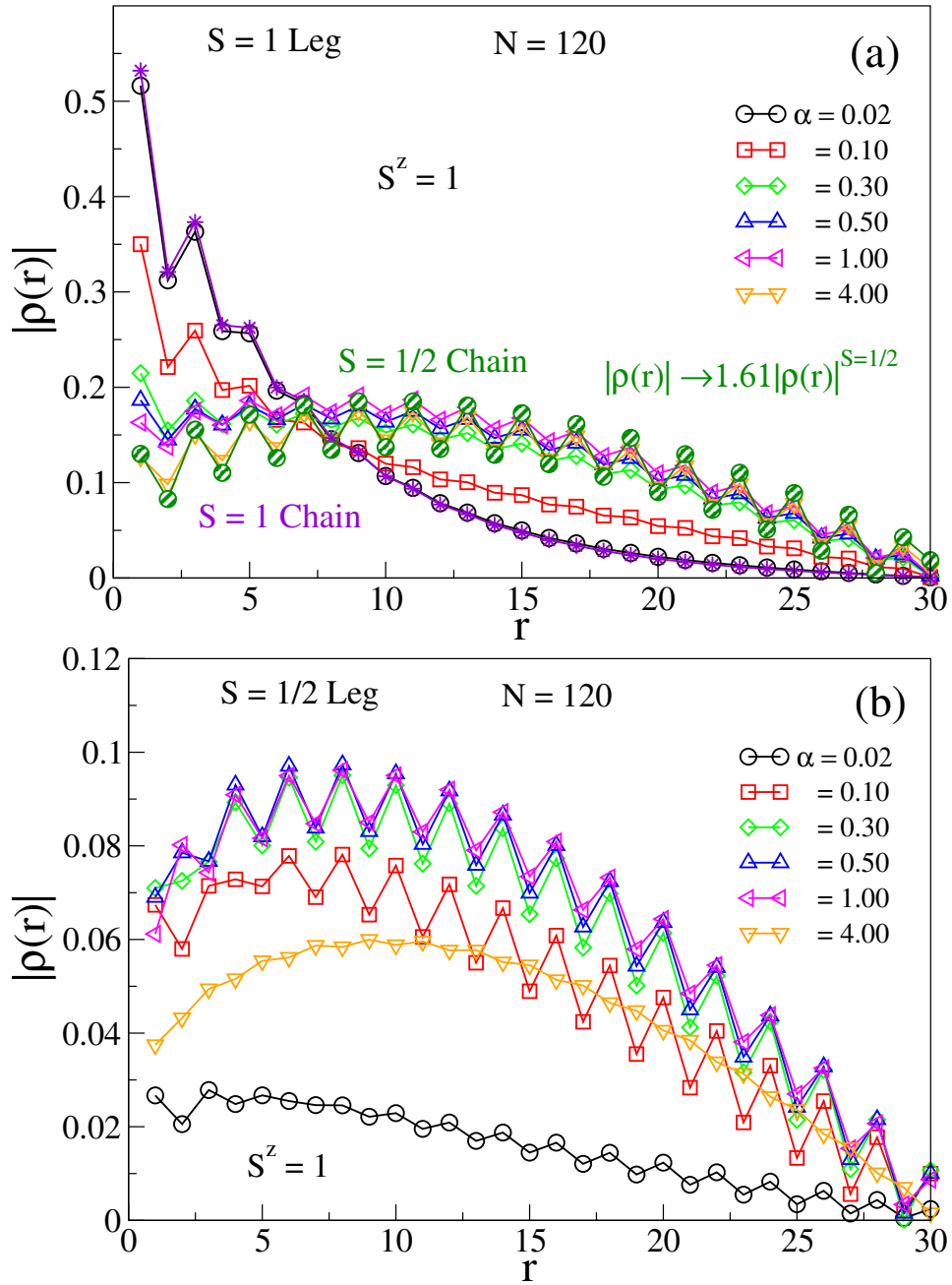
Figure 6.4: (a) The magnitude of spin densities on the spin-1 are shown in upper panel and (b) for spin-1/2 leg, spin densities are shown in lower panel for AFM J_1.
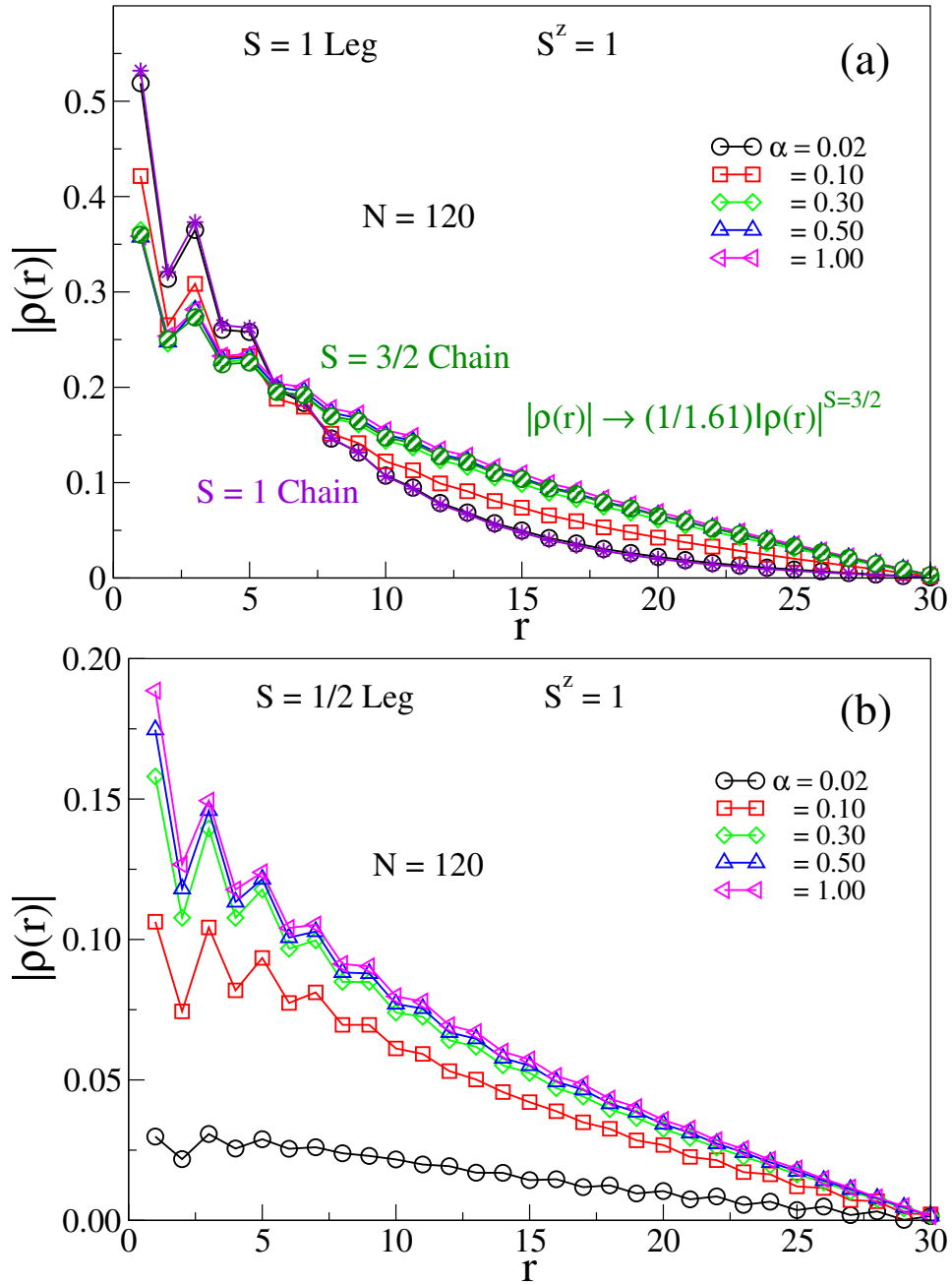
Figure 6.5: (a) The magnitude of spin densities on the spin-1 are shown in upper panel and (b) for spin-1/2 leg, spin densities are shown in lower panel for FM J_1.

consider the AFM J_1 and notice that correlations in the spin-1 leg for very small $\alpha(=0.02)$ agrees with the correlations in $S = 1$ HAF chain up to 2/3 of the chain length as shown the Fig. 6.6(a). $C(r)$ becomes similar to the $S = 1/2$ HAF chain for large α. $C(r)$ of spin-1 chain is similar to spin-1/2 chain with a scaling factor 4.2 in large α limit. For small $\alpha(=0.02)$ the correlations in spin-1/2 leg of the mixed spin ladder agrees with the correlations in $S = 1/2$ HAF chain as shown in the Fig. 6.6(b). Also in large α limit, $C(r)$ of the spin-1/2 leg behaves similar to an individual spin-1/2 chain and need a scaling factor 0.75 to that of spin-1/2 chain.

Now let us examine the system with FM J_1. In this limit C(r) is shown in Fig. 6.7. $C(r)$ along the spin-1 leg is shown in Fig. 6.7(a) while the same along the spin-1/2 leg is shown in Fig. 6.7(b). The correlations in both the legs behave similar to the $S = 3/2$ HAF chain for large α. The correlations in both the legs for $\alpha = 2.0$ are matched with $C(r)$ of $S = 3/2$ HAF chain after required scaling. We also note from Fig. 6.6, the correlations first increase and then decrease with increase in α in both the legs. Moreover, $C(r)$ always increase with α with FM J_1 as shown in Fig. 6.7.

Now we will vary x and δ to find the transition of the ferrimagnetic to non-magnetic phase. In Fig. 6.8 the transition points are shown on x-α' plane, for various values of δ. Here α' is defined as the ratio J_2/J_1. The inset shows the scaling for different δ. The scaling parameter $\beta(\delta)$ follows the relation $1/\beta(\delta) = 0.029 + 1.1(1 - \delta))$. We notice that phase boundary α_c decreases with increasing δ.

6.4 DISCUSSIONS AND CONCLUSIONS

In this work we studied a system of mixed spin ladders. we notice that for $\delta = 1$ and $x = 1/2$ limit, the system possesses interesting behavior. For AFM J_1, in the weak coupling limit of α, the system behaves like two decoupled chains. However, in the large α limit the system behaves like an effective spin-1/2 chain. The edge modes for $S = 1$ system disappear for $J_2 > 0.02$. However, the exact transition from decoupled to $S = 1/2$ is still not understood. For FM J_1 the system behaves quite similar to the decoupled phase like that for AFM J_1 at
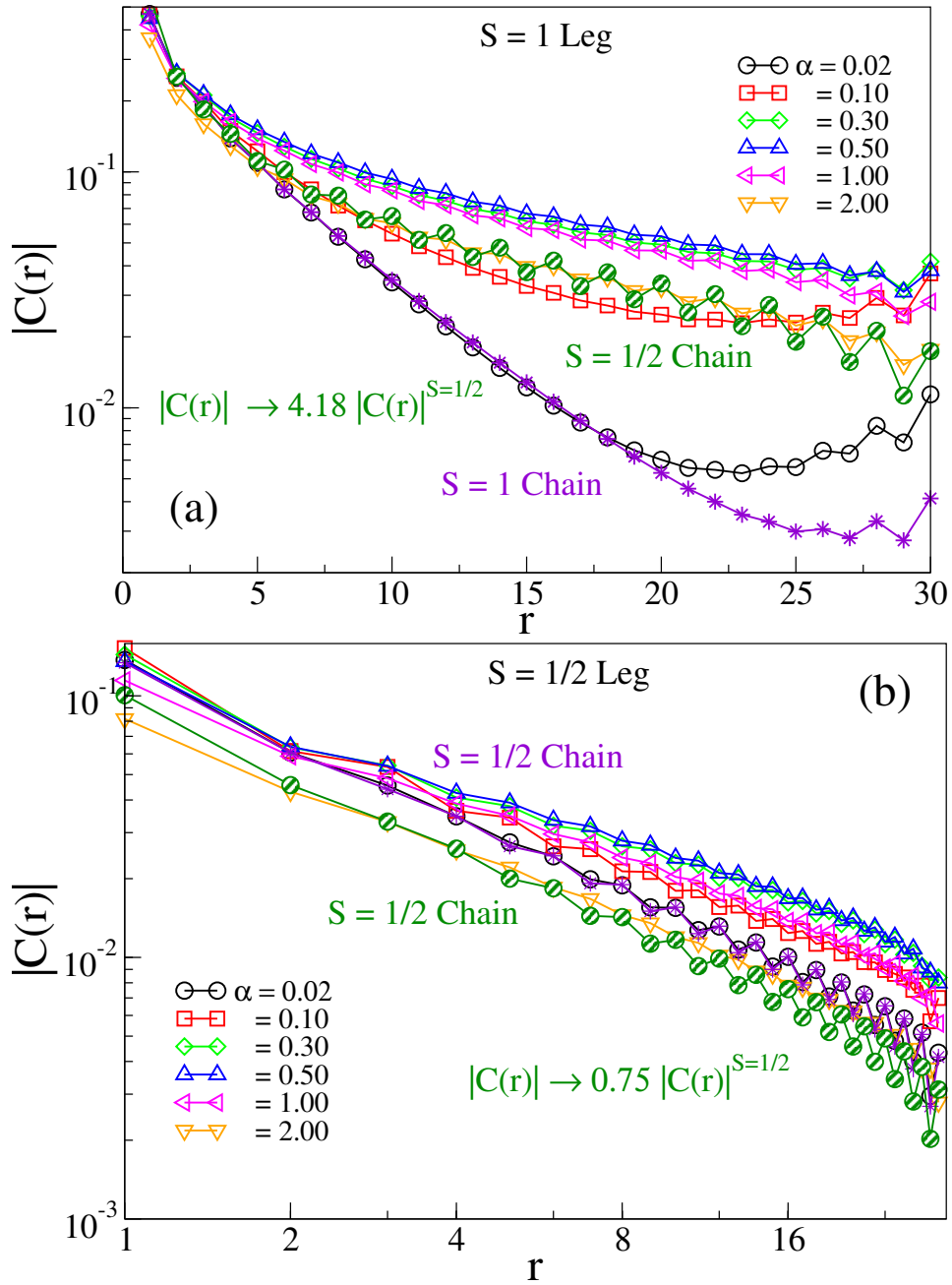
Figure 6.6: (a) The spin-spin correlations on the spin-1 are shown in upper panel and (b) for spin-1/2 leg, spin-spin correlations are shown in lower panel for AFM J_1.
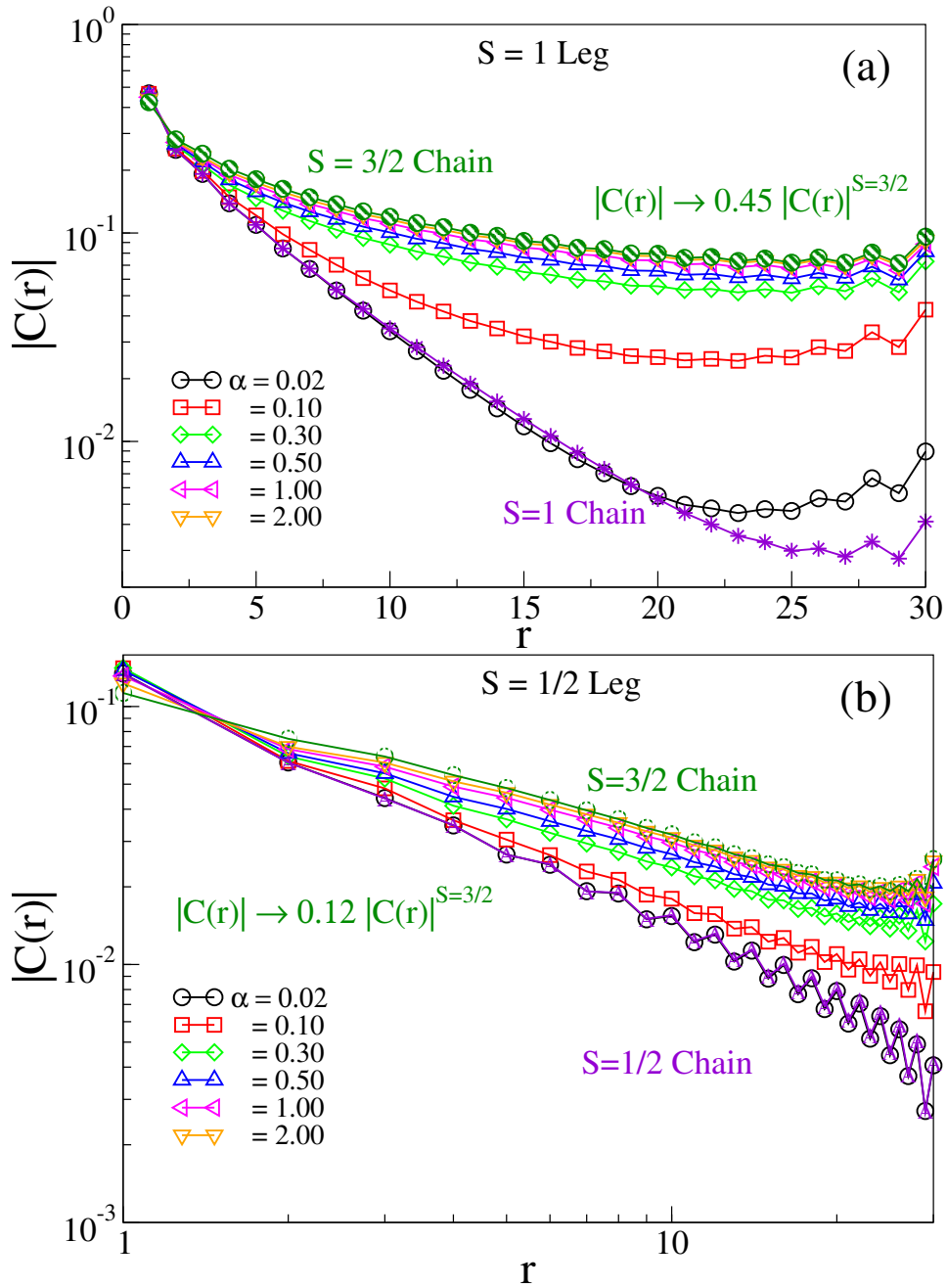
Figure 6.7: (a) The spin-spin correlations on the spin-1 are shown in upper panel and (b) for spin-1/2 leg, spin-spin correlations are shown in lower panel for FM J_1.
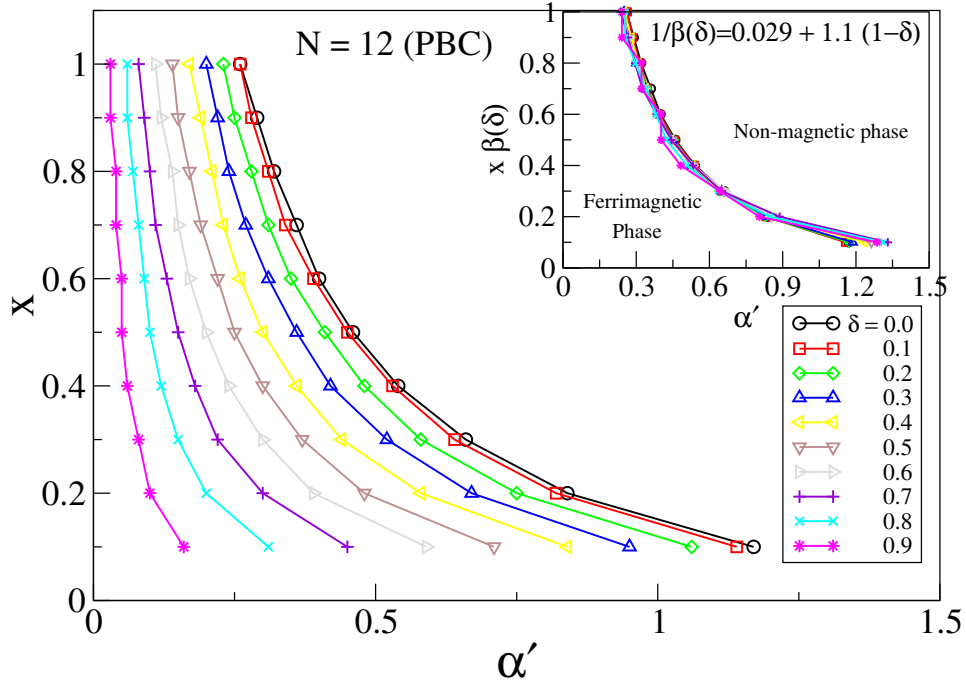
Figure 6.8: Main figure shows ferrimagnetic to non-magnetic phase transition points on x-α' plane for various values of δ. The inset shows the phase boundary point after scaling by a factor $\beta(\delta)$.

small α limit. However, for large FM J_1 limit, the whole system behaves like a spin-3/2 spin chain.

In the later part of this chapter, we studied the effect of x and δ. For small J_2 limit this system behaves like an alternate spin-1 and 1/2 chain with ferrimagnetic gs. But as we increase the J_2, gs goes from a ferrimagnetic state to non-magnetic state. The transition point α_c decreases with δ. The exact spin configuration in the non-magnetic phase is still not completely understood. The further studies on this system will be discussed in somewhere else.

7

CONCLUSION

In this chapter, we provide a brief summary and concluding remarks on all the problems discussed so far.

We propose a modified density matrix renormalization group (DMRG) algorithm for a linear chain with periodic boundary condition, which give accurate results comparable with the results of recently developed matrix product state (MPS) algorithm. The conventional DMRG code can be easily modified to the new algorithm. In the new algorithm, we avoid multiple time renormalization of operators keeping the other parts of the algorithm same as in conventional DMRG. The computation effort using the new algorithm goes as $O(m^3)$, whereas it goes as $O(m^6)$ using conventional DMRG.

In the next problem, We consider two-leg spin-1/2 ladders where a ferromagnetic (FM) leg and an antiferromagnetic leg interact through AFM rung couplings J_1. We study two types of geometrical arrangements; one is zigzag ladder and another one is normal ladder. These systems are frustrated irrespective of their geometry. The frustration gives rise to two kinds of ground state phases in both ladders in thermodynamic limit. These ladders show an incommensurate phase for $0.0 < J_1 < 1.0$. The spin-spin correlation functions in the incommensurate phase follow power law decay, and the behavior is very similar to Heisenberg antiferromagnetic chain in external magnetic field. In large J_1 limit, the normal ladder behaves like a collection of singlet dimers, whereas the zigzag ladder behaves as a one dimensional spin-1/2 antiferromagnetic chain which exhibits spin fluid ground state. Our numerical study shows that magnetization in these ladders decreases linearly with J_1^2 and

this relation is similar with the relation between effective bias field and exchange interaction strength acting between FM and AFM layers, proposed by Suhl and Schuller.

We construct a quantum phase diagram of the trellis ladder on $J_2 - J_3$ plane based on pitch angle and correlation length obtained from spin-spin correlation. We have noted that the collinear to non-collinear transition point J_2^c decreases with rung interaction J_3. In the CS(SRO) phase J_3 induces antiparallel spin arrangement on one zigzag ladder w.r.t to the spins on other zigzag ladder, but spins on each zigzag ladder remain parallel to each other. In this phase the spin-spin correlation decays exponentially along each zigzag leg. In non-collinear (NC) phase both short range order (SRO) and quasi long range order (QLRO) in spin correlation appear for small J_2/J_3 and large J_2/J_3, respectively. The width of the NC(QLRO) region expands with increase in J_2, whereas CS(SRO) phase region shrinks with increase in J_3. The correlation length decreases with J_2 in CS(SRO) phase, whereas the behavior is completely opposite in NC(SRO) phase. The value of pitch angle increases with J_2 . We have performed linear spin wave analysis to find the collinear to non-collinear phase transition, which is quite consistent with our DMRG result. We have used our model to estimate the interaction strengths in trellis lattice material CaV_2O_5 by fitting experimental data of susceptibility and magnetization. It confirms the presence of dominant rung interaction in the system, but J_1 and J_2 interactions are not negligible.

In the final work, we consider a mixed-spin ladder system made up of spin-1 and spin-1/2 legs. The system behaves effectively like a spin-1/2 AFM chain or a spin-3/2 AFM chain in large AFM or FM rung coupling limit, respectively. We have shown the effect of dimerized nearest neighbor bonds between a spin-1/2 and 1, on the transition points from ferrimagnetic phase to non-magnetic phase.

BIBLIOGRAPHY

[1] P. Mohn, "Magnetism in the solid state," in *Magnetism in the solid state* (Springer, Germany, 2003) Chap. 1, pp. 6–7 (cit. on p. 1).

[2] P. Mohn, "Magnetism in the solid state," in *Magnetism in the solid state* (Springer, Germany, 2003) Chap. 3, pp. 23–28 (cit. on p. 1).

[3] P. Fazekas, "Lecture notes on electron correlation and magnetism," in *Lecture notes on electron correlation and magnetism* (World Scientific, Singapore, 2003) Chap. 4,5,6 (cit. on p. 1).

[4] P. Fazekas, "Lecture notes on electron correlation and magnetism," in *Lecture notes on electron correlation and magnetism* (World Scientific, Singapore, 2003) Chap. 6 (cit. on p. 1).

[5] I. Yamada, "Ferromagnetism in k2cuf4," Journal of the Physical Society of Japan **28**, 1585–1585 (1970), eprint: https://doi.org/10.1143/JPSJ.28.1585 (cit. on p. 1).

[6] R. J. A. N. Menyuk K. Dwight and A. Wold, "Ferromagnetism in cdcr2se4 and cdcr2s4," Journal of Applied Physics **37**, 1387–1388 (1966), eprint: https://doi.org/10.1063/1.1708484 (cit. on p. 1).

[7] B. T. Matthias, R. M. Bozorth, and J. H. Van Vleck, "Ferromagnetic interaction in euo," Phys. Rev. Lett. **7**, 160–161 (1961) (cit. on p. 1).

[8] B. D. H. G. Bohn W. Zinn and A. Kollmar, "Neutron scattering study of spin waves and exchange interactions in ferromagnetic eus," Phys. Rev. B **22**, 5447–5452 (1980) (cit. on p. 1).

[9] E Janke, M. T. Hutchings, P Day, and P. J. Walker, "Neutron diffraction study of the crystal and magnetic structure of rb2crcl4: a two-dimensional ionic ferromagnet," Journal of Physics C: Solid State Physics (cit. on p. 1).

[10] A. C. Gossard, V. Jaccarino, and J. P. Remeika, "Nmr in domains and walls in ferromagnetic crbr3," Journal of Applied Physics **33**, 1187–1188 (1962), eprint: https://doi.org/10.1063/1.1728650 (cit. on p. 1).

[11] M. E. Lines and E. D. Jones, "Antiferromagnetism in the face-centered cubic lattice. ii. magnetic properties of mno," Phys. Rev. **139**, A1313–A1327 (1965) (cit. on p. 1).

[12] H. A. G. Will S.J. Pickart and R. Nathans, (cit. on p. 1).

[13] M. J. F. Dale T. Teaney and R. W. H. Stevenson, "Discovery of a simple cubic antiferromagnet: antiferromagnetic resonance in rbmnf3," Phys. Rev. Lett. **9**, 212–214 (1962) (cit. on p. 1).

[14] M Hagiwara, K Katsumata, and J Tuchendler, "Antiferromagnetic resonance in rb2mncl4," Journal of Physics: Condensed Matter **6**, 545–550 (1994) (cit. on p. 1).

[15] T. Komaru, T. Hihara, and Y. Koi, "Nmr study of the magnetic phase of euse," Journal of the Physical Society of Japan **31**, 1391–1398 (1971) (cit. on p. 1).

[16] A. Szabo and N. S. Ostlund, "Modern quantum chemistry," in *Modern quantum chemistry* (Dover Publications, INC., New York, 1996) Chap. 3 (cit. on p. 2).

[17] P. Fazekas, "Lecture notes on electron correlation and magnetism," in *Lecture notes on electron correlation and magnetism* (World Scientific, Singapore, 2003) Chap. 5 (cit. on p. 2).

[18] P. Fazekas, "Lecture notes on electron correlation and magnetism," in *Lecture notes on electron correlation and magnetism* (World Scientific, Singapore, 2003) Chap. 1 (cit. on p. 2).

[19] M. C. Gutzwiller, "Effect of correlation on the ferromagnetism of transition metals," Phys. Rev. Lett. **10**, 159–162 (1963) (cit. on p. 2).

[20] J. Hubbard, "Electron correlations in narrow energy bands," Proc. R. Soc. Lond. A **276** (1963) 10.1098/rspa.1963.0204 (cit. on p. 2).

[21] J. Kanamori, "Electron Correlation and Ferromagnetism of Transition Metals," Progress of Theoretical Physics **30**, 275–289 (1963), eprint: http://oup.prod.sis.lan/ptp/article-pdf/30/3/275/5278869/30-3-275.pdf (cit. on p. 2).

[22] E. H. Lieb and F. Y. Wu, "Absence of mott transition in an exact solution of the short-range, one-band model in one dimension," Phys. Rev. Lett. **20**, 1445–1448 (1968) (cit. on pp. 3, 19).

[23] N. F. MOTT, "Metal-insulator transition," Rev. Mod. Phys. **40**, 677–683 (1968) (cit. on p. 3).

[24] H.-F. Lin, H.-D. Liu, H.-S. Tao, and W.-M. Liu, "Phase transitions of the ionic hubbard model on the honeycomb lattice," Scientific Reports **5** (2015) 10.1038/srep09810 (cit. on p. 3).

[25] A. Mielke and H. Tasaki, "Ferromagnetism in the hubbard model. examples from models with degenerate single-electron ground states," Comm. Math. Phys. **158**, 341–371 (1993) (cit. on p. 3).

[26] S. R. White, D. J. Scalapino, R. L. Sugar, E. Y. Loh, J. E. Gubernatis, and R. T. Scalettar, "Numerical study of the two-dimensional hubbard model," Phys. Rev. B **40**, 506–516 (1989) (cit. on p. 3).

[27] H. Yokoyama, "Variational Monte Carlo Studies of Attractive Hubbard Model. I: Normal-State Properties," Progress of Theoretical Physics **108**, 59–101 (2002) (cit. on p. 3).

[28] R Gersch, C Honerkamp, and W Metzner, "Superconductivity in the attractive hubbard model: functional renormalization group analysis," New Journal of Physics **10**, 045003 (2008) (cit. on p. 3).

[29] A. Georges, G. Kotliar, W. Krauth, and M. J. Rozenberg, "Dynamical mean-field theory of strongly correlated fermion systems and the limit of infinite dimensions," Rev. Mod. Phys. **68**, 13–125 (1996) (cit. on p. 3).

[30] M. Imada, A. Fujimori, and Y. Tokura, "Metal-insulator transitions," Rev. Mod. Phys. **70**, 1039–1263 (1998) (cit. on p. 3).

[31] Y. Park, S. Liang, and T. K. Lee, "Phase diagram of the two-chain hubbard model," Phys. Rev. B **59**, 2587–2590 (1999) (cit. on pp. 3, 23).

[32] R Peters and T Pruschke, "Magnetic phase diagram of the hubbard model with next-nearest-neighbour hopping," New Journal of Physics **11**, 083022 (2009) (cit. on p. 3).

[33] G. Li, A. E. Antipov, A. N. Rubtsov, S. Kirchner, and W. Hanke, "Competing phases of the hubbard model on a triangular lattice: insights from the entropy," Phys. Rev. B **89**, 161118 (2014) (cit. on p. 3).

[34] S. Sachdev, "Quantum phase transitions," in *Quantum phase transitions* (Cambridge University Press, Cambridge, 1999) (cit. on p. 4).

[35]I. U. Heilmann, G. Shirane, Y. Endoh, R. J. Birgeneau, and S. L. Holt, "Neutron study of the line-shape and field dependence of magnetic excitations in cucl2·2n(c5d5)," Phys. Rev. B **18**, 3530–3536 (1978) (cit. on pp. 5, 79).

[36]M. T. Hutchings, J. M. Milne, and H Ikeda, "Spin wave energy dispersion in KCuF3: a nearly one-dimensional spin-1/2antiferromagnet," Journal of Physics C: Solid State Physics **12**, L739–L744 (1979) (cit. on pp. 5, 79).

[37]I. Umegaki, H. Tanaka, N. Kurita, T. Ono, M. Laver, C. Niedermayer, C. Rüegg, S. Ohira-Kawamura, K. Nakajima, and K. Kakurai, "Spinon, soliton, and breather in the spin-$\frac{1}{2}$ antiferromagnetic chain compound kcugaf6," Phys. Rev. B **92**, 174412 (2015) (cit. on pp. 5, 79).

[38]M. Mourigal, M. Enderle, B. Fåk, R. K. Kremer, J. M. Law, A. Schneidewind, A. Hiess, and A. Prokofiev, "Evidence of a bond-nematic phase in licuvo4," Phys. Rev. Lett. **109**, 027203 (2012) (cit. on pp. 5, 41, 58, 59, 76).

[39]S. E. Dutton, M. Kumar, M. Mourigal, Z. G. Soos, J.-J. Wen, C. L. Broholm, N. H. Andersen, Q. Huang, M. Zbiri, R. Toft-Petersen, and R. J. Cava, "Quantum spin liquid in frustrated one-dimensional licusbo4," Phys. Rev. Lett. **108**, 187206 (2012) (cit. on pp. 5, 41, 58, 76).

[40]C. L. Z. S. Park Y. J. Choi and S.-W. Cheon, "Ferroelectricity in an $s = 1/2$ chain cuprate," Phys. Rev. Lett. **98**, 057601 (2007) (cit. on p. 5).

[41]S.-L. Drechsler, O. Volkova, A. N. Vasiliev, N. Tristan, J. Richter, M. Schmitt, H. Rosner, J. Málek, R. Klingeler, A. A. Zvyagin, and B. Büchner, "Frustrated cuprate route from antiferromagnetic to ferromagnetic spin-$\frac{1}{2}$ heisenberg chains: li2zrcuo4 as a missing link near the quantum critical point," Phys. Rev. Lett. **98**, 077202 (2007) (cit. on pp. 5, 41, 58, 76).

[42]A. W. Sandvik, E. Dagotto, and D. J. Scalapino, "Spin dynamics of srcu2o3 and the heisenberg ladder," Phys. Rev. B **53**, R2934–R2937 (1996) (cit. on pp. 5, 41, 58).

[43]D. C. Johnston, "Antiferromagnetic exchange in two-leg spin-1/2 ladders," Phys. Rev. B **54**, 13009–13016 (1996) (cit. on p. 5).

[44]T. Barnes, E. Dagotto, J. Riera, and E. S. Swanson, "Excitation spectrum of heisenberg spin ladders," Phys. Rev. B **47**, 3196–3203 (1993) (cit. on pp. 5, 13).

[45]E. Dagotto and T. M. Rice, "Surprises on the way from one- to two-dimensional quantum magnets: the ladder materials," Science **271**, 618–623 (1996) (cit. on pp. 5, 41, 55, 58).

[46]S. E. Dutton, M Kumar, Z. G. Soos, C. L. Broholm, and R. J. Cava, "Dominant ferromagnetism in the spin-1/2 half-twist ladder 334 compounds, ba3cu3in4o12 and ba3cu3sc4o12," J. Phys.: Condens. Matter **24**, 166001 (2012) (cit. on pp. 5, 41, 58).

[47]M Kumar, S. E. Dutton, R. J. Cava, and Z. G. Soos, "Spin-flop and antiferromagnetic phases of the ferromagnetic half-twist ladder compounds ba3cu3in4o12 and ba3cu3sc4o12," J. Phys.: Condens. Matter **25**, 136004 (2013) (cit. on pp. 5, 41).

[48]A. A. Tsirlin, R. Zinke, J. Richter, and H. Rosner, "Spiral ground state in the quasi-two-dimensional spin-$\frac{1}{2}$ system cu2geo4," Phys. Rev. B **83**, 104415 (2011) (cit. on p. 5).

[49]K.-Y. Choi, J. W. Hwang, P. Lemmens, D. Wulferding, G. J. Shu, and F. C. Chou, "Evidence for dimer crystal melting in the frustrated spin-ladder system bicu2po6," Phys. Rev. Lett. **110**, 117204 (2013) (cit. on p. 5).

[50]E. Manousakis, "The spin-1/2 heisenberg antiferromagnet on a square lattice and its application to the cuprous oxides," Rev. Mod. Phys. **63**, 1–62 (1991) (cit. on p. 5).

[51]B. Sachs, T. O. Wehling, K. S. Novoselov, A. I. Lichtenstein, and M. I. Katsnelson, "Ferromagnetic two-dimensional crystals: single layers of k2cuf4," Phys. Rev. B **88**, 201402 (2013) (cit. on p. 5).

[52]Y. Kitaoka, T. Kobayashi, A. K◼da, H. Wakabayashi, Y. Niino, H. Yamakage, S. Taguchi, K. Amaya, K. Yamaura, M. Takano, A. Hirano, and R. Kanno, "Orbital frustration and resonating valence bond state in the spin-1/2 triangular lattice linio 2," Journal of the Physical Society of Japan **67**, 3703–3706 (1998) (cit. on p. 5).

[53]R. Coldea, D. A. Tennant, K. Habicht, P. Smeibidl, C. Wolters, and Z. Tylczynski, "Direct measurement of the spin hamiltonian and observation of condensation of magnons in the 2d frustrated quantum magnet cs2cucl4," Phys. Rev. Lett. **88**, 137203 (2002) (cit. on p. 5).

[54]Y. Shimizu, K. Miyagawa, K. Kanoda, M. Maesato, and G. Saito, "Spin liquid state in an organic mott insulator with a triangular lattice," Phys. Rev. Lett. **91**, 107001 (2003) (cit. on p. 5).

[55] Y. Kurosaki, Y. Shimizu, K. Miyagawa, K. Kanoda, and G. Saito, "Mott transition from a spin liquid to a fermi liquid in the spin-frustrated organic conductor $\kappa-(et)2cu2(cn)3$," Phys. Rev. Lett. **95**, 177001 (2005) (cit. on p. 5).

[56] Y. Singh and P. Gegenwart, "Antiferromagnetic mott insulating state in single crystals of the honeycomb lattice material na2iro3," Phys. Rev. B **82**, 064412 (2010) (cit. on p. 5).

[57] Y. Singh, S. Manni, J. Reuther, T. Berlijn, R. Thomale, W. Ku, S. Trebst, and P. Gegenwart, "Relevance of the heisenberg-kitaev model for the honeycomb lattice iridates A2iro3," Phys. Rev. Lett. **108**, 127203 (2012) (cit. on p. 5).

[58] M. A. Korotin, I. S. Elfimov, V. I. Anisimov, M. Troyer, and D. I. Khomskii, "Exchange interactions and magnetic properties of the layered vanadates cav2o5, mgv2o5, cav3o7, and cav4o9," Phys. Rev. Lett. **83**, 1387–1390 (1999) (cit. on pp. 5, 58).

[59] M. A. Korotin, V. I. Anisimov, T Saha-Dasgupta, and I Dasgupta, "Electronic structure and exchange interactions of the ladder vanadates cav 2 o 5 and mgv 2 o 5," Journal of Physics: Condensed Matter **12**, 113 (2000) (cit. on pp. 5, 58, 73–75).

[60] A. Koga and N. Kawakami, "Quantum phase transitions in the shastry-sutherland model for $SrCu2(BO3)2$," Phys. Rev. Lett. **84**, 4461–4464 (2000) (cit. on p. 6).

[61] F. D. M. Haldane, "Nonlinear field theory of large-spin heisenberg antiferromagnets: semiclassically quantized solitons of the one-dimensional easy-axis néel state," Phys. Rev. Lett. **50**, 1153–1156 (1983) (cit. on pp. 6, 11, 19, 79).

[62] W. J. L Buyers, R. M. Morra, R. L. Armstrong, M. J. Hogan, P. Gerlach, and K. Hirakawa, "Experimental evidence for the haldane gap in a spin-1 nearly isotropic, antiferromagnetic chain," Phys. Rev. Lett. **56**, 371–374 (1986) (cit. on pp. 6, 79).

[63] T. Delica, W. J. M. de Jonge, K. Kopinga, H. Leschke, and H. J. Mikeska, "Static properties of csnif3: comparison of numerical results, experimental data, and predictions from soliton-bearing models," Phys. Rev. B **44**, 11773–11783 (1991) (cit. on p. 6).

[64] J. P Renard, M Verdaguer, L. P Regnault, W. A. C Erkelens, J Rossat-Mignod, and W. G Stirling, "Presumption for a quantum energy gap in the quasi-one-DimensionalS= 1 heisenberg antiferromagnet ni(c2h8n2)2no2(ClO4)," Europhysics Letters (EPL) **3**, 945–952 (1987) (cit. on pp. 6, 79).

[65]H. Tsujii, Z. Honda, B. Andraka, K. Katsumata, and Y. Takano, "High-field phase diagram of the haldane-gap antiferromagnet $Ni(C_5H_{14}N_2)2n3(pf6)$," Phys. Rev. B **71**, 014426 (2005) (cit. on pp. 6, 79).

[66]M. Hagiwara, K. Minami, Y. Narumi, K. Tatani, and K. Kindo, "Magnetic properties of a quantum ferrimagnet: nicu(pba)(d 2 o) 3âů 2d 2 o," Journal of the Physical Society of Japan **67**, 2209–2211 (1998) (cit. on p. 6).

[67]N. D. Mermin and H. Wagner, "Absence of ferromagnetism or antiferromagnetism in one- or two-dimensional isotropic heisenberg models," Phys. Rev. Lett. **17**, 1133–1136 (1966) (cit. on pp. 6, 7).

[68]U. SchollwÃück, J. Richter, D. Farnell, and R. Bishop, "One-dimensional magnetism," in *Quantum magnetism* (Springer, Germany, 2004) Chap. 1 (cit. on p. 6).

[69]C. M. Bender and T. T. Wu, "Anharmonic oscillator. ii. a study of perturbation theory in large order," Phys. Rev. D **7**, 1620–1636 (1973) (cit. on p. 6).

[70]A. Auerbach, "Spin wave theory," in *Interacting electrons and quantum magnetism* (Springer New York, New York, NY, 1994), pp. 113–127 (cit. on pp. 6, 19).

[71]D. P. Arovas and A. Auerbach, "Functional integral theories of low-dimensional quantum heisenberg models," Phys. Rev. B **38**, 316–332 (1988) (cit. on pp. 6, 19).

[72]K. G. Wilson, "The renormalization group: critical phenomena and the kondo problem," Rev. Mod. Phys. **47**, 773–840 (1975) (cit. on pp. 6, 19, 23).

[73]K. G. Wilson, "The renormalization group and critical phenomena," Rev. Mod. Phys. **55**, 583–600 (1983) (cit. on pp. 6, 19, 23).

[74]D. Sénéchal, "An introduction to bosonization," in *Theoretical methods for strongly correlated electrons*, edited by D. Sénéchal, A.-M. Tremblay, and C. Bourbonnais (Springer New York, New York, NY, 2004), pp. 139–186 (cit. on pp. 6, 19).

[75]S. R. White and D. A. Huse, "Numerical renormalization-group study of low-lying eigenstates of the antiferromagnetic S=1 Heisenberg chain," Phys. Rev. **B48**, 3844–3852 (1993) (cit. on pp. 6, 11, 20, 23, 79).

[76]S. R. White, "Density matrix formulation for quantum renormalization groups," Phys. Rev. Lett. **69**, 2863–2866 (1992) (cit. on pp. 6, 20, 23, 30, 44, 61).

[77]S. R. White, "Density-matrix algorithms for quantum renormalization groups," Phys. Rev. B **48**, 10345–10356 (1993) (cit. on pp. 6, 20, 23, 30).

[78]M. Suzuki, ed., *Quantum monte carlo methods in condensed matter physics* (World Scientific, 1993) (cit. on pp. 6, 20, 30).

[79]J. Biamonte and V. Bergholm, "Tensor Networks in a Nutshell," arXiv e-prints, arXiv:1708.00006, arXiv:1708.00006 (2017), arXiv:1708.00006 [quant-ph] (cit. on p. 6).

[80]P. Jordan and E. Wigner, "Über das paulische Äquivalenzverbot," Zeitschrift für Physik **47**, 631–651 (1928) (cit. on p. 7).

[81]E. Lieb, T. Schultz, and D. Mattis, "Two soluble models of an antiferromagnetic chain," Annals of Physics **16**, 407 –466 (1961) (cit. on p. 7).

[82]B. M. McCoy, "Spin correlation functions of the $x - y$ model," Phys. Rev. **173**, 531–541 (1968) (cit. on p. 7).

[83]F. Bloch, "Zur theorie des ferromagnetismus," Zeitschrift für Physik **61**, 206–219 (1930) (cit. on p. 8).

[84]F. Bloch, "Zur theorie des austauschproblems und der remanenzerscheinung der ferromagnetika," Zeitschrift für Physik **74**, 295–335 (1932) (cit. on p. 8).

[85]T. Holstein and H. Primakoff, "Field dependence of the intrinsic domain magnetization of a ferromagnet," Phys. Rev. **58**, 1098–1113 (1940) (cit. on p. 8).

[86]P. W. Anderson, "An approximate quantum theory of the antiferromagnetic ground state," Phys. Rev. **86**, 694–701 (1952) (cit. on pp. 8, 16).

[87]R. Kubo, "The spin-wave theory of antiferromagnetics," Phys. Rev. **87**, 568–580 (1952) (cit. on p. 8).

[88]T. Oguchi, "Theory of spin-wave interactions in ferro- and antiferromagnetism," Phys. Rev. **117**, 117–123 (1960) (cit. on p. 8).

[89]F. C. Alcaraz, S. R. Salinas, and W. F. Wreszinski, "Anisotropic ferromagnetic quantum domains," Phys. Rev. Lett. **75**, 930–933 (1995) (cit. on p. 8).

[90]D. C. Mattis, "Theory of magnetism made simple," in *Theory of magnetism made simple* (World Scientific, Singapore, 2006) Chap. 5, pp. 186–196 (cit. on p. 8).

[91] H. Bethe, "Zur theorie der metalle," Zeitschrift für Physik **71**, 205–226 (1931) (cit. on pp. 8, 19, 79).

[92] J. des Cloizeaux and J. J. Pearson, "Spin-wave spectrum of the antiferromagnetic linear chain," Phys. Rev. **128**, 2131–2135 (1962) (cit. on p. 8).

[93] L. Faddeev and L. Takhtajan, "What is the spin of a spin wave?" Physics Letters A **85**, 375–377 (1981) (cit. on p. 8).

[94] I Affleck, D Gepner, H. J. Schulz, and T Ziman, "Critical behaviour of spin-s heisenberg antiferromagnetic chains: analytic and numerical results," Journal of Physics A: Mathematical and General **22**, 511–529 (1989) (cit. on pp. 9, 79).

[95] I. Affleck, "Exact correlation amplitude for the heisenberg antiferromagnetic chain," Journal of Physics A: Mathematical and General **31**, 4573–4581 (1998) (cit. on pp. 9, 79).

[96] U. SchollwÃŭck, J. Richter, D. Farnell, and R. Bishop, "One-dimensional magnetism," in *Quantum magnetism* (Springer, Germany, 2004) Chap. 1, pp. 5–12 (cit. on p. 9).

[97] K. Okamoto and K. Nomura, "Fluid-dimer critical point in s = 12 antiferromagnetic heisenberg chain with next nearest neighbor interactions," Physics Letters A **169**, 433 –437 (1992) (cit. on pp. 10, 58).

[98] F. D. M. Haldane, "Spontaneous dimerization in the $s = \frac{1}{2}$ heisenberg antiferromagnetic chain with competing interactions," Phys. Rev. B **25**, 4925–4928 (1982) (cit. on pp. 10, 58).

[99] C. K. Majumdar and D. K. Ghosh, "On nextâăřnearestâăřneighbor interaction in linear chain. i," J. Math. Phys. **10**, 1388–1398 (1969) (cit. on pp. 10, 58).

[100] C. K. Majumdar and D. K. Ghosh, "On nextâăřnearestâăřneighbor interaction in linear chain. ii," J. Math. Phys. **10**, 1399–1402 (1969) (cit. on pp. 10, 41).

[101] S. R. White and I. Affleck, "Dimerization and incommensurate spiral spin correlations in the zigzag spin chain: analogies to the kondo lattice," Phys. Rev. B **54**, 9862–9869 (1996) (cit. on p. 10).

[102] M. Kumar, A. Parvej, and Z. G. Soos, "Level crossing, spin structure factor and quantum phases of the frustrated spin-1/2 chain with first and second neighbor exchange," J. Phys.: Condens. Matter **27**, 316001 (2015) (cit. on pp. 10, 41, 58, 60, 62, 63, 75).

[103]Z. G. Soos, A. Parvej, and M. Kumar, "Numerical study of incommensurate and decoupled phases of spin-1/2 chains with isotropic exchange j_1 , j_2 between first and second neighbors," J. Phys.: Condens. Matter **28**, 175603 (2016) (cit. on pp. 10, 41, 58, 62, 63).

[104]W. Selke, "Spin chains with nearest and next nearest neighbour interactions," Zeitschrift für Physik B Condensed Matter **27**, 81–84 (1977) (cit. on p. 10).

[105]J. Sirker, V. Y. Krivnov, D. V. Dmitriev, A. Herzog, O. Janson, S. Nishimoto, S.-L. Drechsler, and J. Richter, "$J1 - J2$ heisenberg model at and close to its $z = 4$ quantum critical point," Phys. Rev. B **84**, 144403 (2011) (cit. on p. 10).

[106]C. E. Agrapidis, S.-L. Drechsler, J. van den Brink, and S. Nishimoto, "Coexistence of valence-bond formation and topological order in the Frustrated Ferromagnetic J_1-J_2 Chain," SciPost Phys. **6**, 19 (2019) (cit. on pp. 10, 15).

[107]T. Tonegawa and I. Harada, "Magnetization curves in the ground state of spin- 1 2 antiferromagnetic xxz chains with competing interactions," English, Physica B: Condensed Matter **155**, 379–382 (1989) (cit. on p. 11).

[108]T. Tonegawa, K. Okamoto, K. Okunishi, K. Nomura, and M. Kaburagi, "Magnetization plateaux in an anisotropic s = 1/2 antiferromagnetic chain with frustration and bond-alternation," English, Physica B: Condensed Matter **346-347**, 50–54 (2004) (cit. on p. 11).

[109]K. Okunishi and T. Tonegawa, "Magnetic phase diagram of the s=1/2 antiferromagnetic zigzag spin chain in the strongly frustrated region: cusp and plateau," Journal of the Physical Society of Japan **72**, 479–482 (2003), eprint: https://doi.org/10.1143/JPSJ.72.479 (cit. on p. 11).

[110]T. Hikihara, T. Momoi, A. Furusaki, and H. Kawamura, "Magnetic phase diagram of the spin-$\frac{1}{2}$ antiferromagnetic zigzag ladder," Phys. Rev. B **81**, 224433 (2010) (cit. on p. 11).

[111]A. Parvej and M. Kumar, "Multipolar phase in frustrated spin-1/2 and spin-1 chains," Phys. Rev. B **96**, 054413 (2017) (cit. on p. 11).

[112]M. Kaburagi, H. Kawamura, and T. Hikihara, "Spin and chiral orderings of frustrated quantum spin chains," Journal of the Physical Society of Japan **68**, 3185–3188 (1999), eprint: https://doi.org/10.1143/JPSJ.68.3185 (cit. on p. 11).

[113] T. Hikihara, M. Kaburagi, and H. Kawamura, "Ground-state phase diagrams of frustrated spin-s xxz chains: chiral ordered phases," Phys. Rev. B **63**, 174430 (2001) (cit. on p. 11).

[114] F. Haldane, "Continuum dynamics of the 1-d heisenberg antiferromagnet: identification with the o(3) nonlinear sigma model," Physics Letters A **93**, 464 –468 (1983) (cit. on p. 11).

[115] U. SchollwÃűck, J. Richter, D. Farnell, and R. Bishop, "One-dimensional magnetism," in *Quantum magnetism* (Springer, Germany, 2004) Chap. 1, p. 27 (cit. on p. 11).

[116] A. W. Sandvik, "Computational studies of quantum spin systems," AIP Conference Proceedings **1297** (2010) (cit. on pp. 11, 39).

[117] I. Affleck, T. Kennedy, E. H. Lieb, and H. Tasaki, "Rigorous results on valence-bond ground states in antiferromagnets," Phys. Rev. Lett. **59**, 799–802 (1987) (cit. on pp. 12, 79).

[118] K Totsuka and M Suzuki, "Matrix formalism for the VBS-type models and hidden order," Journal of Physics: Condensed Matter **7**, 1639–1662 (1995) (cit. on p. 12).

[119] E. Lieb and D. Mattis, "Ordering energy levels of interacting spin systems," Journal of Mathematical Physics **3**, 749–751 (1962), eprint: https://doi.org/10.1063/1.1724276 (cit. on pp. 12, 80).

[120] S. K. Pati, S. Ramasesha, and D. Sen, "Low-lying excited states and low-temperature properties of an alternating spin-1–spin-1/2 chain: a density-matrix renormalization-group study," Phys. Rev. B **55**, 8894–8904 (1997) (cit. on pp. 12, 80).

[121] N. B. Ivanov, J. Richter, and U. Schollwöck, "Frustrated quantum heisenberg ferrimagnetic chains," Phys. Rev. B **58**, 14456–14461 (1998) (cit. on pp. 12, 80).

[122] S. R. White, R. M. Noack, and D. J. Scalapino, "Resonating valence bond theory of coupled heisenberg chains," Phys. Rev. Lett. **73**, 886–889 (1994) (cit. on pp. 13, 23).

[123] S. R. White, "Equivalence of the antiferromagnetic heisenberg ladder to a single s=1 chain," Phys. Rev. B **53**, 52–55 (1996) (cit. on pp. 13, 23, 55, 58, 59, 75).

[124] K. Hijii, A. Kitazawa, and K. Nomura, "Phase diagram of S=$\frac{1}{2}$ two-leg *xxz* spin-ladder systems," Phys. Rev. B **72**, 014449 (2005) (cit. on pp. 13, 41).

[125]S. P. Strong and A. J. Millis, "Competition between singlet formation and magnetic ordering in one-dimensional spin systems," Phys. Rev. Lett. **69**, 2419–2422 (1992) (cit. on p. 13).

[126]S. P. Strong and A. J. Millis, "Competition between singlet formation and magnetic ordering in one-dimensional spin systems," Phys. Rev. B **50**, 9911–9923 (1994) (cit. on pp. 13, 14).

[127]K. Hida, "Haldane gap in the spin-1/2 double chain heisenberg antiferromagnet -numerical diagonalization and projector monte carlo study-," Journal of the Physical Society of Japan **60**, 1347–1354 (1991), eprint: https://doi.org/10.1143/JPSJ.60.1347 (cit. on p. 13).

[128]K. Hida, "Haldane gap in the spin-1/2double chain anisotropic heisenberg antiferromagnet," Journal of the Physical Society of Japan **60**, 1939–1942 (1991), eprint: https://doi.org/10.1143/JPSJ.60.1939 (cit. on p. 13).

[129]T. Narushima, T. Nakamura, and S. Takada, "Numerical study on the ground-state phase diagram of the s=1/2 xxz ladder model," Journal of the Physical Society of Japan **64**, 4322–4330 (1995), eprint: https://doi.org/10.1143/JPSJ.64.4322 (cit. on p. 14).

[130]M. Roji and S. Miyashita, "Competition between classical ordered state and quantum state in ferromagnetic chains coupled by antiferromagnetic bonds," Journal of the Physical Society of Japan **65**, 883–886 (1996), eprint: https://doi.org/10.1143/JPSJ.65.883 (cit. on p. 14).

[131]A. K. Kolezhuk and H. J. Mikeska, "Phase transitions in the heisenberg spin ladder with ferromagnetic legs," Phys. Rev. B **53**, R8848–R8850 (1996) (cit. on p. 14).

[132]T. Vekua, G. I. Japaridze, and H.-J. Mikeska, "Phase diagrams of spin ladders with ferromagnetic legs," Phys. Rev. B **67**, 064419 (2003) (cit. on pp. 14, 41, 59).

[133]E. H. Kim, G. Fáth, J. Sólyom, and D. J. Scalapino, "Phase transitions between topologically distinct gapped phases in isotropic spin ladders," Phys. Rev. B **62**, 14965–14974 (2000) (cit. on p. 14).

[134]A. Lavarélo, G. Roux, and N. Laflorencie, "Melting of a frustration-induced dimer crystal and incommensurability in the $J1$-$J2$ two-leg ladder," Phys. Rev. B **84**, 144407 (2011) (cit. on p. 15).

[135] Q. Luo, S. Hu, J. Zhao, A. Metavitsiadis, S. Eggert, and X. Wang, "Ground-state phase diagram of the frustrated spin-$\frac{1}{2}$ two-leg honeycomb ladder," Phys. Rev. B **97**, 214433 (2018) (cit. on pp. 15, 59).

[136] P. Müller, J. Richter, and D. Ihle, "Thermodynamics of frustrated ferromagnetic spin-$\frac{1}{2}$ heisenberg chains: role of interchain coupling," Phys. Rev. B **95**, 134407 (2017) (cit. on p. 15).

[137] R. Zinke, S.-L. Drechsler, and J. Richter, "Influence of interchain coupling on spiral ground-state correlations in frustrated spin-$\frac{1}{2}$ $J1-J2$ heisenberg chains," Phys. Rev. B **79**, 094425 (2009) (cit. on pp. 16, 60, 74, 75).

[138] G. I. Japaridze and E Pogosyan, "Magnetization plateau in the spin ladder with alternating rung exchange," Journal of Physics: Condensed Matter **18**, 9297–9306 (2006) (cit. on p. 16).

[139] A. Metavitsiadis and S. Eggert, "Competing phases in spin ladders with ring exchange and frustration," Phys. Rev. B **95**, 144415 (2017) (cit. on p. 16).

[140] F. Elias, M. Arlego, and C. A. Lamas, "Magnetization process in a frustrated plaquette dimerized ladder," Phys. Rev. B **95**, 214426 (2017) (cit. on p. 16).

[141] K. Totsuka, "Magnetization plateau in the $s = \frac{1}{2}$ heinsenberg spin chain with next-nearest-neighbor and alternating nearest-neighbor interactions," Phys. Rev. B **57**, 3454–3465 (1998) (cit. on p. 16).

[142] T. Tonegawa, T. Hikihara, K. Okamoto, S. C. Furuya, and T. Sakai, "Ground-state phase diagram of an anisotropic s = 1/2 ladder with different leg interactions," Journal of the Physical Society of Japan **87**, 104002 (2018), eprint: `https://doi.org/10.7566/JPSJ.87.104002` (cit. on p. 16).

[143] K. Sekiguchi and K. Hida, "Partial ferrimagnetism in s = 1/2 heisenberg ladders with a ferromagnetic leg, an antiferromagnetic leg, and antiferromagnetic rungs," Journal of the Physical Society of Japan **86**, 084706 (2017), eprint: `https://doi.org/10.7566/JPSJ.86.084706` (cit. on p. 16).

[144] U. Schollwãűck, J. Richter, D. Farnell, and R. Bishop, "One-dimensional magnetism," in *Quantum magnetism* (Springer, Germany, 2004) Chap. 2, pp. 100–103 (cit. on p. 16).

[145]P. Anderson, "Resonating valence bonds: a new kind of insulator?" Materials Research Bulletin **8**, 153 –160 (1973) (cit. on p. 17).

[146]P. Fazekas and P. W. Anderson, "On the ground state properties of the anisotropic triangular antiferromagnet," The Philosophical Magazine: A Journal of Theoretical Experimental and Applied Physics **30**, 423–440 (1974), eprint: https://doi.org/10.1080/14786439808206568 (cit. on p. 17).

[147]D. A. Huse and V. Elser, "Simple variational wave functions for two-dimensional heisenberg spin- antiferromagnets," Phys. Rev. Lett. **60**, 2531–2534 (1988) (cit. on p. 17).

[148]T. Jolicoeur and J. C. Le Guillou, "Spin-wave results for the triangular heisenberg antiferromagnet," Phys. Rev. B **40**, 2727–2729 (1989) (cit. on p. 17).

[149]B. Bernu, C. Lhuillier, and L. Pierre, "Signature of néel order in exact spectra of quantum antiferromagnets on finite lattices," Phys. Rev. Lett. **69**, 2590–2593 (1992) (cit. on p. 17).

[150]B. Bernu, P. Lecheminant, C. Lhuillier, and L. Pierre, "Exact spectra, spin susceptibilities, and order parameter of the quantum heisenberg antiferromagnet on the triangular lattice," Phys. Rev. B **50**, 10048–10062 (1994) (cit. on p. 17).

[151]P. Lecheminant, B. Bernu, C. Lhuillier, L. Pierre, and P. Sindzingre, "Order versus disorder in the quantum heisenberg antiferromagnet on the kagomé lattice using exact spectra analysis," Phys. Rev. B **56**, 2521–2529 (1997) (cit. on p. 17).

[152]B Bernu, P Lecheminant, C Lhuillier, and L Pierre, "Néel order versus spin liquid in quantum heisenberg antiferromagnets on triangular and kagomé lattices," Physica Scripta **T49A**, 192–197 (1993) (cit. on p. 17).

[153]J. D. Reger, J. A. Riera, and A. P. Young, "Monte carlo simulations of the spin-1/2heisenberg antiferromagnet in two dimensions," Journal of Physics: Condensed Matter **1**, 1855–1865 (1989) (cit. on p. 17).

[154]J. Oitmaa, C. J. Hamer, and Z. Weihong, "Quantum magnets on the honeycomb and triangular lattices at t=0," Phys. Rev. B **45**, 9834–9841 (1992) (cit. on p. 17).

[155]B. Normand, K. Penc, M. Albrecht, and F. Mila, "Phase diagram of the $s=\frac{1}{2}$ frustrated coupled ladder system," Phys. Rev. B **56**, R5736–R5739 (1997) (cit. on pp. 17, 60).

[156] S. Miyahara, M. Troyer, D. Johnston, and K. Ueda, "Quantum monte carlo simulation of the trellis lattice heisenberg model for srcu2o3 and cav2o5," Journal of the Physical Society of Japan **67**, 3918 (1998), eprint: `cond-mat/9807127` (cit. on pp. 17, 60, 75).

[157] C. Lanczos, "An iteration method for the solution of the eigenvalue problem of linear differential and integral operators," J. Res. Natl. Bur. Stand. B **45**, 255–282 (1950) (cit. on p. 21).

[158] C. Lanczos, "Solution of systems of linear equations by minimized iterations," J. Res. Natl. Bur. Stand **49**, 33–53 (1952) (cit. on p. 21).

[159] R. Riedinger and M. Benard, "Quantum chemistry without diagonalization: an extension of the lanczos method to molecules and solids," The Journal of Chemical Physics **94**, 1222–1228 (1991), eprint: `https://doi.org/10.1063/1.460030` (cit. on p. 21).

[160] E. R. Davidson, "The iterative calculation of a few of the lowest eigenvalues and corresponding eigenvectors of large real-symmetric matrices," Journal of Computational Physics **17**, 87 –94 (1975) (cit. on p. 21).

[161] E. R. Davidson and W. J. Thompson, "Monster matrices: their eigenvalues and eigenvectors," Computers in Physics **7**, 519–522 (1993), eprint: `https://aip.scitation.org/doi/pdf/10.1063/1.4823212` (cit. on p. 21).

[162] S. Rettrup, "An iterative method for calculating several of the extreme eigensolutions of large real non-symmetric matrices," Journal of Computational Physics **45**, 100 –107 (1982) (cit. on p. 21).

[163] K. Hallberg, "Density Matrix Renormalization: A Review of the Method and its Applications," (2003), arXiv:`cond-mat/0303557` [cond-mat] (cit. on p. 23).

[164] K. A. Hallberg, "New trends in density matrix renormalization," Advances in Physics **55**, 477–526 (2006), eprint: `https://doi.org/10.1080/00018730600766432` (cit. on pp. 23, 44, 61).

[165] A. E. Feiguin, "The density matrix renormalization group," in *Strongly correlated systems: numerical methods*, edited by A. Avella and F. Mancini (Springer Berlin Heidelberg, Berlin, Heidelberg, 2013), pp. 31–65 (cit. on p. 23).

[166] E. S. So/rensen and I. Affleck, "S(k) for haldane-gap antiferromagnets: large-scale numerical results versus field theory and experiment," Phys. Rev. B **49**, 13235–13238 (1994) (cit. on p. 23).

[167] E. S. So/rensen and I. Affleck, "Equal-time correlations in haldane-gap antiferromagnets," Phys. Rev. B **49**, 15771–15788 (1994) (cit. on p. 23).

[168] K. Hallberg, X. Q. G. Wang, P. Horsch, and A. Moreo, "Critical Behavior of the S=3/2 Antiferromagnetic Heisenberg Chain," Phys. Rev. Lett. **76**, 4955–4958 (1996), arXiv:cond-mat/9603082 [cond-mat] (cit. on p. 23).

[169] U. Schollwock and T. Jolicoeur, "Haldane Gap and Hidden Order in the S=2 Antiferromagnetic Quantum Spin Chain," Europhys. Lett. **30**, 493 (1995), arXiv:cond-mat/9501115 [cond-mat] (cit. on p. 23).

[170] M. Kumar, S. Ramasesha, and Z. G. Soos, "Bond-order wave phase, spin solitons, and thermodynamics of a frustrated linear spin-$\frac{1}{2}$ heisenberg antiferromagnet," Phys. Rev. B **81**, 054413 (2010) (cit. on pp. 23, 58).

[171] M. Kumar, Z. G. Soos, D. Sen, and S. Ramasesha, "Modified density matrix renormalization group algorithm for the zigzag spin-$\frac{1}{2}$ chain with frustrated antiferromagnetic exchange: comparison with field theory at large $J2/J1$," Phys. Rev. B **81**, 104406 (2010) (cit. on pp. 23, 44, 61).

[172] T. Xiang, J. Lou, and Z. Su, "Two-dimensional algorithm of the density-matrix renormalization group," Phys. Rev. B **64**, 104414 (2001) (cit. on p. 23).

[173] P. Henelius, "Two-dimensional infinite-system density-matrix renormalization-group algorithm," Phys. Rev. B **60**, 9561–9565 (1999) (cit. on p. 23).

[174] C. Aebischer, D. Baeriswyl, and R. M. Noack, "Dielectric catastrophe at the mott transition," Phys. Rev. Lett. **86**, 468–471 (2001) (cit. on p. 23).

[175] B. Srinivasan and M.-B. Lepetit, "Current-current correlations in a cuo3 model system," Phys. Rev. B **66**, 024421 (2002) (cit. on p. 23).

[176] K. Hamacher, C. Gros, and W. Wenzel, "Interaction-induced collapse of a section of the fermi sea in the zigzag hubbard ladder," Phys. Rev. Lett. **88**, 217203 (2002) (cit. on p. 23).

[177]T. Nishino, "Density matrix renormalization group method for 2d classical models," Journal of the Physical Society of Japan **64**, 3598–3601 (1995), eprint: `https://doi.org/10.1143/JPSJ.64.3598` (cit. on p. 23).

[178]T. Nishino and N. Shibata, "Efficiency of asymmetric targeting for finite-t dmrg," Journal of the Physical Society of Japan **68**, 3501–3504 (1999), eprint: `https://doi.org/10.1143/JPSJ.68.3501` (cit. on p. 24).

[179]U. SchollwÃűck and S. R. White, "Methods for time dependence in dmrg," AIP Conference Proceedings **816** (2006) `10.1063/1.2178041` (cit. on p. 24).

[180]R. P. Feynman, "Statistical mechanics: a set of lectures," in *Statistical mechanics: a set of lectures* (The Benjamin/Cummings Publishing Company,Inc., U.S.A., 1982) Chap. 2, pp. 39–41 (cit. on p. 25).

[181]M. Tinkham, *Introduction to Superconductivity: Second Edition (Dover Books on Physics) (Vol I)* (Dover Publications, 2004) (cit. on p. 30).

[182]A. V. Chubukov, "Chiral, nematic, and dimer states in quantum spin chains," Phys. Rev. B **44**, 4693–4696 (1991) (cit. on p. 30).

[183]L. Kecke, T. Momoi, and A. Furusaki, "Multimagnon bound states in the frustrated ferromagnetic one-dimensional chain," Phys. Rev. B **76**, 060407 (2007) (cit. on p. 30).

[184]P. W. Anderson, "The resonating valence bond state in la2cuo4 and superconductivity," Science **235**, 1196–1198 (1987) (cit. on p. 30).

[185]A. Parvej and M. Kumar, "Degeneracies and exotic phases in an isotropic frustrated spin-1/2 chain," Journal of Magnetism and Magnetic Materials **401**, 96 –101 (2016) (cit. on p. 30).

[186]X.-L. Qi and S.-C. Zhang, "Topological insulators and superconductors," Rev. Mod. Phys. **83**, 1057–1110 (2011) (cit. on p. 30).

[187]M. Nakamura, "Tricritical behavior in the extended hubbard chains," Phys. Rev. B **61**, 16377–16392 (2000) (cit. on p. 30).

[188]P. Sengupta, A. W. Sandvik, and D. K. Campbell, "Bond-order-wave phase and quantum phase transitions in the one-dimensional extended hubbard model," Phys. Rev. B **65**, 155113 (2002) (cit. on p. 30).

[189]M. Kumar, S. Ramasesha, and Z. G. Soos, "Tuning the bond-order wave phase in the half-filled extended hubbard model," Phys. Rev. B **79**, 035102 (2009) (cit. on pp. 30, 31).

[190]W. Kohn and L. J. Sham, "Self-consistent equations including exchange and correlation effects," Phys. Rev. **140**, A1133–A1138 (1965) (cit. on p. 30).

[191]K. G. Wilson, "The renormalization group and critical phenomena," Rev. Mod. Phys. **55**, 583–600 (1983) (cit. on p. 30).

[192]U. Schollwöck, "The density-matrix renormalization group," Rev. Mod. Phys. **77**, 259–315 (2005) (cit. on pp. 31, 44, 61).

[193]K. A. Hallberg, "New trends in density matrix renormalization," Advances in Physics **55**, 477–526 (2006) (cit. on p. 31).

[194]Z. G. Soos, A. Parvej, and M. Kumar, "Numerical study of incommensurate and decoupled phases of spin-1/2 chains with isotropic exchange $J1$, $J2$ between first and second neighbors," Journal of Physics: Condensed Matter **28**, 175603 (2016) (cit. on pp. 31, 35, 40).

[195]U. Schollwöck, "The density-matrix renormalization group in the age of matrix product states," Annals of Physics **326**, 96 –192 (2011) (cit. on p. 31).

[196]P. Pippan, S. R. White, and H. G. Evertz, "Efficient matrix-product state method for periodic boundary conditions," Phys. Rev. B **81**, 081103 (2010) (cit. on pp. 31, 33, 34, 37, 39).

[197]E. Dagotto and T. M. Rice, "Surprises on the way from one- to two-dimensional quantum magnets: the ladder materials," Science **271**, 618–623 (1996) (cit. on p. 32).

[198]S. Östlund and S. Rommer, "Thermodynamic limit of density matrix renormalization," Phys. Rev. Lett. **75**, 3537–3540 (1995) (cit. on p. 32).

[199]F. Verstraete, D. Porras, and J. I. Cirac, "Density matrix renormalization group and periodic boundary conditions: a quantum information perspective," Phys. Rev. Lett. **93**, 227205 (2004) (cit. on p. 33).

[200]F. Verstraete, J. I. Cirac, J. I. Latorre, E. Rico, and M. M. Wolf, "Renormalization-group transformations on quantum states," Phys. Rev. Lett. **94**, 140601 (2005) (cit. on pp. 33, 40).

[201] D. Rossini, V. Giovannetti, and R. Fazio, "Stiffness in 1d matrix product states with periodic boundary conditions," Journal of Statistical Mechanics: Theory and Experiment **2011**, P05021 (2011) (cit. on pp. 34, 40).

[202] S. K. Pati, S. Ramasesha, Z. Shuai, and J. L. Brédas, "Dynamical nonlinear optical coefficients from the symmetrized density-matrix renormalization-group method," Phys. Rev. B **59**, 14827–14830 (1999) (cit. on pp. 34, 40).

[203] K. A. Hallberg, "Density-matrix algorithm for the calculation of dynamical properties of low-dimensional systems," Phys. Rev. B **52**, R9827–R9830 (1995) (cit. on pp. 34, 40).

[204] I Affleck, D Gepner, H. J. Schulz, and T Ziman, "Critical behaviour of spin-s heisenberg antiferromagnetic chains: analytic and numerical results," Journal of Physics A: Mathematical and General **22**, 511 (1989) (cit. on p. 39).

[205] D. Rossini, V. Giovannetti, and R. Fazio, "Spin-supersolid phase in heisenberg chains: a characterization via matrix product states with periodic boundary conditions," Phys. Rev. B **83**, 140411 (2011) (cit. on p. 40).

[206] S. R. White, R. M. Noack, and D. J. Scalapino, "Resonating valence bond theory of coupled heisenberg chains," Phys. Rev. Lett. **73**, 886–889 (1994) (cit. on pp. 41, 58, 59, 62).

[207] T. Verkholyak and J. Strečka, "Quantum phase transitions in the exactly solved spin-1/2 heisenberg–ising ladder," Journal of Physics A: Mathematical and Theoretical **45**, 305001 (2012) (cit. on p. 41).

[208] A. Honecker, F. Mila, and M. Troyer, "Magnetization plateaux and jumps in a class of frustrated ladders: a simple route to a complex behaviour," The European Physical Journal B - Condensed Matter and Complex Systems" **15**, 227–233 (2000) (cit. on p. 41).

[209] D. C. Johnston, J. W. Johnson, D. P. Goshorn, and A. J. Jacobson, "Magnetic susceptibility of $(vo)_2p_2o_7$: a one-dimensional spin-1/2 heisenberg antiferromagnet with a ladder spin configuration and a singlet ground state," Phys. Rev. B **35**, 219–222 (1987) (cit. on pp. 41, 58).

[210] N Maeshima, M Hagiwara, Y Narumi, K Kindo, T. C. Kobayashi, and K Okunishi, "Magnetic properties of a s = 1/2 zigzag spin chain compound (n 2 h 5)cucl 3," Journal of Physics: Condensed Matter **15**, 3607 (2003) (cit. on pp. 41, 58).

[211]E. Dagotto, J. Riera, and D. Scalapino, "Superconductivity in ladders and coupled planes," Phys. Rev. B **45**, 5744–5747 (1992) (cit. on pp. 41, 55).

[212]J. Almeida, M. A. Martin-Delgado, and G. Sierra, "Density-matrix renormalization group study of the bond-alternating $s = 12$ heisenberg ladder with ferro-antiferromagnetic couplings," Phys. Rev. B **76**, 184428 (2007) (cit. on pp. 41, 59).

[213]O. S. Volkova, I. S. Maslova, R. Klingeler, M. Abdel-Hafiez, Y. C. Arango, A. U. B. Wolter, V. Kataev, B. Büchner, and A. N. Vasiliev, "Orthogonal spin arrangement as possible ground state of three-dimensional shastry-sutherland network in $ba_3cu_3in_4o_12$," Phys. Rev. B **85**, 104420 (2012) (cit. on pp. 41, 58).

[214]D. I. Badrtdinov, O. S. Volkova, A. A. Tsirlin, I. V. Solovyev, A. N. Vasiliev, and V. V. Mazurenko, "Hybridization and spin-orbit coupling effects in the quasi-one-dimensional spin-1/20 magnet $ba3cu3sc4o12$," Phys. Rev. B **94**, 054435 (2016) (cit. on p. 41).

[215]M. Kumar and Z. G. Soos, "Decoupled phase of frustrated spin-$\frac{1}{2}$ antiferromagnetic chains with and without long-range order in the ground state," Phys. Rev. B **88**, 134412 (2013) (cit. on pp. 41, 55, 62).

[216]R. Chitra, S. Pati, H. R. Krishnamurthy, D. Sen, and S. Ramasesha, "Density-matrix renormalization-group studies of the spin-1/2 heisenberg system with dimerization and frustration," Phys. Rev. B **52**, 6581–6587 (1995) (cit. on pp. 41, 55, 58, 59, 62).

[217]H. Suhl and I. K. Schuller, "Spin-wave theory of exchange-induced anisotropy," Phys. Rev. B **58**, 258–264 (1998) (cit. on pp. 42, 55).

[218]T. M. Hong, "Simple mechanism for a positive exchange bias," Phys. Rev. B **58**, 97–100 (1998) (cit. on pp. 42, 55).

[219]W. H. Meiklejohn and C. P. Bean, "New magnetic anisotropy," Phys. Rev. **102**, 1413–1414 (1956) (cit. on p. 42).

[220]W. H. Meiklejohn and C. P. Bean, "New magnetic anisotropy," Phys. Rev. **105**, 904–913 (1957) (cit. on p. 42).

[221]J NoguÃľs and I. K. Schuller, "Exchange bias," J. Magn. Magn. Mater. **192**, 203 –232 (1999) (cit. on p. 42).

[222] M. Kiwi, "Exchange bias theory," J. Magn. Magn. Mater. **234**, 584 –595 (2001) (cit. on p. 42).

[223] A. Berkowitz and K. Takano, "Exchange anisotropy – a review," J. Magn. Magn. Mater. **200**, 552 –570 (1999) (cit. on p. 42).

[224] M. Finazzi, "Interface coupling in a ferromagnet/antiferromagnet bilayer," Phys. Rev. B **69**, 064405 (2004) (cit. on p. 42).

[225] A. P. Malozemoff, "Random-field model of exchange anisotropy at rough ferromagnetic-antiferromagnetic interfaces," Phys. Rev. B **35**, 3679–3682 (1987) (cit. on p. 42).

[226] N. C. Koon, "Calculations of exchange bias in thin films with ferromagnetic/antiferromagnetic interfaces," Phys. Rev. Lett. **78**, 4865–4868 (1997) (cit. on p. 42).

[227] T. C. Schulthess and W. H. Butler, "Consequences of spin-flop coupling in exchange biased films," Phys. Rev. Lett. **81**, 4516–4519 (1998) (cit. on p. 42).

[228] T. C. Schulthess and W. H. Butler, "Coupling mechanisms in exchange biased films (invited)," J. Appl. Phys. **85**, 5510–5515 (1999) (cit. on p. 42).

[229] J.-V. Kim and R. L. Stamps, "Defect-modified exchange bias," Applied Physics Letters **79**, 2785–2787 (2001) (cit. on p. 42).

[230] U. Nowak, A. Misra, and K. D. Usadel, "Domain state model for exchange bias," J. Appl. Phys. **89**, 7269–7271 (2001) (cit. on p. 42).

[231] Y. Sakurai, H. Kitatani, T. Ishiguro, Y. Ichinose, and N. S. Kazama, "Monte carlo approach for f-af coupling layers," IEEE Trans. Magn. **29**, 3879 (1993) (cit. on p. 42).

[232] D. Mauri, H. C. Siegmann, P. S. Bagus, and E. Kay, "Simple model for thin ferromagnetic films exchange coupled to an antiferromagnetic substrate," J. Appl. Phys. **62**, 3047–3049 (1987) (cit. on p. 42).

[233] H. Xi, R. M. White, and S. M. Rezende, "Irreversible and reversible measurements of exchange anisotropy," Phys. Rev. B **60**, 14837–14840 (1999) (cit. on p. 42).

[234] H. Xi and R. M. White, "A theoretical study of interfacial spin flop in exchange-coupled bilayers," IEEE Trans. Magn. **36**, 2635 (2000) (cit. on p. 42).

[235] J. Geshev, "Analytical solutions for exchange bias and coercivity in ferromagnetic/antiferromagnetic bilayers," Phys. Rev. B **62**, 5627–5633 (2000) (cit. on p. 42).

[236]T. C. Schulthess and W. H. Butler, "First-principles exchange interactions between ferromagnetic and antiferromagnetic films: co on nimn, a case study," J. Appl. Phys. **83**, 7225–7227 (1998) (cit. on p. 42).

[237]D. Dey, D. Maiti, and M. Kumar, "An efficient density matrix renormalization group algorithm for chains with periodic boundary condition," Papers in Physics **8**, 080006 (2016) (cit. on p. 44).

[238]P. Fulde, *Electron correlations in molecules and solids*, 3rd ed. (Springer-Verlag, 1995) Chap. 4, p. 76 (cit. on p. 53).

[239]F. Mila, "Ladders in a magnetic field: a strong coupling approach," Eur. Phys. J. B **6**, 201–205 (1998) (cit. on p. 53).

[240]K. Sekiguchi and K. Hida, "Partial ferrimagnetism in $s = 1/2$ heisenberg ladders with a ferromagnetic leg, an antiferromagnetic leg, and antiferromagnetic rungs," J. Phys. Soc. Jpn. **86**, 084706 (2017) (cit. on p. 55).

[241]B. S. Shastry and B. Sutherland, "Excitation spectrum of a dimerized next-neighbor antiferromagnetic chain," Phys. Rev. Lett. **47**, 964–967 (1981) (cit. on p. 58).

[242]A. V. Chubukov, "Chiral, nematic, and dimer states in quantum spin chains," Phys. Rev. B **44**, 4693–4696 (1991) (cit. on p. 58).

[243]S. Furukawa, M. Sato, S. Onoda, and A. Furusaki, "Ground-state phase diagram of a spin-$\frac{1}{2}$ frustrated ferromagnetic xxz chain: haldane dimer phase and gapped/gapless chiral phases," Phys. Rev. B **86**, 094417 (2012) (cit. on p. 58).

[244]M. E. Zhitomirsky and H. Tsunetsugu, "Magnon pairing in quantum spin nematic," EPL (Europhysics Letters) **92**, 37001 (2010) (cit. on p. 58).

[245]A. Parvej and M. Kumar, "Multipolar phase in frustrated spin-1/2 and spin-1 chains," Phys. Rev. B **96**, 054413 (2017) (cit. on p. 58).

[246]M Kumar, S. E. Dutton, R. J. Cava, and Z. G. Soos, "Spin-flop and antiferromagnetic phases of the ferromagnetic half-twist ladder compounds ba3cu3in4o12and ba3cu3sc4o12," Journal of Physics: Condensed Matter **25**, 136004 (2013) (cit. on p. 58).

[247] B Koteswararao, A. V. Mahajan, F Bert, P Mendels, J Chakraborty, V Singh, I Dasgupta, S Rayaprol, V Siruguri, A Hoser, and S. D. Kaushik, "Magnetic behavior of ba3cu3sc4o12," Journal of Physics: Condensed Matter **24**, 236001 (2012) (cit. on p. 58).

[248] D. Maiti and M. Kumar, "Melting of ferromagnetic order on a trellis ladder," Journal of Magnetism and Magnetic Materials **486**, 165266 (2019) (cit. on p. 62).

[249] D. C. Johnston, M. Troyer, S. Miyahara, D. Lidsky, K. Ueda, M. Azuma, Z. Hiroi, M. Takano, M. Isobe, Y. Ueda, M. A. Korotin, V. I. Anisimov, A. V. Mahajan, and L. L. Miller, "Magnetic susceptibilities of spin-1/2 antiferromagnetic heisenberg ladders and applications to ladder oxide compounds," arXiv:cond-mat/0001147 (cit. on pp. 72, 73, 75).

[250] M. Onoda and N. Nishiguchi, "Letter to the editor: crystal structure and spin gap state of cav2o5," Journal of Solid State Chemistry **127**, 359 –362 (1996) (cit. on p. 74).

[251] J. S. Miller and M. Drillon, "Magnetism: molecules to materials iv," in *Magnetism: molecules to materials iv* (Wiley-VCH, Germany, 2002) Chap. 4, p. 148 (cit. on p. 80).

[252] J. Lou, C. Chen, and S. Qin, "Low-energy properties and magnetization plateaus in a two-leg mixed spin ladder," Phys. Rev. B **64**, 144403 (2001) (cit. on p. 80).

[253] A. Langari, M. Abolfath, and M. A. Martin-Delgado, "Phase diagram of ferrimagnetic ladders with bond alternation," Phys. Rev. B **61**, 343–348 (2000) (cit. on p. 80).